Manipulation of Magnetic Microparticles in Liquid Phases for On-Chip Biomedical Analysis Methods

THÈSE N^{O} 4072 (2008)

PRÉSENTÉE LE 27 JUIN 2008

À LA FACULTÉ DES SCIENCES ET TECHNIQUES DE L'INGÉNIEUR
LABORATOIRE DE MICROSYSTÈMES 2
PROGRAMME DOCTORAL EN MICROSYSTÈMES ET MICROÉLECTRONIQUE

ÉCOLE POLYTECHNIQUE FÉDÉRALE DE LAUSANNE

POUR L'OBTENTION DU GRADE DE DOCTEUR ÈS SCIENCES

PAR

Ulrike LEHMANN

Dipl.-Ing. (Elektrotechnik), Technische Universität Chemnitz, Allemagne
et de nationalité allemande

acceptée sur proposition du jury:

Prof. Y. Leblebici, président du jury
Prof. M. Gijs, directeur de thèse
Prof. G. Borghs, rapporteur
Dr N. Pamme, rapporteur
Dr C. Vandevyver, rapporteur

ÉCOLE POLYTECHNIQUE
FÉDÉRALE DE LAUSANNE
Suisse
2008

"Magnetism, as you recall from physics class, is a powerful force that causes certain items to be attracted to refrigerators."

Dave Barry (American Writer and Humorist)

ACKNOWLEDGEMENTS

This thesis work was done at the *Laboratory for Microsystems 2*, which is part of the Institute of Microtechnology at the Ecole Polytechnique Fédérale de Lausanne (EPFL). It was funded by the Swiss National Science Foundation (Grant 200020-107372) and the Competence Center for Materials Science and Technology (CCMX).

I would like to acknowledge the members of my jury, Prof. Yussuf Leblebici, Dr. Nicole Pamme, Dr. Caroline Vandervyver, Prof. Gustaf Borghs and Prof. Martin Gijs, for reviewing this thesis and for the challenging and interesting discussion, which encompassed my thesis defense.

Special thanks to my thesis supervisor Prof. Martin Gijs, who gave me the opportunity to work on this very interesting and challenging topic and who's door was always open for a PhD student looking for advice or a second opinion.

A very big „thank you" also to Virendra Parashar, who's knowledge in chemistry helped me a lot in making the droplet manipulation system work, and to Caroline Vandervyver, without whom the experiments on bioanalysis would not have been possible. Another „thank you" is due to Maximilian Sergio and Edoardo Charbon, who helped designing the CMOS chip and who showed a lot of patience until it finally worked.

Further-on I would like to thank my students, Marc Desaules, Damien DeCourten and Stefano Pietrocola, as well as Marta Lombardini, Smail Hadjidj, Michael Friedrich, Fabio Jutzi and Ha Huy Hoang Le, who all contributed for a short time to the work presented here.

Additionally I would like to extend my gratitude to Mr. Amendola and his colleagues at the mechanic's workshop, who were always helpful in fabricating elements for experimental setups as well as the metal masks for the Teflon treatment.

Finally I would like to thank all my colleagues for supporting me in the ups and downs of a PhD's academic life as well as the Polyssons and FlyHighs for helping me to keep my mind fresh during these years.

Last but not least I most heartily thank my friends and family.

Lausanne, April 2008

Ulrike Lehmann

ABSTRACT

Magnetic microparticles and their application in bio-analytical microfluidic systems have been steadily gaining interest in recent years. This progress is fueled by the comparatively large and long range magnetic forces that can be obtained independently of the fluidic flow pattern.

This thesis work presents new approaches for using magnetic microparticles in Lab-on-a-Chip systems. The first approach deals with the design of a magnetic droplet manipulation system and the second combines magnetic particle actuation with integrated optical detection. The applicability of both systems for miniaturized bioanalysis will be shown, demonstrating the potential of magnetic particle based Lab-on-a-Chip systems.

The magnetic droplet manipulation system tackles the handling of small liquid volumes, which is an important task in miniaturized analytical systems. The careful adjustment of hydrophilic/hydrophobic surface properties and interfacial tensions leads to the design of a system, where small droplets are manipulated in a controllable fashion. The system's setup permits the direct implementation of bioanalytical protocols and two different procedures are in consequence examined.
Based on a commercial laboratory kit, a platform for the on-chip extraction and purification of DNA will be designed. The miniaturized setup allows the user to capture and clean the DNA obtained from a raw cell sample containing as little as 10 cells, which is several orders of magnitude lower than known for macroscopic systems.
A similar performance is observed for the colorimetric antibody detection further-on evaluated in the droplet manipulation system, where the small sample volumes permit a significant reduction of the reaction times. With the possibility of concentrating the biomolecules of interest on the particle surface, a sensitive and fast immunosorbent assay can be devised.

A further miniaturization is examined in a CMOS system, which combines magnetic actuation and optical detection. The small dimensions of the actuation system allow the manipulation of single magnetic microparticles and the integration of Single Photon Avalanche Diodes (SPADs) enables their optical detection. An innovative detection algorithm permits hereby to distinguish the particles in size and, in combination with a velocity measurement, to evaluate the magnetic properties of the detected particles. In consequence, bioanalysis on a single magnetic particle using fluorescent measurements can be performed, as is shown by preliminary experiments.

Keywords: Magnetic Microparticles, Microfluidics, Droplet Manipulation, Lab-on-a-Chip, Optical Detection

ZUSAMMENFASSUNG

Magnetische Mikropartikel und ihre Verwendung in mikrofluidischen Bioanalyse-Systemen (Lab-on-a-Chip) haben in den vergangenen Jahren stetig an Interesse gewonnen. Die Motivation hierfür liegt in den magnetischen Kräften begründet, welche vergleichsweise groß sind, eine lange Reichweite ausweisen und unabhängig vom Strömungsprofil erzeugt werden können.

Diese Doktorarbeit präsentiert neue Ansätze zur Verwendung magnetischer Mikropartikel in "Lab-on-a-Chip" Systemen. Der erste Ansatz beschäftigt sich mit dem Entwurf eines Mikrosystems zur Manipulation von Tröpfchen und der zweite kombiniert magnetische Aktuation mit integrierter optischer Detektion. In diesem Zusammenhang wird ebenfalls der potentielle Einsatz beider Systeme für Bioanalyse in miniaturisierter Form demonstriert.

Die magnetbasierte Manipulation von Tropfen nimmt die Handhabung kleiner Flüssigkeitsvolumen in Angriff, welche eine große Herausforderung für miniaturisierte Analysesysteme darstellt. Die sorgfältige Anpassung der hydrophilen/hydrophoben Oberflächeneigenschaften sowie der Grenzflächenspannungen führt zum Entwurf eines Systems, welches die kontrollierte Manipulation kleiner Tropfen ermöglicht. Die Gestaltung des Systems erlaubt die direkte Übertragung makroskopischer Protokolle aus der Bioanalyse auf den Chip, derer zwei im Folgenden studiert werden.
Ausgehend von einem kommerziellen Laborkit wird ein Prozeß zur chipbasierten Extrahierung und Reinigung von DNS entwickelt. Die Miniaturisierung macht es hierbei möglich, die DNS aus einer Probe von nur 10 Zellen zu gewinnen, was eine Verbesserung von mehreren Größenordnungen, im Vergleich zu makroskopischen Systemen, darstellt. Ähnliches ist für die colorimetrische Detektion von Antikörpern zu beobachten, welche ebenfalls mit dem Tropfenmanipulationssystem durchgeführt werden kann und aufgrund des geringen Probenvolumens zu einer deutlichen Verringerung der Reaktionszeit führt.

Ein größerer Miniaturisierungsschritt wird an einem CMOS System untersucht, welches magnetische Aktuation und optische Detektion miteinander verbindet. Aufgrund der geringen Abmessungen können einzelne magnetische Mikropartikel manipuliert werden, wobei die Integration von Single Photon Avalanche Dioden (SPADs) deren optische Detektion erlaubt. Ein innovativer Messalgorithmus macht es möglich, die Partikel hierbei nach Größe zu unterscheiden und, in Kombination mit der Messung der Partikelgeschwindigkeit, ihre magnetischen Eigenschaften zu bestimmen. Somit kann ein Protokoll entworfen werden, welches einzelne magnetische Partikel für fluoreszenzbasierte bioanalytische Untersuchungen verwendet.

Schlagwörter: Magnetische Mikropartikel, Mikrofluidik, Tropfenmanipulation, Lab-on-a-Chip, Optische Detektion

VERSION ABRÉGÉE

La manipulation de microparticules magnétiques et leur application dans des systèmes micro-fluidiques pour l'analyse biologique a continuellement gagné en intérêt ces dernières années. Ce progrès est propulsé par l'utilisation des forces magnétique qui, d'une grande intensité, peuvent être appliquées sur de grandes distances indépendamment du mouvement des fluides.

Dans ce travail de thèse, on propose deux nouveaux concepts pour l'utilisation et la manipulation de particules magnétiques dans les systèmes Lab-on-a-Chip. Lors d'une première approche, on présentera un système permettant la manipulation de microgouttes à l'aide de particules magnétiques. Une seconde approche consistera à combiner l'actuation magnétique de microparticules avec une détection optique intégrée. La faisabilité de ces deux systèmes pour la réalisation d'analyses biologiques miniaturisées sera expérimentalement démontrée, prouvant leur potentiel pour l'analyse de type Lab-on-a-Chip.

Dans la première approche, les particules magnétiques permettrons la manipulation de très faibles quantités de liquide sous forme de gouttes, répondant ainsi à une grande exigence pour les systèmes d'analyses miniaturisés. Le contrôle précis des propriétés hydrophobes/hydrophiles des surfaces et des tensions interfaciales conduira à un système où les petites gouttes seront manipulées d'une façon très précises. La structure de ce système permettra la réalisation de protocoles bioanalytiques, et l'étude de deux cas bien définis sera réalisée. Dans un premier temps, l'utilisation d'un kit commercial pour l'extraction et la purification d'ADN sera démontrée sur chip. Ce système miniaturisé permettra la capture et la purification de l'ADN de seulement 10 cellules, inférieur de plusieurs ordres de grandeur comparé aux systèmes macroscopiques. Des performances similaires seront observées lors de la détection colorimétrique d'anticorps.

Lors de la seconde approche, une miniaturisation encore plus poussée a été étudiée dans un système CMOS, combinant actuation magnétique des microparticules et détection optique. Les très petites dimensions du système d'actionnement permettront la manipulation d'une seule particule et l'intégration de Single Photon Avalanche Diodes (SPADs) donnera la possibilité de la détecter. Avec un algorithme de détection innovant, les particules peuvent être discernées par leur taille et, combiné avec une mesure de leur vitesse, les propriétés magnétiques des ces particules peuvent être évaluées. En conséquence, la bioanalyse sur une seule particule magnétique devient possible, comme démontré par les premières mesures réalisées sur des particules fluorescentes.

Mots-clés: microparticules magnétiques, microfluidique, manipulation des gouttes, Lab-on-a-Chip, détection optique

TABLE OF CONTENTS

Acknowledgements ..... **i**

Abstract ..... **iii**

Zusammenfassung ..... **iv**

Version Abrégée ..... **v**

Table of Contents ..... **vii**

1. Introduction **1**

1.1. From Microfluidics to Lab-on-a-Chip 1

1.2. Magnetic Particles in Bioanalysis 3

1.3. Scope and Outline of this Work 4

2. Theory on Magnetic Particles and Magnetic Droplet Manipulation **7**

2.1. Magnetic Microparticles in Liquid Phases 7

2.1.1. Magnetic Microparticles 7

2.1.2. Forces on Magnetic Microparticles 14

2.1.3. Magnetophoretic Mobility 16

2.2. Droplets and Interfacial Tension 17

2.2.1. Droplet Breakup 20

2.3. The Magnetic Field of a Multilayer of Square Coils 23

2.4. Conclusion 26

3. State of the Art **29**

3.1. Microfluidics 29

3.1.1. Continuous Flow Microfluidics 29

3.1.2. Digital Microfluidics 31

3.1.3. Literature Review of Droplet Manipulation Systems 31

3.1.4. Magnetic Droplet Manipulation 35

3.2. Magnetic Particle Manipulation 38

3.2.1. Magnetic Manipulation via Permanent Magnets 38

3.2.2. Magnetic Manipulation via Electromagnetic Fields 39

3.2.3. Literature Review of Magnetic Microparticle Manipulation Systems 40
3.3. Magnetic Microparticles in Lab-on-a-Chip Systems 42
3.4. Conclusion 47

4. Magnetic Droplet Manipulation 49
4.1. Introduction 49
4.2. Magnetic Droplet Actuation System 50
4.2.1. The Magnetic Actuation Unit 50
4.2.2. The Oil Medium 55
4.2.3. The Magnetic Particles 58
4.3. Droplet Handling 60
4.3.1. Droplet Transport 60
4.3.2. Droplet Merging and Mixing 63
4.3.3. Droplet Splitting 64
4.4. Conclusion 72

5. Droplet Based Lab-on-a-Chip for Miniaturized Bioanalysis 75
5.1. Introduction 75
5.1.1. Biology on a Bead 75
5.1.2. Bioanalysis in Droplets 76
5.2. DNA Purification and Extraction 78
5.2.1. Protocol and Materials 78
5.2.2. Results and Discussion 80
5.2.3. Conclusion 88
5.3. On-chip antibody binding and detection 89
5.3.1. Protocol and Methods 90
5.3.2. Results and Discussion 93
5.3.3. Conclusion 99
5.4. Conclusion 99

6. Manipulation and Integrated Optical Detection of Single Magnetic Particles 103
6.1. Introduction 103
6.2. System Setup 104
6.2.1. Magnetic Actuation 106

6.2.2. Optical Detection Elements 108
6.2.3. Optical Detection - Theory and Model 110
6.3. Experiments and Results 113
6.4. Towards a Lab-on-a-Chip 119
6.4.1. Microfluidic Network 119
6.4.2. Fluorescent Detection 121
6.4.3. Conclusion 124
6.5. Conclusion 125

7. Conclusion and Outlook 127
7.1. Magnetic Droplet Manipulation 127
7.2. Magnetic Particle Manipulation with Integrated Optical Detection 129
7.3. Summary 130
7.4. Going Forward 131

Nomenclature 135

References 141

Publications 159
Journal Articles 159
Conference Contributions 159
Conference Abstracts 161

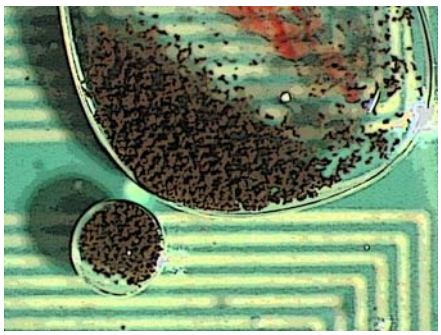

CHAPTER 1

INTRODUCTION

The 1990s have seen the successful rise of the Micro-Electro-Mechanical Systems (MEMS) and their integration into our daily life [85]. A MEMS device or microsystem can combine mechanical elements, sensors, actuators and electronics on a common silicon substrate through microfabrication technology [115]. When adding sensors for gathering information from the environment, the decision making capability of the microelectronics is augmented. The measurement of mechanical, thermal, biological, chemical, optical and magnetic phenomena results in creating an "intelligent" system capable of sensing and controlling its environment. One of the most prominent and successful examples of MEMS technology is the accelerometer. First introduced by Analog Devices in 1991, accelerometers can now be found in most automobiles, where they control the airbag's release in case of an accident.

One of the strengths and characteristics of MEMS is their versatility and interdisciplinarity, which as a consequence requires highly flexible means of microfabrication [115], and leads to an ever increasing number of micromachining technologies. Fueled by the development of new fabrication methods [1, 12, 201], the MEMS community recently started taking an interest in the miniaturization of applications used for bioanalysis. This field of activity is generally termed BioMEMS, since it combines microtechnology and biology, such as the handling of cells or the detection and processing of DNA and antibodies, within microfluidic channels [186].

1.1 From Microfluidics to Lab-on-a-Chip

Microfluidics, which deals with the miniaturized handling of liquid samples [11, 63, 70] - a requirement for bioanalysis - is steadily gaining

interest, as the increasing number of publications shows (Figure 1.1). Recently, more specific applications of microfluidics are emerging and an increasing diversity of techniques and applications can be observed in literature [1, 163]. Continuous flow microfluidics of the first generation is joined by droplet-based approaches [48, 128], cells are cultured, transported and studied on a microfluidic chip [47] and particles are manipulated within the microfluidic system [181].

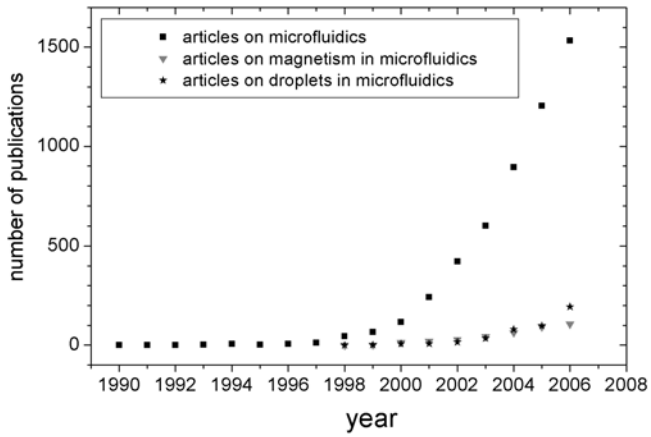

Figure 1.1 Number of articles on microfluidics and its variations, including droplets and magnetism, published in recent years (taken from ISI Web of Knowledge).

Lab-on-a-Chip

The increasing complexity of microfluidic systems and their application to bioanalytical problems led to the introduction of the concept of Micro Total Analysis Systems (μTAS) or Lab-on-a-Chip (LOC) [118]. Such systems aim at shrinking a laboratory filled with people down to a chip the size of a credit card. All necessary sample handling and analysis steps are performed within the chip, as schematically shown in Figure 1.2.

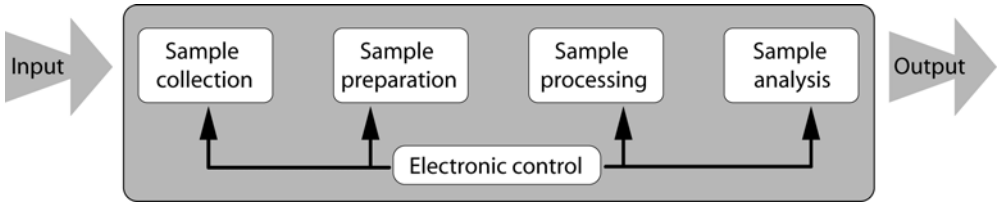

Figure 1.2 Schematic of a Lab-on-a-Chip system.

Thus an LOC can be represented by a black-box that generates a meaningful output signal upon the insertion of a real world sample, such as an aqueous droplet or blood.

The advantages of miniaturized bioanalysis procedures are manifold. Most important is the reduction of sample and reagent volumes and thus

the reduction of overall costs [7, 149]. In addition, the miniaturization leads to decreased reaction times and allows a high parallelization of reactions, which is an enormous advantage in screening-based protocols. In many cases, applications known from macroscopic bioanalysis can be directly converted into the miniaturized format, which has the advantage, that reactions and reagents are already well known and characterized.

1.2 Magnetic Particles in Bioanalysis

Magnetic micro- and nanoparticles ("beads") have proven to be a very versatile and reliable tool in biomedical analysis procedures within recent years [100, 174].

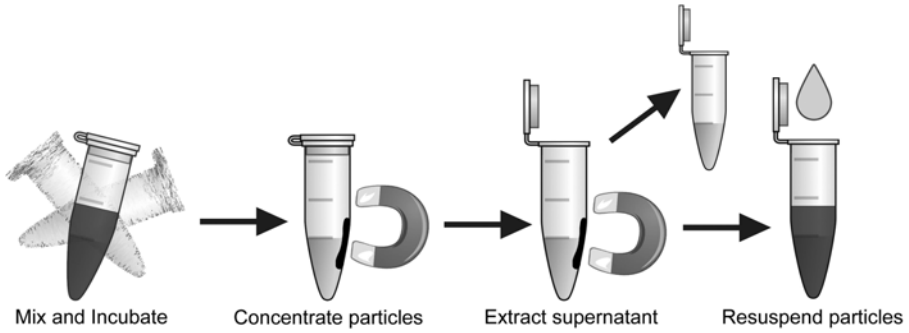

Figure 1.3 Procedural sequence for magnetic particle-based bioanalysis. The particles are mixed with a first medium and concentrated via an external permanent magnet. The first medium is removed and the particles are resuspended in a second medium. The sequence is repeated for the subsequent step of the protocol.

They are used, among others, in DNA extraction [182, 205], cell separation [119, 124] and antibody detection [61]. The advantages of the magnetic particles are their easy handling and the ever increasing choice of surface functionalizations available on the market [58, 167]. In general, bioanalytical protocols employing magnetic particles repeat a series of particle handing steps, as shown in Figure 1.3. The mixing with a sample solution is followed by the concentration of the particles via a permanent magnet. The sample solution is removed and the particles are resuspended in the medium of the subsequent step, such as a washing solution or detection substrate. In comparison with other concentration or separation procedures, magnetic separation does not require additional elaborate equipment, but simply a field gradient generated by a permanent magnet [138] or a specially designed electromagnet [65]. A

common setup for lab-bench magnetic particle supported bioanalysis is presented in Figure 1.4.

Figure 1.4 Standard setup for the magnetic separation. The magnetic particles in solution are attracted towards a permanent magnet and the liquid is extracted from the vial.

Furthermore, the magnetic particles serve not only as markers for the biomolecules of choice, but also as substrates and handles for manipulation. This multi-functionality of the magnetic particles makes them ideal candidates for being the active component in miniaturized bioanalytical systems [21]. Subsequently, LOC-type systems employing magnetic microparticles as either active or passive components are steadily gaining impact and importance, as recent publications show [137].

1.3 Scope and Outline of this Work

Within the last years, a wide range of solutions for the handling of liquids in microfluidic systems have been developed [6, 63, 130, 171]. In parallel, a multitude of sensors and actuators, ready to be implemented in these systems, have been demonstrated, resulting in new approaches for Lab-on-a-Chip systems. Based on the schematic shown in Figure 1.2 we can envision a μTAS toolbox containing different solutions for the LOC steps. These solutions form groups of building blocks, which can be combined and permuted depending on the requirements of a specific bioanalytical application.

The goal of this thesis is to study the combination of magnetic particle manipulation with other elements of the μTAS toolbox and to examine the applicability of the thus arising solution for miniaturized bioanalysis. The

elements chosen for combination are digital microfluidics, as suggested by Shikida at the 2004 IEEE MEMS conference [160], and integrated optical detection [131].

After an overview of the theoretical background of the magnetic particle manipulation and a discussion of the principles and forces dominating the manipulation of droplets in chapter 2, I am going to look into existing solutions in a state-of-the-art study in chapter 3.

Chapter 4 presents the combination of the manipulation of magnetic microparticles with digital microfluidics resulting in a magnetic droplet manipulation system. I will demonstrate the different droplet manipulation steps and their implementation, resulting in a system capable of on-chip bioanalyis. Subsequently, chapter 5 shows the potential of such a system for miniaturized bioanalysis, with the advantage of keeping the reagents and steps of well-known standard protocols, while simply reducing the processing time and consumption.

In chapter 6 the system for the manipulation of magnetic microparticles is further reduced in size and is combined with integrated optical detection in a hybrid CMOS system. The reduction in size permits the manipulation and detection of single microparticles. I will demonstrate the capability of the CMOS system to distinguish the microparticles in size and magnetic properties.

Finally the results and findings are summarized in chapter 7 and I will conclude this work with recommendations for future developments and applications.

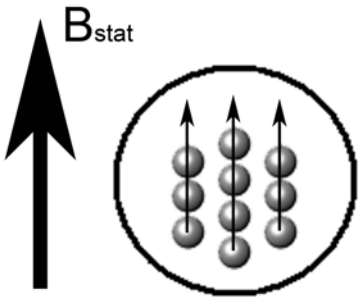

CHAPTER

2

THEORY ON MAGNETIC PARTICLES AND MAGNETIC DROPLET MANIPULATION

This chapter presents the governing principles behind the magnetic droplet manipulation starting from the actuation of magnetic microparticles. The basic properties of magnetic microparticles will be discussed as well as their behavior in the presence of liquids and magnetic fields. Subsequently, I will present the concept of microdroplets with enclosed magnetic particles and the parameters guiding their interaction during the droplet handling steps. The final section of this chapter discusses the generation of a two dimensional flexible field topology used for the droplet manipulation.

2.1 Magnetic Microparticles in Liquid Phases

Magnetic microparticles are steadily gaining interest in macroscopic bioanalysis as well as Lab-on-a-Chip systems. The use of micrometric particles in bioassays offers hereby the advantage of a large specific surface for chemical binding combined with a high mobility, as compared to solutions based on solids of larger volume [58].

2.1.1 Magnetic Microparticles

Fueled by the increasing interest, magnetic microparticles can be obtained in an ever rising multitude of sizes, materials and surface properties [74]. The choice of the type of magnetic microparticles depends on the

individual application and the respective advantages and disadvantages of the different particle variants.

Magnetic Properties

Most commonly magnetic microparticles are made of magnetic nanocrystals enclosed in a matrix of inert and bio-compatible material such as polymer or silicon dioxide [58]. The nanocrystals can be composed of iron oxide (maghemite or magnetite), amalgams of transition metals (Ni, Fe, Co, Mg or Zn) or rare earth materials (NdFeB or SmCo). Figure 2.1 summarizes via a table of elements the magnetic character of the different elements in their bulk state.

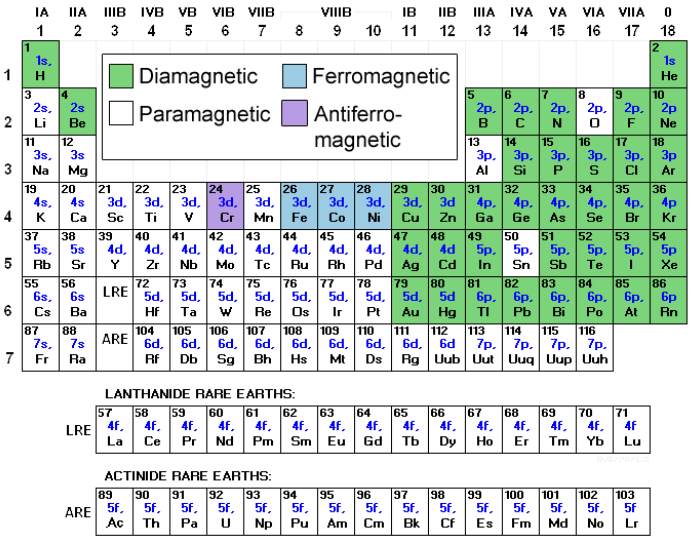

Figure 2.1 Table of elements indicating the magnetic properties of the elements in their solid state.

The magnetism of materials has its origin at the atomic level, where the orbital and spin angular momenta contribute to the magnetic moment μ of an atomic electron.

$$\mu = -g_L \mu_B \mathbf{J} \tag{2.1}$$

with the Landé factor g_L [96], the Bohr magneton μ_B = 9.274 10^{-24} J/T and the resultant total angular momentum $\boldsymbol{J} = \boldsymbol{S} + \boldsymbol{L}$, were S is the angular momentum from the electron's spin and L the orbital angular momentum [31]. The strength of an atom's magnetic dipole moment is determined by the inner structure of the atom, especially its number of electrons and their placement in the atomic shells and their quantum states.

Type of Magnetism	Susceptibility	Atomic/Magnetic Behavior		Example (Susceptibility χ_r)	
Diamagnetism	- small ($\lvert\chi_r\rvert \ll 1$) - negative	- atoms have no magnetic moment	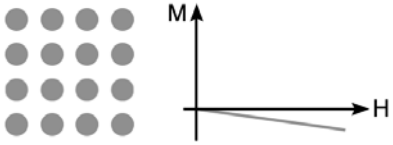	Au Cu	-2.74 10^{-6} -0.77 10^{-6}
Paramagnetism	- small ($\ll 1$) - positive	- atoms have randomly oriented magnetic moments - negligible interaction energy between atomic magnetic moments	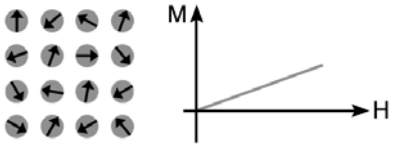	β-Sn Pt Mn	0.19 10^{-6} 21.04 10^{-6} 66.10 10^{-6}
Ferromagnetism	- large ($\gg 1$) - positive - function of applied field	- atoms have parallel aligned magnetic moments within domains	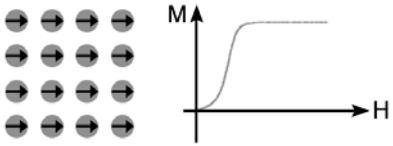	Fe	~100,000
Antiferromagnetism	- small ($\ll 1$) - positive	- atoms have parallel and anti-parallel magnetic moments aligned in a regular pattern	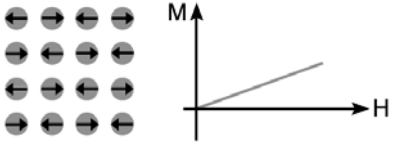	Cr	3.6 10^{-6}
Ferrimagnetism	- large ($\gg 1$) - positive - function of applied field	- anti-parallel aligned magnetic moments of different atom types do not cancel completely	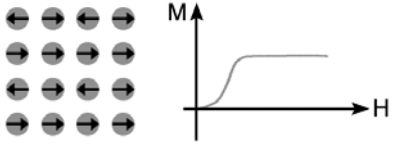	ferrite	~ 1000

Table 2.1 Overview and comparison of the different types of magnetism (adapted from http://www.aacg.bham.ac.uk/magnetic_materials/type.htm).

Depending on the interaction of the solid material with an external magnetic field various types of magnetism can be distinguished, such as diamagnetism, paramagnetism, ferromagnetism, antiferromagnetism and ferrimagnetism [31], which are schematically presented in Table 2.1.

This table shows that the magnetic character of a material is represented by its relative magnetic susceptibility χ_r, which describes the material's response to an applied magnetic field $\vec{H}$, i.e. its magnetization $\vec{M}$, via:

Magnetization

$$\vec{M} = \chi_r \cdot \vec{H} \tag{2.2}$$

The magnetization $\vec{M}$ of the material increases the total induced magnetic flux density $\vec{B} = \mu_0 \vec{H}$ by $\mu_0 \vec{M}$ to form:

$$\vec{B} = \mu_0(\vec{H} + \vec{M}) \tag{2.3}$$

with the permeability constant $\mu_0 = 4\pi\ 10^{-7}$ Vs/Am. The combination with equation (2.2) yields:

Magnetic flux density

$$\vec{B} = \mu_0(1 + \chi_r)\vec{H} = \mu_0\mu_r\vec{H} \tag{2.4}$$

with the relative magnetic permeability μ_r. The dimensionless parameter μ_r is usually expressed as a function of applied field H and temperature T depending on the type of magnetism [31, 133].

Since magnetic microparticles should react strongly to an applied magnetic field, a high relative susceptibility χ_r is required. For this reason, most magnetically responsive particles contain ferro- or ferrimagnetic material[1], such as maghemite or magnetite. These materials exhibit, in combination with a high susceptibility, internal long-range ordering effects between the non-zero magnetic dipole moments of the atoms. These ordering effects, which are a result of the magnetic exchange interaction [67, 72, 188], lead to the spontaneous alignment of neighboring atomic magnetic moments even in the absence of an applied magnetic field. Since the influence of the exchange energy decreases over longer distances, the anti-alignment of classic electromagnetism overrules the exchange interaction and results in the formation of magnetic domains [188]. In consequence, these *Weiss domains* are aligned at short range, but

1. In the following summarized as ferromagnetic material for brevity.

neighboring domains are anti-aligned. The transition between two domains, where the magnetization flips, is called a *Bloch domain wall* and is a gradual transition over the range of a few hundred atoms or ions. The presence of domains usually prevents the spontaneous magnetization of ferromagnetic materials and in addition leads to a non-linear magnetization behavior, know as magnetic hysteresis (Figure 2.2) [31].

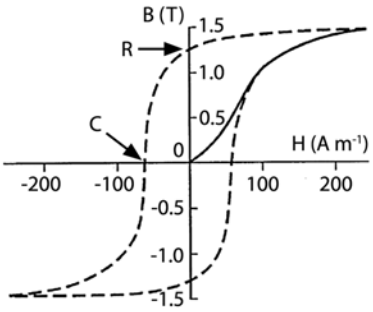

Figure 2.2 Magnetic hysteresis loop (broken line). After being magnetized from the unordered state until saturation (full line), the material will retain a magnetic moment even in the absence of an external field (remanence R). Only at the application of the coercitive field C, the net magnetic moment of the material will return to zero.

Superpara-magnetism

The effect of the *Weiss domain* formation leads to an additional phenomenon when reducing the size of a ferromagnetic crystal below the typical domain size, i.e. smaller than 30 nm for magnetite. In such a case, the thermal energy suffices to randomly change the magnetization of the entire complex, while the individual atomic moments maintain their ordered state relative to each other [101]. Thus the thermally induced fluctuations of the direction of magnetization cause the overall magnetic moment of a group of such nanocrystals to average to zero in the absence of an external magnetic field. In the presence of an external magnetic field, however, the magnetic moments of the crystallites tend to align with the field lines (Figure 2.3), expressing a relative magnetic susceptibility in the range of $\chi_r \sim 10^{-2} - 10^{2}$.

Due to its similarity with paramagnetism and its strong interaction with an applied magnetic field this type of magnetic behavior is described as **superparamagnetism** [87]. However, in contrast to paramagnetic materials (see Table 2.1), whose relative magnetic susceptibility is significantly lower, the magnetization of superparamagnetic materials remains constant after reaching the saturation magnetization M_S, as known for ferromagnetic material. The interaction of the nanoparticles

and the applied magnetic field is further-on influenced by the surrounding medium. When in suspension, the magnetic nanoparticles align with the applied field via particle rotation, but when fixed in a polymer matrix, the moment of the particle aligns with the field via rotation of the atomic magnetic moments, which can result in a non-linear magnetization curve for larger superparamagnetic microparticles.

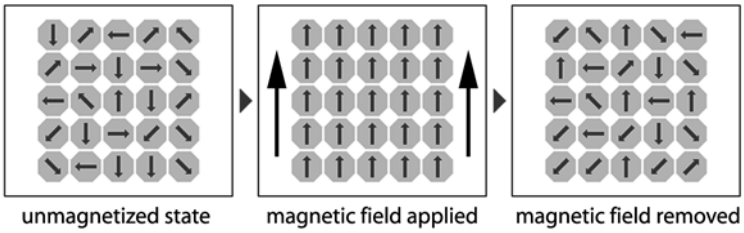

Figure 2.3 Superparamagnetic behavior of a group of freely suspended nanocrystals of ferromagnetic material (< 10 nm) in the absence and presence of an external magnetic field.

Particle Structure

To form a magnetic microparticle, superparamagnetic cores are embedded in a polymer shell, thus protecting the surrounding liquid from direct contact with the magnetic material. The advantage of the polymer shell lies in the possibility of surface functionalization and subsequent immobilization of biomolecules. The inner morphology of the particle, which is determined by the size and the amount of the enclosed magnetic crystallites, influences the overall magnetic behavior of the compound [101, 135]. A selection of commercially available composites is presented in Figure 2.4 [74].

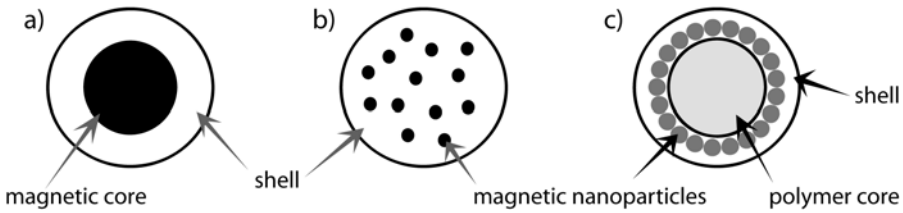

Figure 2.4 Configuration of magnetic microparticles. a) magnetic core in a non-magnetic shell (single-core). b) magnetic nanoparticles in a non-magnetic matrix/shell (multi-core). c) magnetic nanoparticles assembled around an inner polymer core and covered with an inert polymer shell (strawberry).

In general, the overall magnetic moment m_p of a magnetic microparticle containing weakly interacting magnetic nanoparticles is the sum of the individual magnetic moments of the nanocrystals enclosed in the polymer

matrix. For this reason, the fill factor, which describes the ratio of magnetic versus non-magnetic material in the particle, is an important parameter with respect to the magnetic behavior. It is usually highest for particles of the single- and multi-core type.

The overall relative magnetic susceptibility of the composite is further-on influenced by the demagnetization effect, which is related to the self-generated magnetic field in the space surrounding the particle. In consequence, the effective relative magnetic susceptibility χ_{eff} of a magnetic microparticle can be expressed as:

$$\chi_{eff} = \frac{\chi_{np}}{1 + N_d \cdot \chi_{np}} \tag{2.5}$$

with the relative magnetic susceptibility of the enclosed nanoparticles χ_{np} and the demagnetization factor N_d. The latter amounts to N_d = 1/3 for a spherical particle [133].

Finally, the choice of a certain type of particle depends on the intended application. Superparamagnetic single-core particles are generally in the nm-range, due to the size constraints, whereas multi-core and strawberry type superparamagnetic particles can be of any chosen size. The latter have hereby the advantage of a very good size control due to the use of highly mono-disperse polymer cores [60]. In comparison, an increase in particle size leads to a decrease in the surface-to-volume ratio, which results in a disadvantageous reduction of the specific surface area available for the attachment of functional groups to a given volume, while a decrease in particle size leads to a reduced magnetic moment and thus less magnetic force. For this reason, the choice of a type of magnetic particle is generally a compromise between magnetic and bioanalytic responsiveness.

Besides the size and the fill factor of the particle, the material of the non-magnetic shell [58, 112] has an important impact on the particle behavior and its interaction with the sample. The most widely used magnetic microparticles are polystyrene-coated. They can be produced in many sizes ranging from 6 nm to 10 μm and generally have a spherical shape and an excellent size distribution [74, 140]. The polymer shell also permits a wide choice of possible surface coatings, including the incorporation of fluorescent dyes and quantum-dots as well as the attachment of bio-active

molecules such as streptavidin, specific antibodies or nucleic acids [81, 174, 205]. However, the generally hydrophobic nature of polystyrene requires additional surface treatments in order to prevent aggregation in the presence of aqueous solutions.

Silica magnetic microparticles, which are per se hydrophilic, form the second largest group, and are often used in bioanalysis procedures involving DNA capture [16]. They are most commonly fabricated via a sol-gel process [114] and are available in sizes ranging from as small as 250 nm to more than 20 μm diameter but have the disadvantage of wide size distributions and - especially for larger silica coated microparticles - of non-spherical shape.

In addition to polystyrene and silica, a variety of further particle coatings [59, 107, 202], such as polysaccharine, poly-(lactic acid), PMMA or PHEMA, are available to cater to the needs of the various applications and protocols.

2.1.2 Forces on Magnetic Microparticles

A magnetic particle that is freely floating in a liquid and is being pulled by a magnetic force, experiences a set of forces as schematically presented in Figure 2.5. For microscopic particles the gravitational and buoyancy forces are very small and can usually be neglected [120, 195].

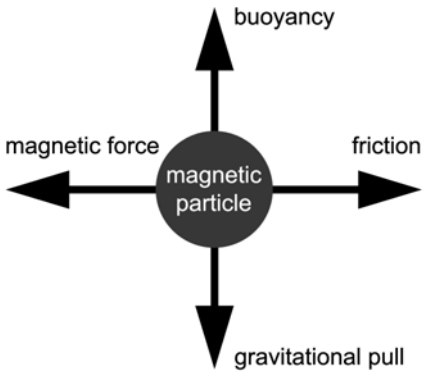

Figure 2.5 Diagram of the forces acting on a floating magnetic microparticle subjected to a magnetic force perpendicular to the direction of gravitation.

In consequence, the manipulation of magnetic particles in liquid phases is mainly guided by the two remaining diametrically opposed forces, the magnetic force that pulls the magnetic particles and the liquid friction or drag that acts against the pull. For a moving particle we obtain thus:

$$\vec{F}_{mag} = -\vec{F}_{drag} \tag{2.6}$$

The magnetic force on F_{mag} on a point-like magnetic dipole can hereby generally be expressed as:

Magnetic force

$$\vec{F}_{mag} = (\vec{m}_p \cdot \nabla)\vec{B} \tag{2.7}$$

with m_p the magnetic moment of the dipole and $\nabla\vec{B}$ the gradient of the magnetic flux density [119]. We see from equation (2.7) that a non-homogeneous magnetic field is required in order to obtain a translating magnetic force on the particle.

The character of the opposing liquid drag is determined by the Reynold's number R [11], which describes wether the flow conditions lead to laminar or turbulent flow. The limit is defined by the critical Reynold's number R_{crit}, which for water arises to R_{crit} = 2100 [189].

Reynold's Number

$$R = \frac{Inertial\,forces}{Viscous\,forces} = \frac{v_s \cdot D_h}{\nu} \tag{2.8}$$

with the mean velocity difference between liquid and particle v_s, the hydraulic diameter of the moving particle D_h and the kinematic viscosity ν of the fluid. The hydraulic diameter is expressed via:

Hydraulic diameter

$$D_h = \frac{4A}{U} \tag{2.9}$$

with the cross sectional area A and the wetted perimeter of the cross section U.

Thus, according to equation (2.8), a microparticle of 50 µm diameter moving with a relative velocity of 1 m/s in water (ν = 1.004 m^2/s) has a Reynold's number of R = 5 10^{-5}, which indicates a laminar flow regime called Stokes flow, where viscous effects are larger than inertial forces [144]. Therefore, the viscous drag force F_{drag} in that regime follows Stokes's Law:

Stokes's Law

$$\vec{F}_{drag} = -3\pi \cdot D_h \cdot \eta \cdot \vec{v}_s \tag{2.10}$$

with the fluid's dynamic viscosity η. The dynamic viscosity η and the kinematic viscosity ν are linked via the density ρ of the liquid via the expression [122]:

$$\eta = \nu \cdot \rho \tag{2.11}$$

2.1.3 Magnetophoretic Mobility

Magnetic microparticles, as stated above, are generally super-paramagnetic. Thus, the magnetic moment m_p of a magnetic particle, for a field strength below saturation, can be expressed as follows:

Magnetic Moment

$$\vec{m}_p = \int \Delta\chi \cdot \vec{H} \cdot dV_m \tag{2.12}$$

with $\Delta\chi$ the difference in relative magnetic susceptibility between the magnetic material (χ_b) and the surrounding medium (χ_f), V_m the volume of magnetic material per microparticle and $\vec{H}$ the magnetic field. Equation (2.12) indicates the strong influence of a high static magnetic field on the magnetization and thus on the magnetic force (equation (2.7)). When assuming a homogeneous susceptibility of the magnetic material over the volume V_m, equation (2.12) can be simplified and thus equation (2.7) yields:

$$\vec{F}_{mag} = \Delta\chi\, V_m (\vec{H} \cdot \nabla)\vec{B} = \frac{1}{2\mu_0}\Delta\chi\, V_m\, \nabla\vec{B}^2 \tag{2.13}$$

The right-hand term is obtained via the application of the rules for the nabla operator ∇ and equation (2.4), with μ_r = 1 for the non-magnetic surrounding medium.

Based on equations (2.6) and (2.10)(2.6)(2.6), we can therefore express the velocity of a magnetic particle as a function of the applied flux density B or the magnetophoretic driving force S.

$$\vec{v}_s = \frac{1}{3\pi}\frac{\Delta\chi\, V_m}{\eta\, D_h} \cdot \frac{\nabla\vec{B}^2}{2\mu_0} = \frac{1}{3\pi}\frac{\Delta\chi\, V_m}{\eta\, D_h} \cdot S \tag{2.14}$$

Magneto-phoretic mobility

The quotient of particle velocity v_s and magnetophoretic driving force S determines the magnetophoretic mobility m_s - a "normalized" parameter analogous to electrophoretic mobility - of a magnetic microparticle, which depends only on properties of the particle and the surrounding medium [120].

$$m_s = \frac{1}{3\pi} \frac{\Delta\chi \, V_m}{\eta \, D_h} \tag{2.15}$$

The above equation shows that particles of different sizes, whose susceptibilities differ, can express the same magnetophoretic mobility. Thus, when separating and transporting magnetic particles, neither their geometry nor their magnetic properties but a combined parameter, their magnetophoretic mobility, becomes the guiding entity.

2.2 Droplets and Interfacial Tension

When replacing the magnetic microparticles with small droplets filled with such particles, the equations above still apply, as long as $R < 1$ is fulfilled. Based on equation (2.8) the Reynold's number of a droplet with a diameter of $\varnothing = 3$ mm and a speed of $v = 1$ m/s amounts to $R = 0.003$, and therefore fits the requirement for Stokes flow. Since a droplet can contain a multitude N of particles, the volume V_m of the magnetic material in equation (2.13) needs to be multiplied by that factor. As a consequence the magnetic force acting on a droplet is:

Magnetic force on a droplet

$$\vec{F}_{mag,\,d} = \Delta\chi \, N \, V_m (\vec{H} \cdot \nabla)\vec{B} = \frac{1}{2\mu_0} \Delta\chi \, N \, V_m \, \nabla \vec{B}^{\,2} \tag{2.16}$$

In addition, the drag force will now act on the droplet, whose hydraulic diameter $D_{h,drop}$ replaces the particle diameter. Thus, the concentration C, given in g/ml, of the magnetic particles becomes the guiding parameter for the magnetophoretic mobility of the droplet. When replacing N, the amount of particles in the droplet, with the following expression

$$N = C \cdot \frac{V_{drop}}{\rho_m V_m} \tag{2.17}$$

equation (2.15) can be transformed into:

(2.18)
$$m_s = \frac{1}{3\,\pi} \cdot \frac{\Delta\chi}{\rho_m} \cdot \frac{V_{drop}}{\eta\, D_{h,drop}} \cdot C$$

Magneto-phoretic Droplet Mobility

with ρ_m the density of the magnetic particles and V_{drop} the droplet volume. We obtain a linear relation between the magnetophoretic mobility of the droplet and the concentration of magnetic particles for constant droplet size. Since a particle's magnetic susceptibility as well as its density are relative to its fill factor, a variation of the latter does not influence the droplets magnetophoretic mobility for a constant particle concentration C of the droplet. The total volume (NV_m) of the magnetic particles however increases, as can be deduced from equation (2.17), which leads to a larger spread of the particles and subsequently of the magnetic force inside the droplet's volume.

Upon the introduction of a magnetic field gradient, the magnetic force acting on the microparticles is transferred onto the droplet via their interaction with the droplet surface. In order to achieve a movement of the droplet, the droplet surface therefore needs to withstand the magnetic pressure. The parameter describing the stability of the droplet surface is hereby the surface or interfacial tension σ, which determines how much energy ΔW_{surf} is required to increase the droplet surface by ΔA [122, 177], or if projected onto a plane the force ΔF_{line} needed to elongate the projected circumference of the droplet by Δs.

(2.19)
$$\sigma = \frac{\Delta W_{surf}}{\Delta A} = \frac{\Delta F_{line}}{\Delta s}$$

Interfacial Tension

The energy required for changing the surface area A of a droplet results in a change of the pressure P_1 inside the droplet, while the outside pressure P_2 remains constant. This results in a pressure difference ΔP, termed Laplace pressure, over the droplet membrane, which depends on the radii of curvature of the droplet [3, 53].

(2.20)
$$P_1 - P_2 = \Delta P = \sigma \left(\frac{1}{r_1} + \frac{1}{r_2} \right)$$

Kelvin equation

The radii r_1 and r_2 describe the local radii of curvature at the point of interest as demonstrated in Figure 2.6.

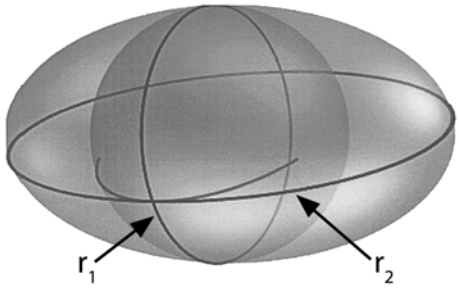

Figure 2.6 Illustration of an oblate droplet's radii of curvature. For a spherical droplet both radii are equal (Schematic after [23]).

In the most general case, the Laplace pressure along a droplet wall can differ depending on the position at the droplet surface. For negative curvatures, resulting from droplet deformations, the pressure can take on negative values, which will lead to droplet fission at that position. This effect is of high interest for a droplet manipulation system, where the splitting of a droplet is the most challenging step.

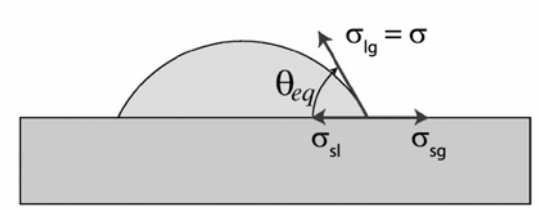

Figure 2.7 Schematics of standard equilibrium wetting, indicating the tensions associated with each interface and the resulting equilibrium contact angle θ_{eq}.

The interfacial tension σ also determines the wetting properties of a droplet when it is in contact with a surface. Since the droplet is also in contact with the surrounding medium and the medium itself with the surface, all three interfacial tensions must balance, which results in the equilibrium contact angle θ_{eq} (Figure 2.7).

The equilibrium situation can generally be described by the Young's equation [122]:

Young's Equation

$$0 = \sigma_{sg} - \sigma_{sl} - \sigma \cos\theta_{eq} \tag{2.21}$$

which translates into the equilibrium contact angle θ_{eq} via:

Equilibrium Contact Angle

$$\theta_{eq} = \arccos\left(\frac{\sigma_{sg} - \sigma_{sl}}{\sigma}\right) \tag{2.22}$$

In the droplet manipulation system, described in this thesis, the droplets are submerged in modified octamethytrisiloxane (OMTS), which therefore replaces the gaseous phase in the above equations. The interfacial tensions between the different media present in the droplet manipulation system are summarized in Table 2.2. The configuration of the droplet manipulation system necessitates that the interfacial tensions in equation (2.22) are replaced by values of the respective interfaces according to Figure 2.7, resulting in the following relation:

$\sigma_{lg} = \sigma$(water/OMTS), $\sigma_{sl} = \sigma$(PTFE/water) and $\sigma_{sg} = \sigma$(PTFE/OMTS).

σ [mN/m]	**water**	**modified OMTS**	**air**
water		1.5	72
modified OMTS	1.5		N.A.
PTFE	36.6 [82]	35.1 (eq. (2.21))	20 [122]

Table 2.2 Interfacial tensions between the different components of the droplet manipulation system.

The equilibrium contact angle of a water droplet suspended in the modified silicone oil will therefore approach 180°, as required for free floating droplets.

2.2.1 Droplet Breakup

Among the different droplet manipulation steps, the extraction of a liquid fraction from a droplet (droplet splitting) is the most challenging. Generally the droplet splitting can be divided into two stages, the droplet deformation and the droplet breakup (Figure 2.8). In the first stage, the droplet is deformed against the interfacial tension until a daughter-droplet is created but stays linked to the initial droplet via a liquid bridge (meniscus). In the second stage, the liquid bridge is broken due to the negative Laplace pressure, while the daughter-droplet is held in place against the capillary force using magnetic force.

Droplet deformation

The force needed for the droplet deformation is determined by the interfacial tension as described in equation (2.19). In Figure 2.8 a) we see that the shape of the object deforming the droplet from the inside influences the change in surface area, since the latter depends on the variation in the shape of the droplet deformation.

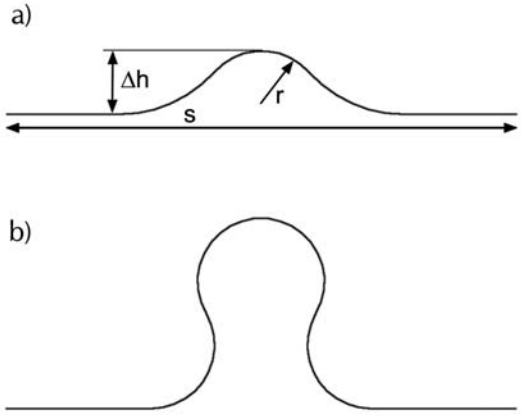

Figure 2.8 Schematics of the droplet splitting stages. The droplet is (a) deformed and subsequently (b) the link between the daughter- and the bulk-droplet (meniscus) is broken.

Table 2.3 summarizes the results of a "Gedanken-experiment" for the droplet deformation using objects of with points of different radii. For simplification, the usually round droplet is hereby represented by a line of s = 1 mm length that is indented by Δh = 0.25 mm, as demonstrated schematically in Figure 2.8 a).

tip radius *r* [mm]	**force due to surface change [nN] (σ = 1.5 mN/m)**
0 ("needle")	177
0.125	184
0.25	192
0.5	215
0.625	240

Table 2.3 Comparison of the forces needed to deform a droplet using points of different radii.

We can clearly see that a sharp tip requires less force than a blunt tip, with an exponential dependence between the tip radius and the force. With respect to the droplet separation we can therefore deduce that the magnetic particles should be concentrated in the smallest possible volume in order to easily deform a droplet towards its breakup point.

Droplet breakup

Another parameter that influences droplet deformation and also the breakup during the second stage is the capillary number Ca [19], which describes the competition between viscous forces and interfacial stress.

The capillary number is a function of the viscosity η of the surrounding liquid, the interfacial tension σ and the velocity v of the shear flow.

Capillary number

(2.23) $$Ca = \frac{\eta\, v}{\sigma}$$

An increasing velocity v leads to a larger shear rate G, which results in a deformation and finally fission of a droplet placed in the flow. In the droplet manipulation system, the shear rate is created via the magnetic particles pressing against the droplet wall. Depending on the undeformed droplet's radius r the capillary number Ca can therefore be expressed as:

(2.24) $$Ca = \frac{\eta\, G\, r}{\sigma}$$

We learn from Figure 2.9 that a increasing capillary number results in unstable elongated droplets and ultimately leads to droplet breakup in the presence of a shear force. The transition from stable to unstable droplet deformation is marked by the critical capillary number, which depends on the ratio of the viscosities of droplet medium and surrounding liquid. For equal viscosities (viscosity ratio = 1), the critical capillary number is lowest. In consequence, we can assume that the droplet splitting will be facilitated by submerging the aqueous droplet in a medium with close-to-equal viscosity.

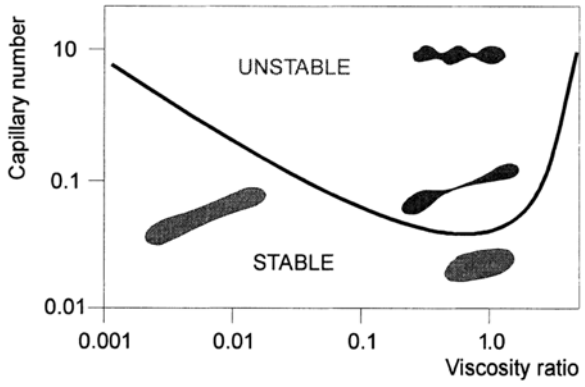

Figure 2.9 Droplet deformation and break-up in simple shear flow, depending on viscosity ratio and capillary number. The line presents the critical capillary number [19].

Further-on, the behavior of the liquid bridge between the droplets during breakup is guided by the interfacial tension and the Laplace pressure,

which combine to the capillary force F_{cap} [28, 50]. The component of the force based on the Laplace pressure can either be positive or negative, while the component based on the interfacial tension is always positive.

Capillary Force

$$F_{cap} = \oint_{Area} \Delta p_{Laplace} \cdot dA + \oint_{Perimeter} \sigma_{lg} \cdot cos(\theta) \cdot ds \tag{2.25}$$

Since the two objects that are connected via the capillary force are of the same medium as the meniscus linking them, they are virtually fully wetted. As a result the equilibrium angle has the value of $\theta = 0°$.

We can see from the above equation that the capillary force is strongly dependent of the shape of the meniscus, since both integrals are related to its dimensions. In consequence, varying the width of the liquid bridge and its radii of curvature by defining the form of the two objects connected by it, will help to influence the characteristics of the droplet breakup [28]. Thus a solution needs to be found for giving an aqueous droplet a defined shape.

2.3 The Magnetic Field of a Multilayer of Square Coils

The magnetic force required for the manipulation of microdroplets can be achieved via a field of magnetic gradients, as indicated in equation (2.16). Since the magnetic field of every permanent magnet and electromagnet varies with the observer's position, a field of magnetic gradients can be obtained by an array of such magnets [46]. The use of permanent magnets has the advantage of large magnetic fields and subsequently of large field gradients, but the permanence of the field does not allow a flexible field topology. In that respect, the use of electromagnets permits a greater control and variability of the field gradient [150]. The flux density $\vec{B}$ and thus the magnetic field $\vec{H} = \vec{B}/\mu_0$ of any electromagnet, composed of windings of wire, can be determined following the law of Biot-Savart:

Biot-Savart's Law

$$\vec{B} = \frac{\mu_0}{4\pi} I \int \frac{\vec{dl}}{\vec{r}^{\,2}} \times \frac{\vec{r}}{|\vec{r}|} \tag{2.26}$$

with the current I, the distance between the wire and the point of interest r and the length of the wire section dl.

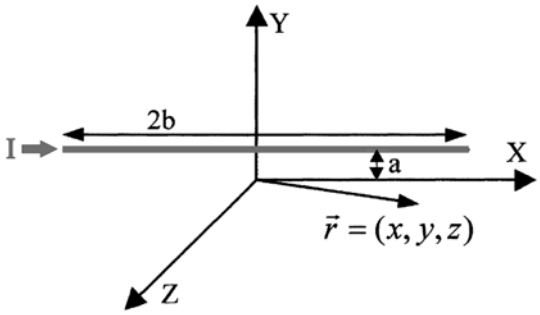

Figure 2.10 Spatial arrangement of the current line of finite length for analytical calculations of a coil's magnetic field [55].

In the case of a square coil, which is a compound of several wires of finite length, the magnetic field can be determined via the superposition of the fields generated by each finite section of wire forming the coil. Based on equation (2.26) and the spatial arrangement of the wire segment as depicted in Figure 2.10, we can determine the expression for a wire of finite length [55]. The components of the magnetic field $\vec{H}$ of the wire segment with the position and dimensions shown in Figure 2.10 can thus be calculated as follows:

$$H_x = 0 \tag{2.27}$$

$$H_y = -\frac{z\,I}{4\pi\left[(a-y)^2+z^2\right]} \cdot \left[\frac{b-x}{\sqrt{(b-x)^2+(a-y)^2+z}} + \frac{b+x}{\sqrt{(b+x)^2+(a-y)^2+z^2}}\right] \tag{2.28}$$

$$H_z = -\frac{(a-y)\,I}{4\pi\left[(a-y)^2+z^2\right]} \cdot \left[\frac{b-x}{\sqrt{(b-x)^2+(a-y)^2+z}} + \frac{b+x}{\sqrt{(b+x)^2+(a-y)^2+z^2}}\right] \tag{2.29}$$

For a square coil, the different spacial positions of the individual wire segments need to be taken into account and, in consequence, the variables of equations (2.27) to (2.29), describing the geometry of the wire, have to be varied according to the coordinate system of reference. Subsequently,

the magnetic fields generated by the segments of a coil of multiple windings can be superimposed as well as the fields of the individual coils of an array.

Super-position of the fields

$$H_{PCB} = \sum_{coils}^{i} \sum_{wires}^{j} H_{i,j} \tag{2.30}$$

In the droplet manipulation system, a multilayer of square coils is used to generate a flexible field topology over a two dimensional surface. The design of the coil multilayer, as presented in Figure 2.11, is based on the thesis work of A. Rida [150], and contains four partially overlapping layers of square coils. The stack of coils is fabricated in a standard Printed Circuit Board technology with coil windings of 125 µm width and a wire spacing of equally 125 µm.

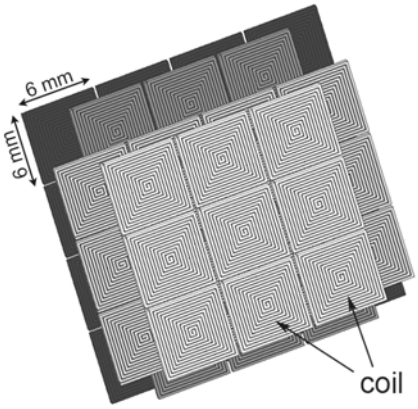

Figure 2.11 Schematic explosion view of the multilayer of square coils. The PCB is fabricated in standard technology resulting in a layer thickness of 150 µm.

The magnetic field of such a multilayer of square coils can be determined by superposing the fields of each wire-section of each coil of the chip according to equation (2.30). Figure 2.12 presents the results of the analytical simulation of the field component H_z for the whole coil multilayer, as calculated using the algorithm discussed above in the mathematical software Mathematica, in comparison with a measurement done with a flat Hall probe oriented in the z-direction. We can see that the model is in a very good agreement with the results of the measurement. We obtain a maximum flux density in the z-direction of B_z = 2 mT for a DC-current of I = 1 A in each layer, which results in a field gradients of the order of 1 T/m.

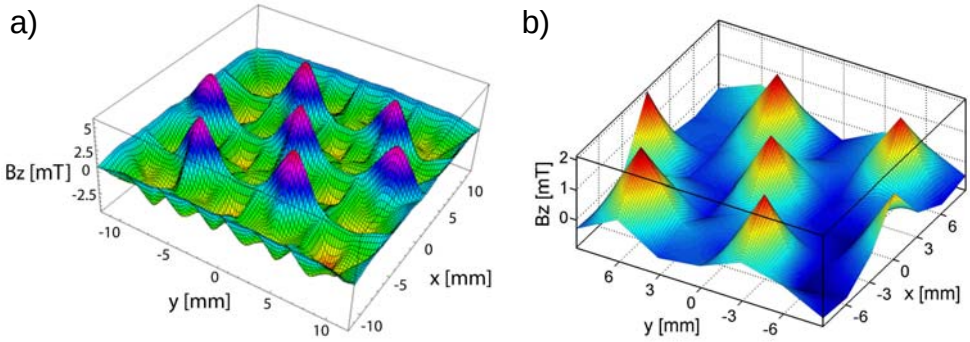

Figure 2.12 Topography of the magnetic field of the PCB with one positive phase and two negative phases. a) analytical simulation of the magnetic field b) graphic representation of a 7 x 7 points measurement.

The field gradients generated via such a coil multilayer exert a force on magnetic microparticles floating inside a droplet, while the latter resides close to the chip surface. The particles move into the direction of the gradient and transfer their energy, and thus the force, onto the droplet wall they encounter in their path. The interaction of the droplet with the enclosed magnetic particles is hereby guided by properties of the droplet and the surrounding medium, as discussed previously.

2.4 Conclusion

In this chapter the theoretical framework behind the manipulation of magnetic microparticles was discussed. I looked into the physical properties of the magnetic particles that will be used in this thesis work and into their interaction with a surrounding liquid medium and the physical principles guiding their impact on a liquid-liquid interface. We see that, when enclosed in a small liquid volume (microdroplet), the magnetic microparticles can serve as handles, on which the magnetic field engages a force in order to actuate a generally non-magnetic aqueous medium. The interaction between the droplet and the magnetic particles is hereby guided by the droplet parameters such as its dimensions, its shape and its interfacial tension towards the surrounding liquid. A Gedanken-experiment, based on the interfacial and capillary forces acting on a small droplet, provides a first estimation of the forces required for the functioning of a magnetic droplet manipulation system.

Further-on, I presented a model for the analytical evaluation of the magnetic field generated by a multi-layered Printed Circuit Board. The

algorithm can be easily implemented in any mathematical program and allows a precise prediction of the field strength and, in consequence, the magnetophoretic driving force as shown via a comparison with the measured magnetic flux density.

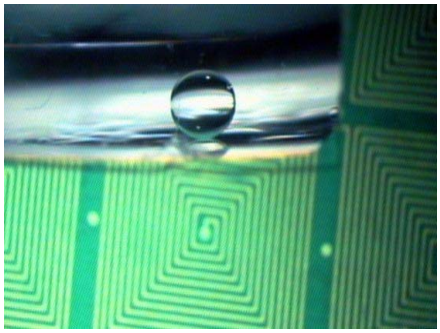

CHAPTER 3

STATE OF THE ART

This chapter gives an overview over the different concepts that come together in the magnetic droplet manipulation system as well as the CMOS chip for single particle manipulation and detection. I will look into microfluidic systems, with an emphasis on droplet manipulation as well as into current systems dealing with the manipulation of magnetic particles. Furthermore, I will introduce the use of magnetic particles for bioanalytical applications and the methods currently used for detecting them.

3.1 Microfluidics

Microfluidics are an important component of most bioanalytical microsystems [11, 63, 190]. Within the last decade a wide range of possible systems have been presented together with different means for driving the liquids in such systems [168, 170, 171]. The majority of microfluidic applications relies hereby on continuous flows driven through channels via valves and pumps that guide and regulate the flow [130]. Another concept is the multiphase flow, where immiscible liquids or phases are present in the same system or channel. The main representatives of this fluidic approach are the droplet-based systems, which are often summarized as digital microfluidics, since the droplets form small self-contained sample containers [80, 128].

3.1.1 Continuous Flow Microfluidics

Pressure Driven Flow

The major part of microfluidic applications still rely on continuous flow, where the liquids are pumped through the system [10, 187]. The most common mechanism for pumping the fluid is the use of pressure, either

applied at the entrance or at the exit of the system. Following one of the basic laws of fluid mechanics for pressure-driven laminar flow, the so-called no-slip boundary condition, the fluid velocity at the walls must be zero [69, 189]. This produces a parabolic velocity profile within the channel, and has significant implications for the distribution of the transported molecules. The main advantage of pressure-driven flow is, that it is an inexpensive and reliable approach to pumping fluids through microdevices and that it can be applied with any type of system geometry, material and liquid. The main challenge for the pressure driven flow is, in contrast, the integration and connection of the pumping system [1, 132], especially when low flow rates and small dead volumes are required.

Electrokinetic Flow

Another common technique for driving fluids in a microchannel is electroosmotic pumping [117]. If the walls of the microchannel have an electric charge, as most surfaces do, an electric double layer of counter-ions will form a liquid/solid interface [69]. When an electric field is applied between in- and outlet of the channel, the ions in the double layer move towards the electrode of opposite polarity. This creates a motion of the fluid near the walls that is transferred via viscous forces into convective motion of the bulk fluid [8]. One of the advantages of electrokinetic flow is that its blunt velocity profile avoids many of the diffusion and transport related non-uniformities that occur with pressure driven flow [171]. Another advantage is the possibility to easily couple the pumping mechanism to other electronic applications on-chip. However, electrokinetic flow often requires very high voltages, making it difficult to miniaturize without off-chip power supplies. Another significant disadvantage is its dependence on surface properties. Proteins, for example, when adsorbed to the channel-walls [106, 116], substantially change the surface charge characteristics and, thereby, the fluid velocity [108]. This can result in an unpredictable long-term time dependence in the fluid flow.

Capillary Flow

A third method, which arises from the small dimensions of the microchannels, is capillary flow. In contrast to pressure-driven flow, capillary flow is highly dependent on the geometry of the channel and its surface properties. Since it requires small channel dimensions it is a very convenient means of driving miniature liquid volumes in microchannels [63]. However, once the channel surface is fully wetted the fluid flow stops. Thus, the duration of the flow depends on the length of the capillary and the properties of the transported liquid.

3.1.2 Digital Microfluidics

In contrast to continuous flow microfluidics, where comparatively large liquid volumes are pumped through the microsystem, droplet microfluidics, also called "digital microfluidics", handles only small self-enclosed liquid entities [83]. The advantage of droplet handling is the strong reduction of the transported volumes and the possibility of working with a plethora of different samples at the same time [80]. In order to perform reactions between the different droplets, the system needs to be able to execute various droplet manipulation steps. The transport of droplets serves for displacing a droplet within the system, the merging and mixing of droplets allows the reaction of samples contained in two droplets and the droplets splitting extracts a liquid fraction from a droplet or a microreservoir. Among these steps, the droplet splitting is the most challenging, since it requires the addition of energy due to the surface tension of the droplet (equation (2.19)).

3.1.3 Literature Review of Droplet Manipulation Systems

The most commonly used approach for the manipulation of small droplets is based on microfluidic networks, where droplets are generated, merged, mixed and split at joining or bifurcating channels [75, 84, 172, 176]. Figure 3.1 shows an example of channel-based droplet manipulation, which permits the creation of droplets containing two reagents and their subsequent mixing. The figure already demonstrates one drawback of these systems, where the forced contact between the droplet medium and the channel walls during the droplet creation stage can lead to uncontrolled reagent absorption and a subsequent cross-contamination between droplets. The well controlled droplet generation mechanism makes them, however, ideal for the creation of emulsions and for single-stage chemical reactions involving minute amounts of reagents.

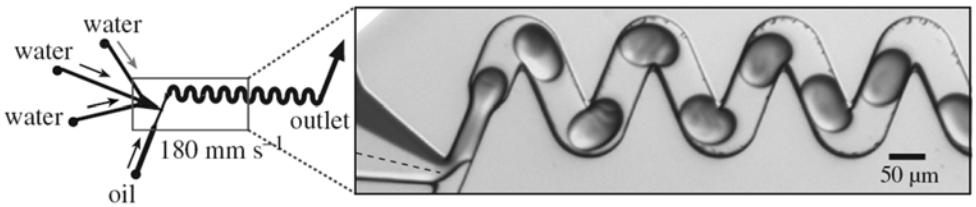

Figure 3.1 Channel-based droplet manipulation system [18] - Reprinted with permission of the Royal Society. Droplet splitting and mixing are controlled by the channel geometry.

The manipulation of aqueous droplets without microfluidics networks has been tackled within recent years based on a multitude of principles, whereby most of them use the properties of the manipulated liquid to generate the actuating forces [41, 128]. Since water-based solutions are usually the droplet medium of choice, its dielectric properties, its asymmetrical wetting angles [69] and the variability of its surface tension are frequently exploited [20, 168].

Chemical Modifications

One of the first examples of droplet transport is based of the **chemical modification** of a surface's wetting properties [29]. In order to obtain a droplet movement, an asymmetry of the wetting angle is required, which can be achieved by creating a hydrophobicity gradient on a surface. The subsequently induced asymmetry of the wetting angle allows a droplet to even move upwards on an inclined slope, as Figure 3.2 shows. The first examples using the approach of wetting angle variation did not have a wide range, since the wetting gradient could not be stretched infinitely. Therefore new solutions for an improved and more flexible control of the wetting angles had to be found.

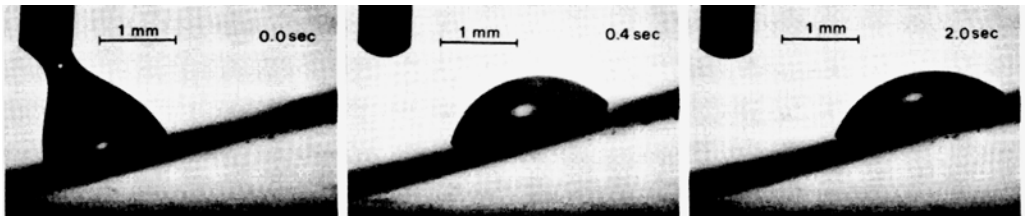

Figure 3.2 Uphill motion of a drop of water (1 µl) on a gradient surface. The surface was inclined by 15° from the horizontal plane. From Chaudhury & Whitesides, Science 256: 1539-1541 (1992) [29]. Reprinted with permission from AAAS.

Electrowetting

One such solution of flexible wetting angle variation is **electrowetting**, where the dependency between the wetting angle and a voltage applied to the droplet is exploited [32, 126]. Figure 3.3 a) demonstrates the effect that a droplet spreads over a surface upon the application of a voltage. For manipulation, the droplets are usually squeezed between the controlling electrodes and a covering slide of conductive glass (ITO), representing the counter electrode (Figure 3.3 b)). Additionally, the bottom electrodes are covered with a dielectric layer in order to prevent electrolysis at the electrodes. Electrowetting based systems are able to perform all droplet manipulation steps required for a Lab-on-a-Chip system, as presented in Figure 3.3 c). Recent publications also demonstrate EWOD (electrowetting on dielectric) without the counter electrode in the cover slide, which increases the number of possible applications [125].

The advantage of droplet manipulation based on EWOD is the high switching speed of the electrodes resulting in high droplet speeds of up to 10 cm/s. Additionally, EWOD can be easily combined with integrated circuitry, which allows a full automation of the droplet treatment [48]. In contrast, the necessary application of an electric field presents at the same time the main challenge for the application of EWOD systems for bioanalytical procedures, due to the field's interaction with charged molecules, such as DNA, as well as ionic solutions [27]. Furthermore, the close contact between the droplet and the dielectric layer can lead to a fouling of the dielectric due to the absorption of biomolecules [206].

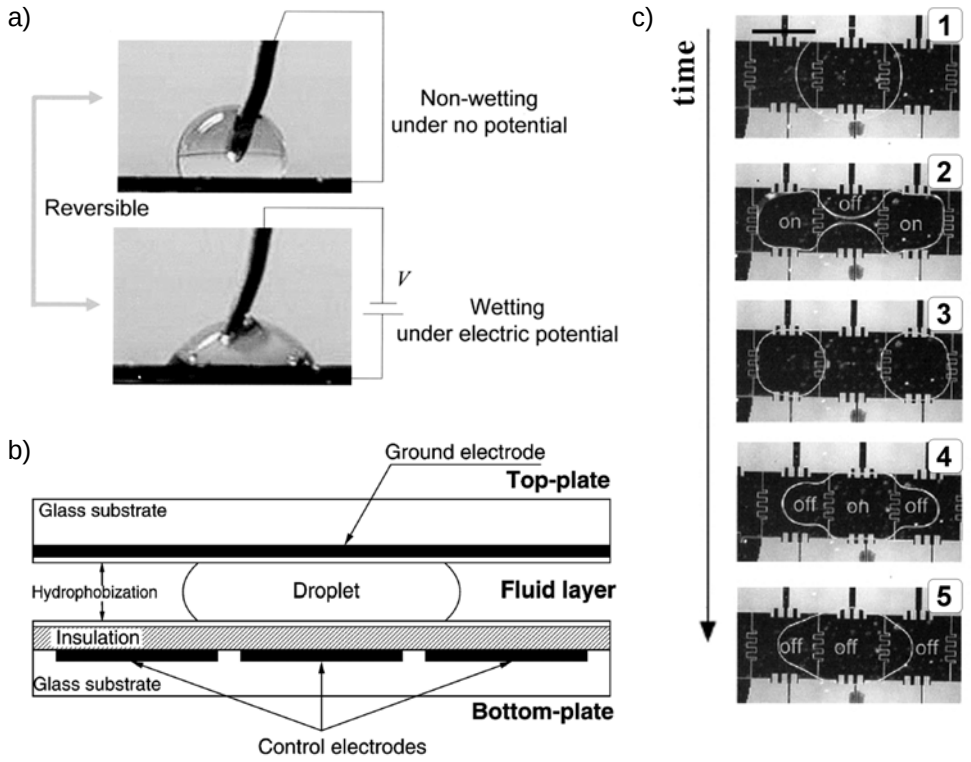

Figure 3.3 Droplet manipulation via electrowetting: a) Electrowetting effect: A droplet of conducting liquid initially forms a contact angle θ with a solid hydrophobic insulator. Application of a voltage V between the droplet and a counter-electrode reduces the solid–liquid interfacial energy, leading to a reduction in θ and improved wetting of the solid by the droplet [32] - Reproduced from Cho, Moon & Kim, Journal of Microelectromechanical Systems, vol. 12, pp. 70-80, 2003, © 2003 IEEE. b) Schematic cross-section of the electrowetting chip [143] - Reproduced by permission of The Royal Society of Chemistry. c) Sequential images of successful cutting and merging of droplets at 25 V (gap size d = 70 µm, electrode: 1.4 mm x 1.4 mm, volume: 0.2 µl) [32] - Reproduced from Cho, Moon & Kim, Journal of Microelectromechanical Systems, vol. 12, pp. 70-80, 2003, © 2003 IEEE.

Dielectro-phoresis

A different approach presents the **dielectrophoretic manipulation**, presented in Figure 3.4, of water droplets floating in silicone oil, which

uses the polarity of the water molecules and allows the transport of droplets via an electric field gradient [185]. The droplets are suspended in a silicone oil higher density and hoover over the electrodes at a certain distance [173, 180]. The strength of this principle is the use of the manipulated medium's intrinsic properties and the contactless manipulation of the droplets. Recent publications demonstrate the dielectrophoretic manipulation of droplets, including droplet splitting, using a matrix of pixels [76]. The careful composition of the surrounding oil medium permits in that case droplet manipulation using voltages as low as 5V.

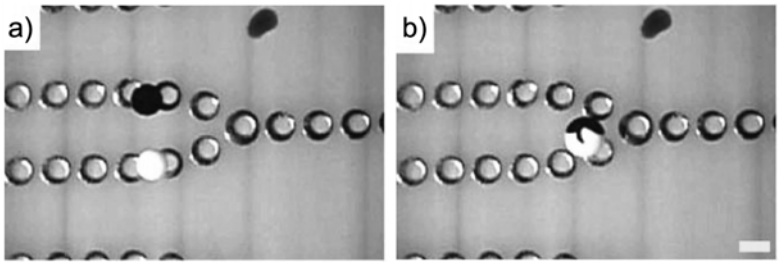

Figure 3.4 Droplet manipulation via dielectrophoresis: a) Droplets (750 nl) containing latex microspheres (white) and gold nanoparticles (black) are transported; b) the droplets mix upon close contact near the track junction. (Scale bar: 1mm) [180] - Reprinted by permission from Macmillan Publishers Ltd: Nature, Velev, Prevo & Bhatt, vol. 426, pp. 515-516, 2003, copyright (2003).

Mechanical Actuation

Another droplet driving mechanism exploits the difference between the advancing and receding wetting angles of an aqueous droplet. In the presence of **vibrations** or **surface acoustic waves** (SAW) [13, 62, 196, 199], a droplet will advance towards the smaller of these angles, as Figure 3.5 demonstrates. In addition, the surface can be structured to prepare superhydrophobic pathways or to modulate the droplet direction and its speed using ratchet-like structures [22]. The advantage of mechanical droplet manipulation is the absence of a direct electrical or chemical interaction with the droplet medium, which permits the manipulation of a wide range of liquids and enclosed biomolecules.

All methods for driving a droplet on a flat surface presented above rely on the properties of the liquid contained inside the droplet. In consequence, these principles are highly sensitive to changes of the droplet medium, for example via contamination through surface contact. In addition, systems exploiting the wetting angle variabilities are easily influenced by variations in the medium surrounding the droplet (see equation (2.21)),

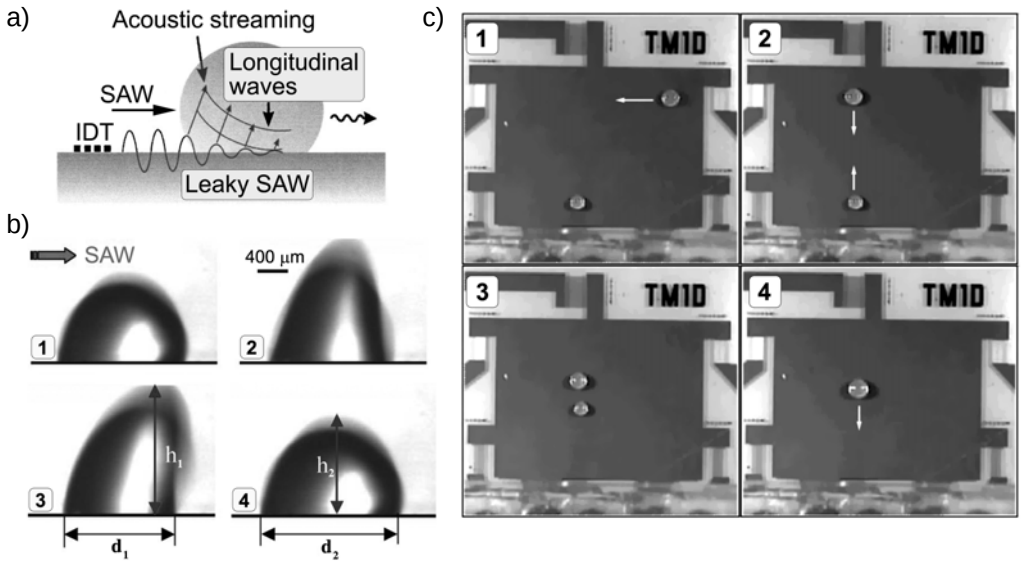

Figure 3.5 Droplet actuation via SAW: **a)** Schematics of the driving mechanism [199]. Reprinted from Wu & Chang, Journal of Applied Physics, vol. 98, 024903, 2005. Copyright 2005 American Institute of Physics. **b)** Periodical distortion of a droplet due to SAW [13]. (1) the droplet adopts a spherical shape on hydrophobic coating, (2) the droplet stands up and the solid/liquid interface decreases, (3) the droplet top bends to the side, in the direction of SAW propagation, (4) the three-phase contact line advances and the droplet adopts a spherical shape again. Reprinted from Beyssen, Le Brizoual, Elmazria & Alnot, Sensors and Actuators B-Chemical, vol. 118, pp. 380-385, 2006 with permission from Elsevier. **c)** 2D droplet movement with SAW on a microfluidic processor chip. The droplets are brought together and merge (droplet volume: V = 200–300 nl) [62] - Reproduced by permission of The Royal Society of Chemistry.

and therefore require a controlled atmosphere, which reduces the systems flexibility and ease of use.

3.1.4 Magnetic Droplet Manipulation

A further principle for the manipulation of droplets introduced recently does not rely on the intrinsic properties of the manipulated medium, but is based on magnetic force mediators contained inside the droplet.

When magnetic microparticles are added either to the droplet volume or the droplet boundary, they translate an applied magnetic field gradient into a force pulling the droplet into the direction of the gradient [127]. In addition, the magnetic microparticles can serve as functionalized components of the system, such as optical indicators [24, 44] or mobile substrates [142]. The challenge in magnetic droplet manipulation is the application of the magnetic field gradient. In most cases, an external magnet is used, which can be moved according to the requirements of the

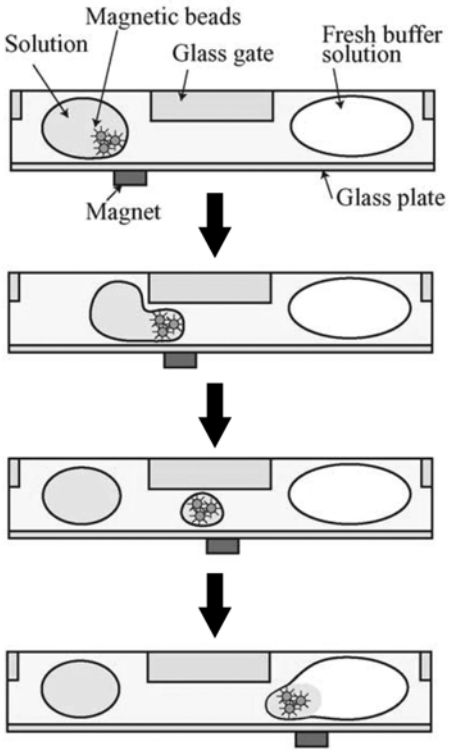

Figure 3.6 Magnetic droplet manipulation using an external moving permanent magnet. The droplet splitting requires a 3D structuring of the chip. [160]

droplet manipulation [162]. In combination with a suitable 3D structuring of the surface, all droplet manipulation steps can be implemented, but at the cost of increasing system complexity and decreasing flexibility [160]. The magnetic manipulation of droplets, which does not require external moving permanent magnets or 3D structured substrates still remains a challenge and is a major subject of this thesis work. The approach presented in the following chapters is based on stacked square coils, which permit a control of the magnetic field applied over a comparatively large surface. In combination with a static magnetic field it allows the manipulation of magnetic particles without moving parts [151] and in consequence the magnetic manipulation of droplets.

The following table summarizes the most commonly used methods for droplet manipulation. The majority of these principles have already been demonstrated as being applicable to Lab-on-a-Chip systems [25, 136, 142, 153, 169, 183, 207]. Shikida et al. [162] demonstrated the potential of the magnetic droplet manipulation for the on-chip bioanalysis by using magnetic particles as mobile substrate for the capture and detection of bio-active molecules (alkaline phosphatase), as presented in Figure 3.7.

	handled volumes	advantages	disadvantages	references
Microfluidic Channel	fl - nl range	- highly parallel - high throughput	- low flexibility - microstructuring of channel network - surface contact	[80, 84]
Electrowetting	pl - nl range	- electronic control - CMOS compatible - fast droplet transport	- surface contact - surface fouling due to biomolecule adsorption - limited number of liquids (DI water)	[32, 143, 158]
Dielectrophoresis	nl - µl range	- electronic control - no surface contact	- small forces - dependent on liquid properties - interaction with polar molecules inside the droplets	[76, 180, 185]
Acoustics/Mechanics	µl range	- fast droplet transport - high flexibility - electronic control	- wetting angle hysteresis required - surface contact - air environment required	[13, 196]
Magnetic Actuation	µl range	- long range - large forces - electronic control - independent of liquid's properties - no interaction with organic material	- force mediators required - small distance between field source and particles necessary	[24, 127, 160]

Table 3.1 Comparison of the most widely used droplet manipulation mechanisms.

Recently, droplet manipulation systems have been presented that combine several actuation methods, such as the magnetic separation and mixing of particles inside an EWOD system [48,184].

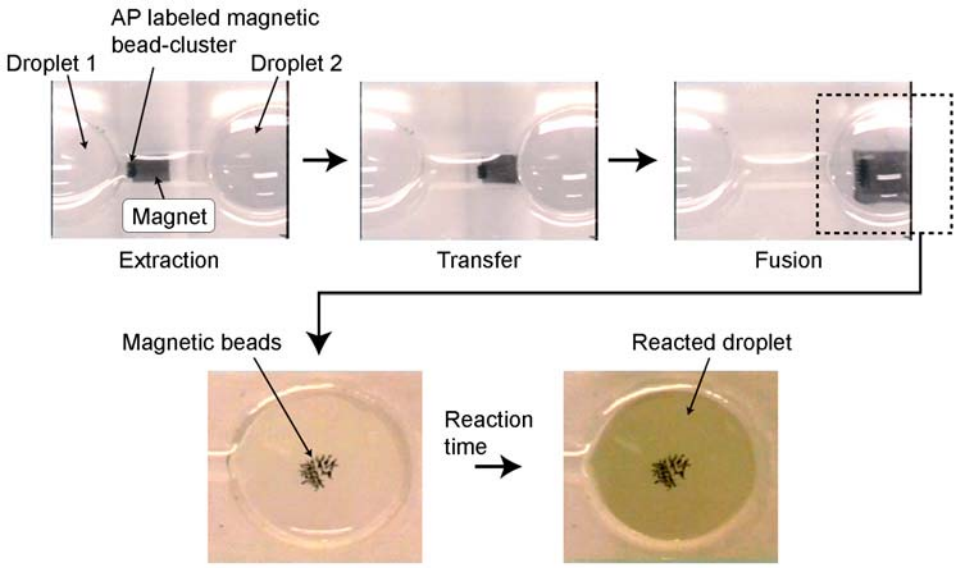

Figure 3.7 Enzymatic reaction performed in a magnetic droplet manipulation system [162]. The magnetic particles carry bioactive molecules, which react with the chromogen in the second droplet. The magnetic actuation is achieved via the displacement of a small permanent magnet. Reprinted from Shikida, Takayanagi, Honda, Ito & Sato, Journal of Micromechanics and Microengineering, vol. 16, pp. 1875-1883, 2006 with permission from IOP Publishing Ltd.

3.2 Magnetic Particle Manipulation

Since the magnetic manipulation of droplets is driven by the actuation of the enclosed magnetic microparticles, the principles used for the manipulation of the latter can be equally applied to magnetic droplet manipulation systems. The following section will present examples taken from recent literature on how to actuate magnetic particles and in consequence droplets via magnetic fields in microfluidic systems.

3.2.1 Magnetic Manipulation via Permanent Magnets

Permanent magnets can generate high magnetic fields and are available in a wide range of shapes and sizes. Thus their application in the microfluidic manipulation of magnetic microparticles is of increasing popularity [92, 139]. Permanent magnets are hereby mainly used for the separation or sorting of magnetic microparticles, either by their size or by

their magnetic properties [86]. In such systems, the permanent magnets are generally placed alongside a microfluidic channel and the magnetic field gradient is adjusted by controlling the distance between the magnet and the channel, as well as the shape of the magnetic poles. The main advantage of using permanent magnets in such systems is the stability of the magnetic field, which at the same time is also its main disadvantage, since the generated field cannot be easily modulated.

3.2.2 Magnetic Manipulation via Electromagnetic Fields

Compared to permanent magnets, electromagnets offer a higher flexibility but generate lower magnetic fields. In order to maximally profit from the generated forces, the distance between the magnetic elements and the magnetic particles needs to be very small. Since small dimensions are a main feature of microfluidic systems, their combination with microelectromagnets offers a promising approach towards electronically controlled magnetic particle manipulation systems, as is shown by a wide range of microfluidic systems with integrated magnetic elements that have been presented recently. In these systems the magnetic field is generated in a multitude of ways, either using wires [4, 43, 97], coils [145, 151], tapered electrodes [195] or soft-magnetic elements that concentrate the magnetic field generated outside the chip [166, 204].

The advantage of systems using electromagnets as compared to permanent magnets is the possibility of improved field control as well as the possibility of system automation. Further-on, electromagnets can be fabricated in smaller dimensions thus allowing to not only move clusters of magnetic beads, but also single magnetic particles or single cells labeled with magnetic particles.

The systems for the manipulation of magnetic microparticles can be divided into two groups: separation and trapping of the particles from a sample flow on the one hand [155, 166, 204] and the guided transport of magnetic particles inside a reservoir or channel on the other hand [4, 43, 97, 145, 151]. Since the magnetic droplet manipulation is based on the transport of magnetic particles, I will concentrate in the following literature review on electromagnetic systems for the magnetic displacement of particles.

3.2.3 Literature Review of Magnetic Microparticle Manipulation Systems

Wire-based Systems

The first examples for microfluidic systems with electronic control of the movement of magnetic microparticles were presented in 2001 [43, 97]. Both systems use multiple wires in order to generate consecutive gradients of the magnetic field, as shown in Figure 3.8 and rely on the attraction of the magnetic particles towards the controlled shifting of the field maximum.

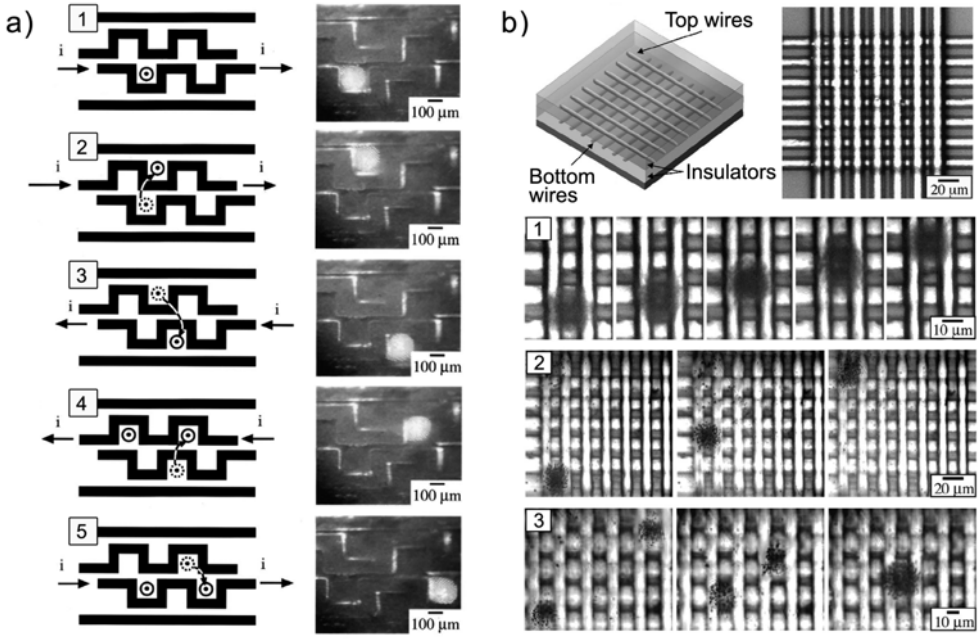

Figure 3.8 Wire based systems for the manipulation of a cloud of magnetic microparticles. a) Meandering wires [43] - Reprinted from Deng, Whitesides & Radhakrishnan, Applied Physics Letters, vol. 78, pp. 1775-1777, 2001. Copyright 2001, Americal Institute of Physics, b) Crossing wires [97] - Reprinted from Lee, Lee & Westervelt, Applied Physics Letters, vol. 79, pp. 3308-3310, 2001. Copyright 2001, American Institute of Physics.

While the system of Deng et al. (see Figure 3.8 a)) is based on meandering wires, whose currents are modulated depending on the particles' position, the system presented by Lee et al. (see Figure 3.8 b)) employs a matrix of wires, which are activated with respect to the particle's position. We see that the two wire system does not require a large number of current sources, but allows a manipulation along only one dimension (Figure 3.8 a)). In contrast, the matrix system permits a two-dimensional manipulation of the particles, but requires a current source for every wire on the chip (Figure 3.8 b)).

Improved Electrode shapes

Based on the two-wire solution, new designs of the electromagnets were examined, which led to systems based on tapered electrodes [194] as well as coil-based magnetic manipulation systems [146, 151]. We see from Figure 3.9 that both systems move the magnetic particles in a sequential pattern, as used for the two meandering wires presented earlier. The current switching between the tapered electrodes results in a zig-zag movement of the magnetic particles, which can be handled one at a time due to the small size of the system. Coil based systems generally have larger dimensions, which therefore results in the transport of clouds of particles. Additionally, Rida et al. [151] introduced the idea of applying a static magnetic field for a fixed magnetization of the magnetic microparticles. In consequence, larger forces could be obtained due to the increased magnetic moment as well as a larger magnetic field gradient.

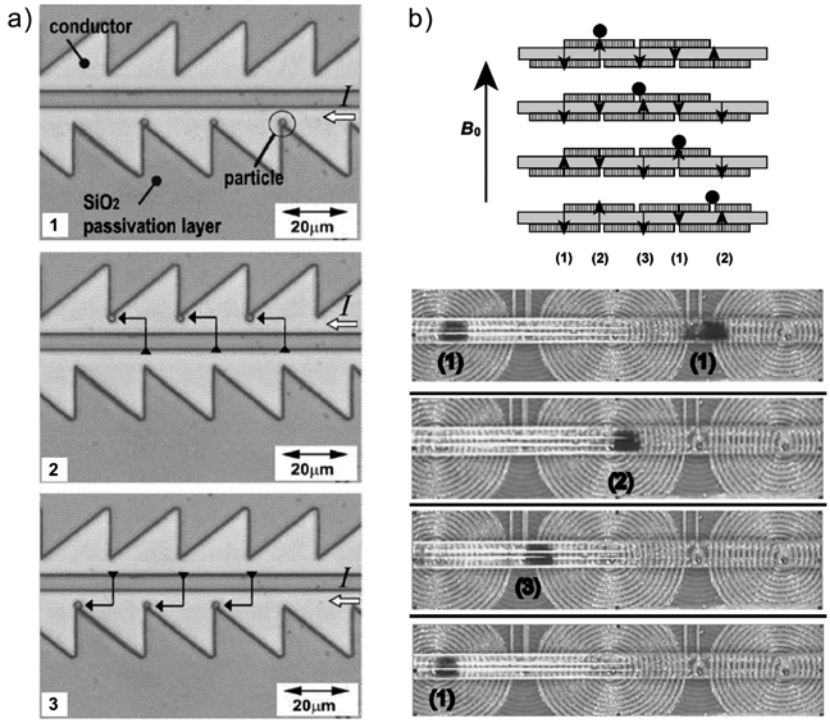

Figure 3.9 **a)** Tapered electrodes [194]: Sequence of microscopic images showing the step-wise movement of a single magnetic particle on a transporting device based on tapered conductors. »I« indicates through which conductor the current is flowing. Reprinted from Wirix-Speetjens & de Boeck, IEEE Transactions on Magnetics, vol. 40, pp. 1944-1946, 2004, © 2004 IEEE. **b)** Coil-based magnetic particle manipulation system [151]: Top) Time-dependent actuation scheme of the planar coils, arranged in a three-phase (1, 2, 3) geometry. The arrows represent the sense of the coil-generated magnetic field; magnetic microbead clusters (represented by the black circle) will always be attracted to a position, where B_0 is in the same sense as the coil field. Bottom) Transport of magnetic beads (1 μm diameter, Promega) by sequential actuation of the coils in a three-phase scheme (1, 2, 3) - Reprinted from Rida, Fernandez & Gijs, Applied Physics Letters, vol. 83, p. 2396, 2003. Copyright 2003, American Institute of Physics.

Recent publications demonstrate the potential of a matrix configuration of the magnetic elements, which allows the handling of single magnetic particles or magnetically labeled cells [99, 204], as Figure 3.10 shows. At a larger scale, a matrix of square coils enables the two dimensional transport of a cluster of magnetic particles [146, 150]. The magnetic droplet manipulation system, presented in this work, is based on the previous work of A. Rida [150] on two dimensional particle manipulation, where the system's large dimensions allow the generation of the forces needed for the different droplet manipulation steps.

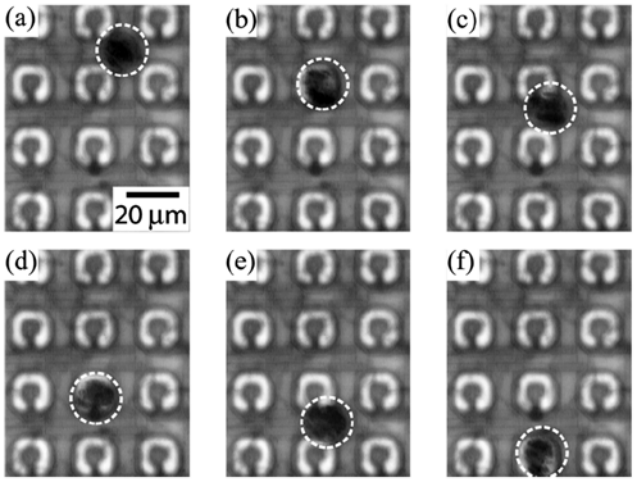

Figure 3.10 Manipulation of a single BCE cell loaded with magnetic nanoparticles via a matrix of coils [99] - Lee, Liu, Westervelt & Ham, IEEE Journal of Solid-State Circuits, vol. 41, pp. 1471-1480, 2006, © 2006 IEEE.

3.3 Magnetic Microparticles in Lab-on-a-Chip Systems

Using magnetic particles in non-magnetic liquids offers the advantage of having a mobile substrate at hand, that can be positioned in a controlled manner. The magnetic particles can be used to capture, transport or label biomolecules or cells, based on applications known from lab-bench macroscopic procedures [36, 121, 124, 182]. Recently, various microfluidic systems have been presented, which profit from the duality (active element and mobile substrate) of the magnetic particles for performing bioanalytical procedures on a chip. The systems differ in their use of the magnetic particles, which either serve as vehicles for the transport of molecules or cells to points of interest [93, 99, 113, 148], as magnetic labels for the detection [103, 152, 193] or as traps for capturing the molecules before and during reaction [35, 52, 73, 92, 156]. Most Lab-on-a-Chip

systems employing magnetic microparticles follow hereby the procedure of macroscopic lab-bench protocols [61], which include incubation, washing and detection steps, as Figure 3.11 demonstrates.

We can see that the immobilization of the magnetic particles in the presence of a sample flow is an important feature of most channel based Lab-on-a-Chip solutions. Such a trapping of the magnetic particles is most commonly done using planar electromagnets, which hold the particles in place during the reaction (Figure 3.12) [34, 166].

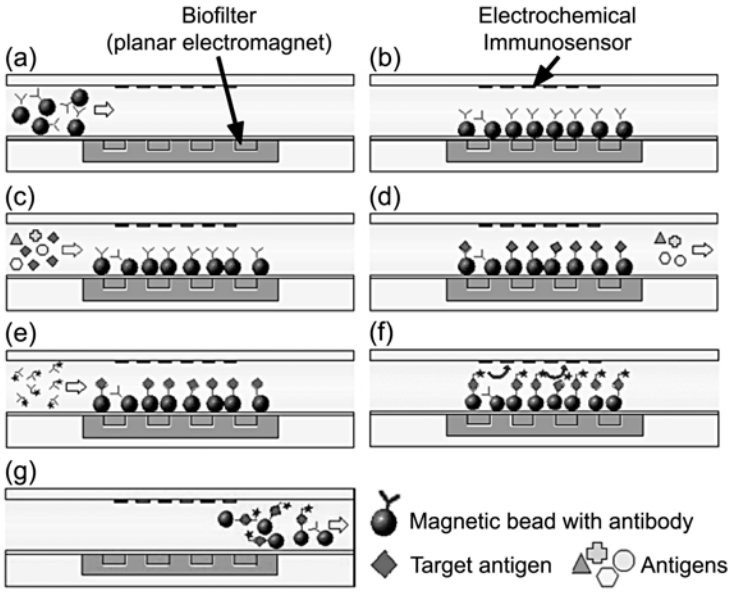

Figure 3.11 Conceptual illustration of bio-sampling and immunoassay procedure using the magnetic bead approach [35] - Reproduced by permission of The Royal Society of Chemistry: (a) injection of magnetic beads; (b) separation and holding of beads; (c) flowing sample; (d) immobilization of target antigen; (e) flowing labeled antibody; (f) electrochemical detection after adding enzyme substrate; and (g) flushing of the magnetic beads.

After the procedure, the magnetic field is switched off and the particles can be flushed out of the system or can be transported to another reaction or detection site. The particles are hereby either transported via the fluid flow or via mechanisms presented in the previous section. When removed from the system, the magnetic character of the particles can be employed to extract the particles, and with them the captured biomolecules from the solution, and to transfer them or the supernatant to an off-chip detection setup [73].

Since magnetic microparticles can be easily trapped inside a microchannel and held against a fluid flow, they offer a tunable increase in active surface for bio-assays performed inside a microfluidic channel. In

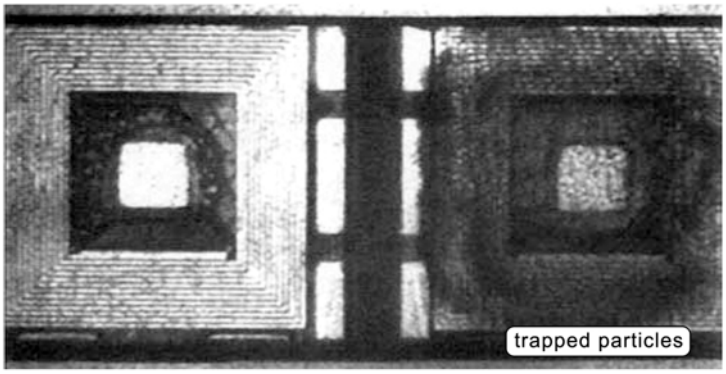

Figure 3.12 Separation of magnetic beads with ∅ = 1 μm from a fluid flow. (Coil width: 50 μm) [34] - Reprinted from Choi, Liakopoulos & Ahn, Biosensors & Bioelectronics, vol. 16, pp. 409-416, 2001 with permission from Elsevier.

consequence, most chip-based bio-assays are performed on clusters of magnetic particles held by an externally applied magnetic field [9, 92], magnetically active elements such as soft magnetic elements [165] or electromagnets [34]. Such systems allow the capture of already labeled or processed magnetic microparticles as well as the immobilization of the particles during the reaction process. The use of electromagnets permits hereby the tuning of the magnetic force and thus the release of the particles after the procedure is finished [35].

Generally, Lab-on-a-Chip systems follow macroscopic bioanalytical procedures and therefore employ the same reagents and reaction steps as in the laboratory. This has the advantage that the reaction steps are already well known and also that the results can be easily compared with a macroscopic benchmark. In consequence, the majority of the magnetic Lab-on-a-Chip systems are applied to DNA extraction and detection [5, 45, 94, 123], cell capture [51, 105, 156, 204] and antigen detection [33, 54, 68, 141].

Even though most of these systems are designed to work with a continuous sample flow, new concepts are being developed based on various principles including the use of magnetic microparticles as mobile substrates. Figure 3.13 presents a Lab-on-a-Chip system, where an ELISA protocol is performed with the help of actively displaced magnetic beads. The particles serve as mobile substrates and are used to magnetically transfer the captured molecules from the complexion site to the reaction site. The spatial separation of the different reaction stages and also of the detection improves the system's sensitivity significantly as Herrmann et al. [68] show. The use of a permanent magnet for the manipulation of the magnetic particles reminds of the magnetic droplet manipulation system

presented earlier in this chapter, and indicates the potential of a microsystem combining separated microreservoirs of reagents, e.g. in the form of droplets, with the manipulation of magnetic microparticles via electromagnets.

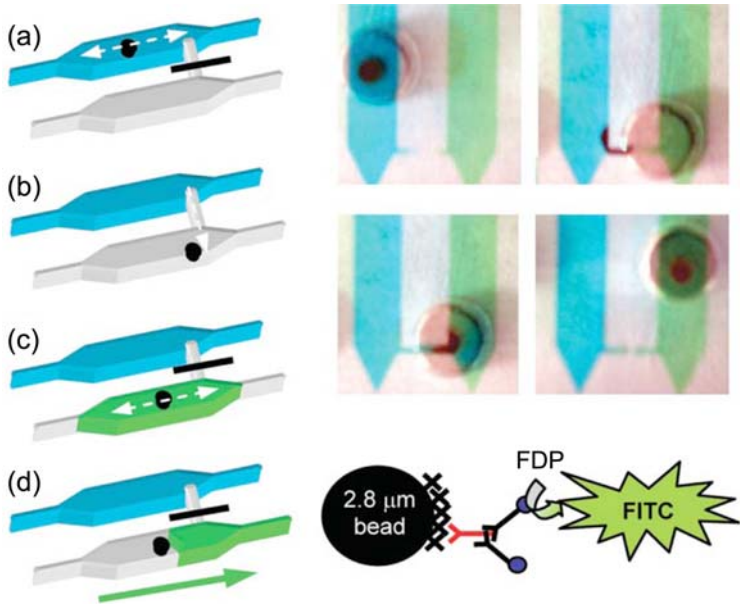

Figure 3.13 Schematic of the on-chip ELISA [68] - Reproduced by permission of The Royal Society of Chemistry: (a) streptavidin-coated magnetic beads are trapped inside the complexion chamber. The trapped beads are mixed and incubated with a series of biomelecules and washing solutions to form the reactive immune complex. (b) After thorough washing, the valve is transiently opened and the beads are magnetically transferred into the reaction chamber. (c) The enzyme labeled beads lead to a fluorescent reaction. (d) The reacted solution is pushed into the detection area. The images on the right side present snapshots taken during the process and a schematic of the assay on the bead surface.

Detection

For the detection of the captured biomolecules (on- but also off-chip) a multitude of principles can be employed, ranging from magnetoresistive [103] sensing to optical [165] and electrochemical [35] methods. During magnetoresistive detection, the magnetic particles serve as labels for the biomolecules, which specifically attach to receptors at the surface of the sensor. A suitable dimensioning of the sensor allows hereby the detection of single magnetic particles, as demonstrated in Figure 3.14.

Fluorescent, colorimetric and electrochemical methods generally allow the quantification of the captured biomolecules, but require additional labels [81, 181]. These methods have the advantage of being independent from the magnetic properties of the system and are therefore not influenced by the magnetic actuation, as is the case for spin-valve sensors [104]. In consequence, optical detection is often the method of choice or

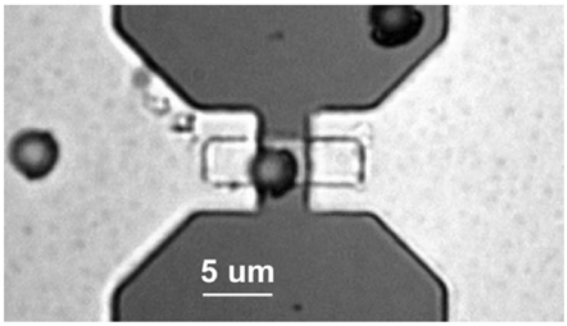

Figure 3.14 Optical image of a 3x12 μm^2 spin valve sensor strip (center) with a single magnetic bead of 2.8 µm diameter (Dynabeads M-280) [103] - Reprinted from Li, Joshi, White, Wang, Kemp, Webb, Davis & Sun, Journal of Applied Physics, vol. 93, pp. 7557-7559, 2003. Copyright 2003, American Institute of Physics.

supplements other detection methods, since the magnetic particles or the respective labels can be observed directly using standard optical microscopy or indirectly via fluorescent microscopy. The advantage of optical detection is the absence of interaction between the magnetic actuation and the optical detection. Thus single particles can be detected without the need for additional corrections, given the necessary resolution of the optical setup. It can be seen that a high performance optical setup is necessary to obtain a high sensitivity, since the sample volumes are very small and therefore generate only very low optical signals. This is also at present the main drawback when using fluorescent detection and quantification in a Lab-on-a-Chip system, because the required high-performance fluorescent microscope results in a large and costly setup, which reduces the systems flexibility and in addition increases the system's complexity and usability. In that respect, the integration of optical detection elements, as presented by Choi et al. [35], can offer a solution. The main challenge is hereby the integrated optical detection and characterization of a single microparticle, as can be achieved using spin-valve sensors [104] or impedance spectroscopy [37], and in combination, the quantification of the molecules captured at the particle surface.

Potential candidates for the on-chip optical detection are integrated photosensitive elements, such as photodiodes and single photon avalanche diodes [26, 147]. These elements have a high sensitivity and can be combined with a microfluidic system as demonstrated in Figure 3.15. The additional advantage of photon avalanche diodes is their inherent amplification as compared to simple photodiodes, resulting in the possibility of detecting very small optical signals with a very good signal

to noise ratio. Comparable optical detection setups are known from cytometry systems, which already proved the capability of optical detection to sense and distinguish single particles and cells [89]. In addition to detecting the presence of magnetic microparticles, integrated SPADs will also offer the ability the perform on-chip fluorescent measurements, such as fluorescence lifetime imaging (FLIM) [109].

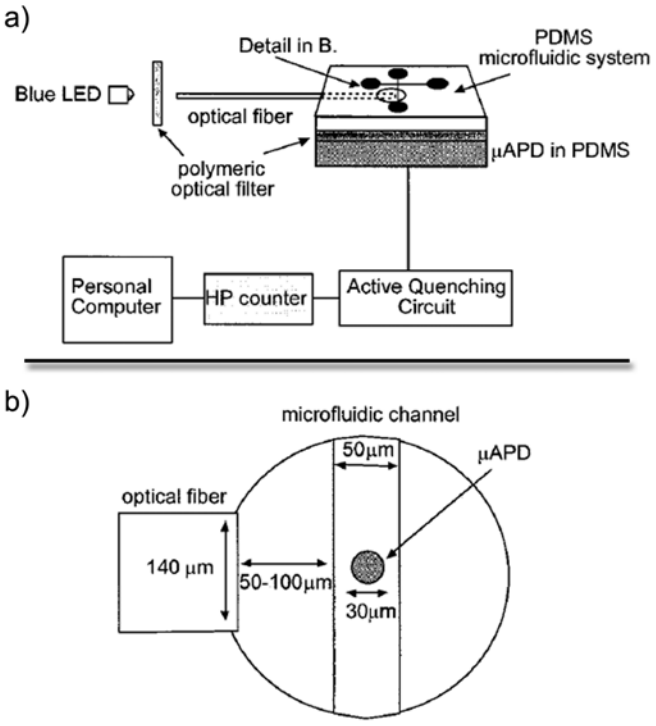

Figure 3.15 Diagrams of experimental setup and arrangement of the microfluidic systems with integrated optical detection using a μAPD (micro avalanche photo diode) combined with an optical fiber and channel [26]. a) The light from a blue LED was coupled into the optical fiber to excite fluorophores in the channel. The emitted photons were detected by the actively quenched μAPD. The photocounts from the quenching circuit were counted with an HP universal counter interfaced with a personal computer. b) The detail of the excitation/detection region. Reprinted with permission from Chabinyc, Chiu, McDonald, Stroock, Christian, Karger & Whitesides, Analytical Chemistry, vol. 73, pp. 4491-4498, 2001. Copyright (2001) American Chemical Society..

3.4 Conclusion

In this chapter I presented different solutions for elements of the μTAS toolbox with an emphasis on digital microfluidics and the manipulation of magnetic microparticles as possible components of modular Lab-on-a-Chip systems. Recent publication show that the challenge of designing a droplet manipulation system, capable of performing all necessary droplet

manipulation steps, while only minimally interacting with the sample, is being tackled using a multitude of different approaches. One interesting approach is hereby the manipulation of droplets via enclosed magnetic microparticles that are actuated using small permanent magnets. In parallel, literature also shows an increasing number of microfluidic systems, where magnetic microparticles are manipulated using electromagnets. The latter are favored over permanent magnets due to their higher flexibility in design and field control.

In consequence, I decided to study the possibilities of combining magnetic particle manipulation via electromagnets with digital microfluidics. The goal is to obtain a Lab-on-a-Chip system that offers the advantages of droplet based microfluidics, such as small, self-contained sample volume of different chemistry on one chip, combined with the potential of mobile substrates, as offered by the magnetic particles. The use of electromagnets allows hereby the design of an automated setup, known from EWOD and SAW systems, in contrast to previous magnetic droplet manipulation approaches relying on the displacement of permanent magnets.

Another μTAS component, which still presents a large challenge with respect to its miniaturization, is the detection unit. A section of this chapter presented different solutions, demonstrating the potential of integrated detection but lacking the sensitivity to examine single magnetic particles on-chip. Thus, in Chapter 6 a system will be presented that combines magnetic particles manipulation with optical detection elements in a CMOS chip. It will be the goal to study the capability of that type of setup for in-situ optical measurements of high sensitivity. The advantage of such a combination is the independence of the actuation and the detection principles, which can result in a high sensitivity and resolution, as known for high performance microscopy setups.

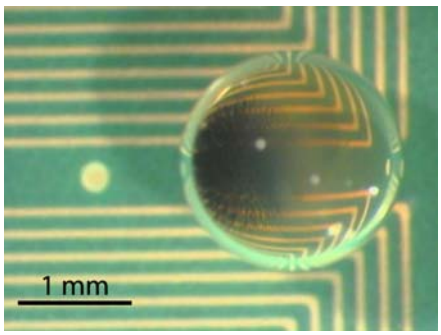

CHAPTER

4

MAGNETIC DROPLET MANIPULATION

The following chapter describes the setup of a system for the magnetic manipulation of aqueous droplets. The different droplet manipulation steps and their implementation into the system are discussed and characterized. This chapter also shows the influence of the medium surrounding the droplets and explains the effects of hydrophilic surface patterning with respect to the different droplet manipulation steps. Furthermore, I will look into the impact of particle size on droplet manipulation.

adapted from the journal article (with permission from Elsevier): U. Lehmann, S. Hadjidj, V.K. Parashar, C. Vandevyver, A. Rida, and M.A.M. Gijs. Two-dimensional magnetic manipulation of microdroplets on a chip as a platform for bioanalytical applications. Sensors and Actuators B: Chem. 117, 2 (2006), pp. 457-463.

4.1 Introduction

The manipulation of small droplets is steadily gaining impact on the development of Lab-on-a-Chip systems [83, 128]. Among the solutions presented in recent years (see Chapter 3), the magnetic droplet manipulation offers the advantage of long range magnetic forces, which do not interact with most biological materials. This non-interaction requires however the introduction of magnetically responsive material into the droplets. Such magnetic microparticles have the advantage that they can serve as mobile substrates in addition to being the force mediators. For the actuation of the magnetic microparticles enclosed in the droplets, present magnetic droplet manipulation systems rely on the displacement of small external permanent magnets [161]. Such external moving elements increase the system's complexity and in consequence have a negative impact on their usability.

In the following chapter I will describe a magnetic droplet manipulation system, where external moving magnets are replaced by a multilayered Printed Circuit Board (PCB), as previously proposed for the manipulation of magnetic microparticles [150]. In combination with hydrophilic/ hydrophobic surface patterning a modular and highly flexible platform is created, where all droplet manipulation steps - transport, merging, mixing and splitting - can be performed.

4.2 Magnetic Droplet Actuation System

The magnetic droplet manipulation system, whose components are shown in Figure 4.1, can be divided into two main units. The **actuation unit** contains the multilayered PCB and the magnetic circuit for the static magnetic field, while the **reaction unit** consists of a small box-shaped reservoir with an exchangeable Teflon bottom. The reaction chamber is filled with silicone oil in order to provide a suitable environment for the free suspension of aqueous droplets.

The modularity of the system allows the permanent installation of the actuation unit, while the reaction unit can be exchanged and adjusted according to the requirements of the experiments. This makes the setup highly flexible, versatile and user-friendly.

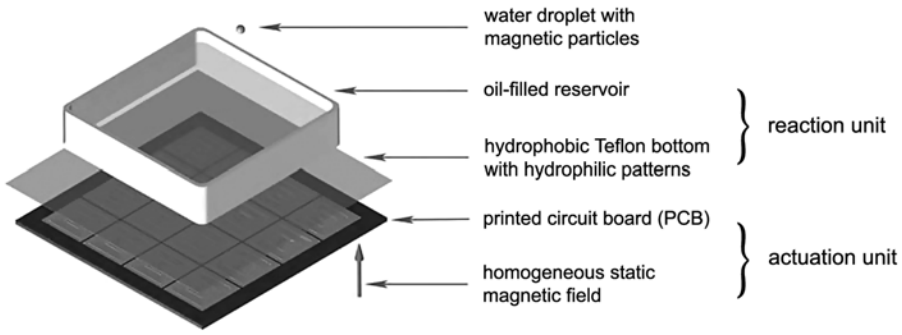

Figure 4.1 Schematic explosion view of the magnetic droplet manipulation system placed inside a homogeneous static magnetic field

4.2.1 The Magnetic Actuation Unit

The magnetic force, which drives the droplet manipulation, is generated via a multilayered PCB. Each layer contains a matrix of square coils, arranged to partially overlap between layers, as demonstrated in Section

2.3. The coils can be addressed in a variable pattern that allows the generation of a changeable magnetic field topology and thus the creation of varying field gradients. The currents driving the coils are controlled via a matrix of switches that can be addressed either manually or with the help of a LabView interface.

Magnetic Circuit

The PCB is placed on a soft-magnetic metal sheet, which - in combination with two stacks of permanent magnets placed alongside the PCB - serves to generate a homogeneous static magnetic field over the chip surface, as presented in Figure 4.2. The simulation as well as the measurement, see Figure 4.3, show that the magnetic flux is perpendicular to the PCB surface and its density amounts to B = 11 - 12 mT. The perpendicular static field, which is higher than the magnetic field generated by the PCB, sets the direction of magnetization of the magnetic microparticles inside the droplets and in consequence determines which component of the magnetic field will interact with the particles.

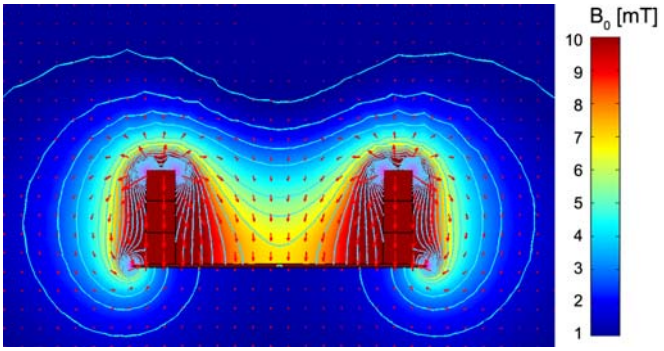

Figure 4.2 FEM simulation of the field generated by the two stacks of permanent magnets placed on a sheet of soft-magnetic steel.

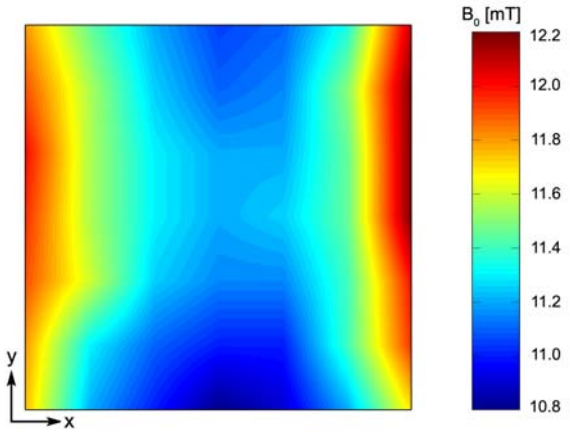

Figure 4.3 7x7 point measurement of the perpendicular static magnetic field at the PCB surface showing the expected relative homogeneity of the perpendicular field over the chip's surface.

Since the permanent magnetic field is oriented in the z-direction, the respective component of the magnetic field generated by the PCB will govern the particle actuation. Thus the magnetic force on the particles and in consequence the droplets can be expressed as:

$$\vec{F}_{mag} = (m_z \cdot \nabla) B_z \tag{4.1}$$

B_z presents hereby the sum of the static magnetic field and the magnetic field generated by the PCB, see Section 2.3.

Figure 4.4 shows the setup of the magnetic actuation system, including the PCB, the steel sheet and the permanent magnets. The ohmic heating of the coils, caused by the comparatively high current densities (J = 230 A/mm^2), necessitates the addition of a cooling device. For this reason a Peltier elements is placed underneath the PCB, where it prevents the destruction of the circuit and, with regard to bioanalytical applications, allows controlling the temperature at the chip surface.

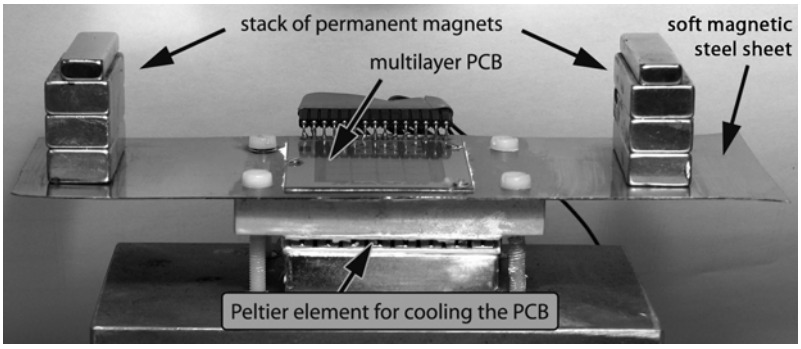

Figure 4.4 Photograph of the complete magnetic actuation unit. The PCB is placed in the perpendicular homogeneous magnetic generated by the two stacks of permanent magnets. A peltier element reduces the ohmic heat produced during actuation.

Characterization of the PCB

Printed Circuit Board

The topology of the magnetic field generated by the PCB depends on the currents in the individual coils. When driving all coils of two selected layers with currents of the same amplitude and direction, the magnetic field expresses channel-like patterns. Figure 4.5 shows the expression of such parallel lines of minima and maxima according to simulation and measurement. In consequence, the magnetic particles and with them the droplets will assemble along the lines according to the orientation of the external magnetic field. The direction and position of the magnetic channels depend hereby on the choice of the PCB's layers. Due to the

PCB's inner circuitry, the number of possible channel patterns is four, out of which only two combinations are generally used.

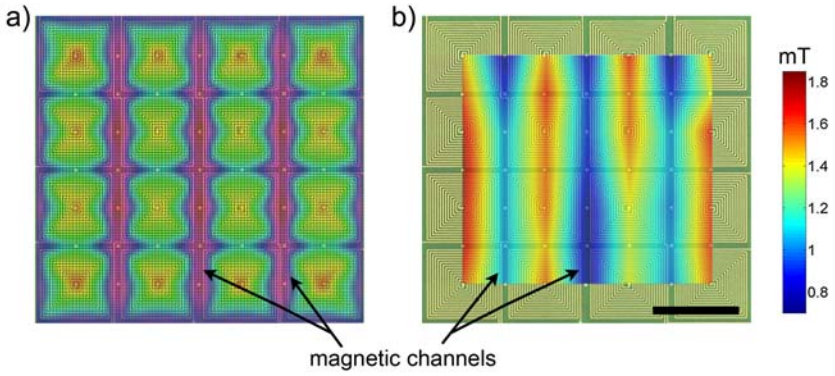

Figure 4.5 Formation of virtual magnetic channels over the PCB. The fields of two layers of coils overlap to form a channel-like field profile confining the magnetic particles. (a) Result of analytical simulation, (b) 7 x 7 point measurement overlaid over a photograph of the circuit.

With two layers of the PCB in "channel-mode", the coils in the remaining two layers are subjected to currents of varying direction according to a three phase scheme [151], schematically shown in Figure 4.6 a). The coils of each PCB layer are hereby interconnected in a pattern that allows to reduce the number of current inputs per layer to three, thus facilitating the system's current control. The currents are chosen according to the

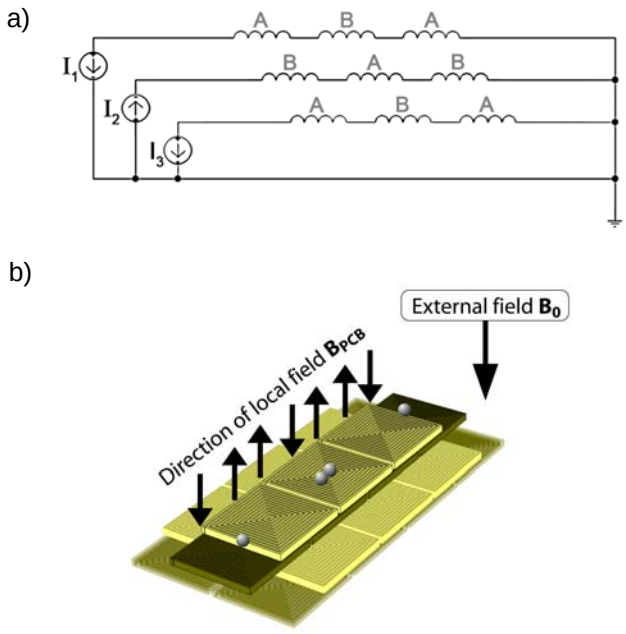

Figure 4.6 Mechanism of the magnetic actuation along the virtual channel. a) Schematic representation of the three phase current scheme (A: layer A, B: layer B). b) The magnetic particles are attracted towards the positions where the local field is aligned with the external field, leading to a local maximum of the absolute field strength.

three-phase scheme, with the result that the field of every third coil is aligned with the external field, while all other local fields are anti-aligned, as Figure 4.6 b) demonstrates. This leads to local field maxima and minima along the virtual channel, resulting in the accumulation of the magnetic particles at defined spots. When changing the position of the aligned local field, the particles will follow, thus enabling the controlled magnetic manipulation of the droplet containing them [151].

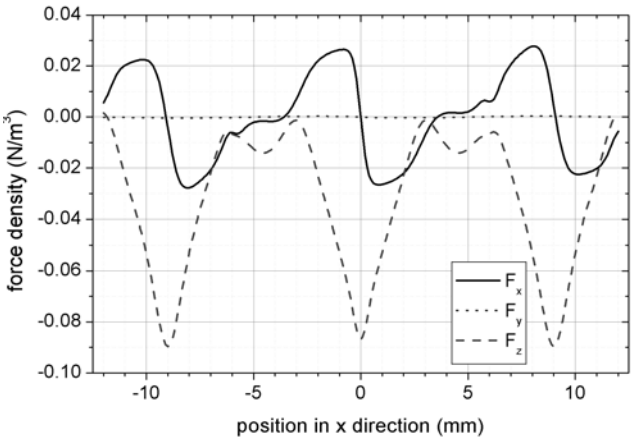

Figure 4.7 Magnetic force per volume on a magnetic particle along a virtual channel obtained from the analytical model.

The forces acting on a magnetic particle, magnetized in the z-direction and positioned in the center of the virtual channel, are presented in Figure 4.7. We see that the particles experience a force along the channel (F_x), while the perpendicular force inside the same plane (F_y) is close to zero, demonstrating the influence of the magnetic channel. However, the simulation also indicates that the particles are subjected to a strong force towards the chip surface (F_z). This emphasizes the importance of a low friction surface at the reaction unit's bottom, since this force will give rise to the surface friction F_{sf} acting against the magnetic transport.

$$\vec{F}_{sf} = -\alpha_r \cdot (|\vec{F}_z| + |\vec{F}_g|) \cdot \frac{\vec{v}}{|\vec{v}|} \tag{4.2}$$

with the friction coefficient α_r, the gravitational force F_g and the particle or droplet velocity v. For this reason, the reservoir bottom is made of Teflon (FEP50, DuPont) with a thickness of 25 µm, whose friction coefficient towards a water droplet is $\alpha_r < 0.001$, resulting in a surface friction that is significantly lower than the magnetic force in x-direction.

4.2.2 The Oil Medium

An important component of the droplet manipulation system is the silicone oil in the reaction unit. The oil prevents the evaporation of the droplet medium, permits the droplets to sink to the reservoir bottom while keeping their spherical shape (Figure 4.8), lowers the droplet's surface tension and, in consequence, makes droplet splitting possible.

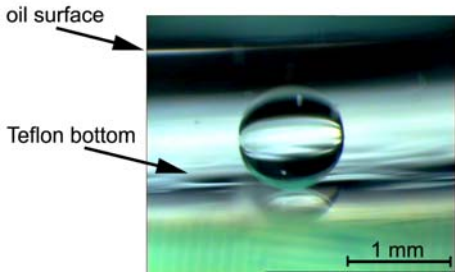

Figure 4.8 Photograph of a submerged droplet sitting on the Teflon bottom layer. The droplet maintains its spherical shape and touches the Teflon only slightly.

The following table summarizes the requirements the silicone oil has to meet in order to be a functional part of the droplet manipulation system.

Parameter	**Requirement**
Density	slightly smaller than water
Viscosity	equal to water
Interfacial Tension towards water	as small as possible

Table 4.1 Requirements for the oil medium present in the droplet manipulation system.

Since the oil should furthermore be compatible with biomaterials, a silicone oil, known for being very inert and immiscible with water, was chosen. With a viscosity of $\eta = 1.2$ cP and a specific gravity of $G = 0.82$, **octamethyltrisiloxane** (OMTS) fulfils the first two requirements, but experiments (Figure 4.9) showed that the interfacial tension towards water is too elevated to successfully split a droplet using the magnetic forces provided by the actuation unit. We see that even a large amount of magnetic microparticles does not suffice to effectively deform a droplet attached to the reservoir's bottom.

It is known from literature that the interfacial tension between two liquids can be lowered via the addition of surfactants [122]. However, since biological molecules can easily react with these surfactants [153], they are not the best choice for bioanalytical systems. In consequence,

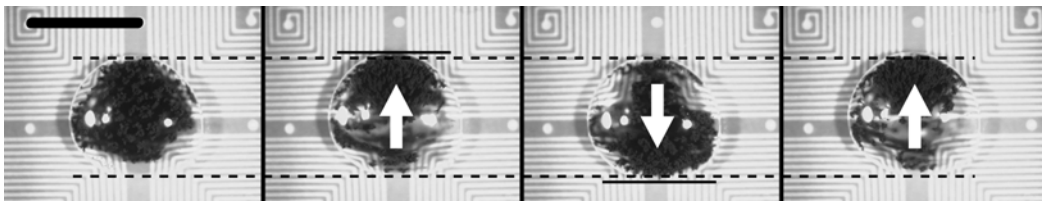

Figure 4.9 Droplet deformation in octamethyltrisiloxane. (Dimension bar = 3 mm)

polymethylphenylsiloxane (Poly-MPS) and dioctylphthalat (DOP) were chosen as additives to the OMTS, and led to a significantly lowered interfacial tension[2]. Furthermore, the presence of the phthalic ester (DOP) in the silicone oil promotes the formation of a molecularly thin protective layer between the aqueous droplet and the OMTS. This layer prevents the direct contact between the oil and the droplet media and permits the handling of saline buffers and even water-ethanol droplets, as required by many bioanalytical protocols. Moreover, the protective layer avoids the permeation of water into the oil medium.

Characterization of the oil medium

Since the properties of a mixture of liquids do not linearly depend on the concentrations and ratios of the components, the mixed oil medium was characterized separately in terms of its density, viscosity and interfacial tension towards water[3].

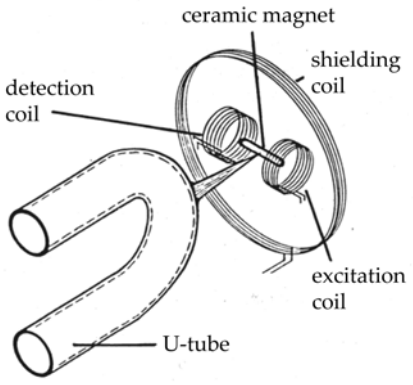

Figure 4.10 Schematics of the vibrating U-shaped tube densimeter (http://www.chemie.uni-rostock.de/pci/Heintz/for_dichte.html).

Density

The density was measured using a **vibrating U-shaped tube densimeter** [77], see Figure 4.10. Here the liquid of interest is inserted into a U shaped tube, whose resonance frequency shifts due to the weight change. The apparatus is calibrated with water and the relative density at a given

2. The silicone oil composition was developed with the support of V.K. Parashar.
3. The measurements were conducted at the University of Rostock with the help of Anja Tschersich.

temperature can be determined. For the modified OMTS the density measurement yielded a value of $\rho = 877.86$ kg/m^3 at room temperature.

Interfacial tension

With the knowledge of the liquid's specific weight, the interfacial tension can be determined using the **pendant drop method** [3]. Here the liquid of higher specific weight is injected at a very low flow-rate via a syringe into a tank filled with the second medium of the two phase system of interest. The droplet forming at the tip of the syringe is recorded with a CCD camera and the shape of the droplet just before detachment is evaluated (see Figure 4.11). The geometry of the droplet can be translated into the interfacial tension between the two media [110]. We measured an interfacial tension of the modified OMTS towards water of $\sigma = 1.52$ mN/m.

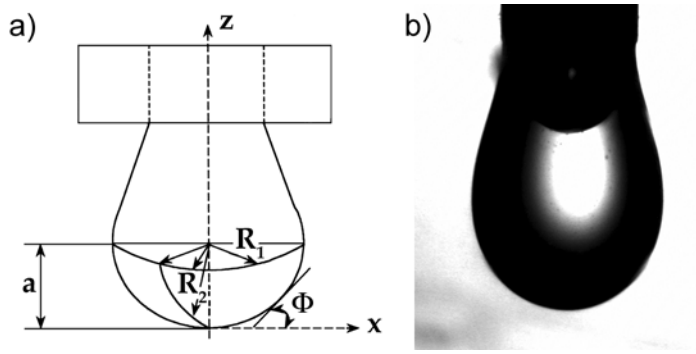

Figure 4.11 Pendant drop method for the measurement of the interfacial tension. a) Pendant drop geometry [110]. b) Picture of a pendant drop of the oil medium in a water tank.

Viscosity

The viscosity of the oil medium was determined, starting from the known specific weight, via the **falling ball method** [111], where a small sphere or droplet sinks a well-defined distance in a column of the medium of interest. The velocity, which can be assumed constant after a short initial phase, can be translated into the liquid's kinematic viscosity via the viscous drag. Thus the kinematic viscosity of the oil solution was measured to be in the range of $\nu = 3.8$-4.2 cSt, which converts to a viscosity of $\eta = 3.3$ - 3.7 mPa s.

The above measurements, summarized in Table 4.2, show that the chosen additives lowered the silicone oil's interfacial tension towards water (σ_{OMTS} = 40.5 mN/m) while maintaining the positive properties of the OMTS regarding its viscosity ($\eta = 1.2$ mPa s) and density ($\rho = 0.82$ kg/m^3).

density	interfacial tension towards water	viscosity
877.86 kg/m^3	1.52 mN/m	3.3 - 3.7 mPa s

Table 4.2 Summary of the measured properties of the modified OMTS used in the droplet manipulation system.

4.2.3 The Magnetic Particles

The successful magnetic manipulation of aqueous droplets employs the effect that magnetic particles are trapped within a droplet and drag this droplet along with them in the direction of a magnetic field gradient. For that reason, the properties of magnetic microparticles chosen for this application are important.

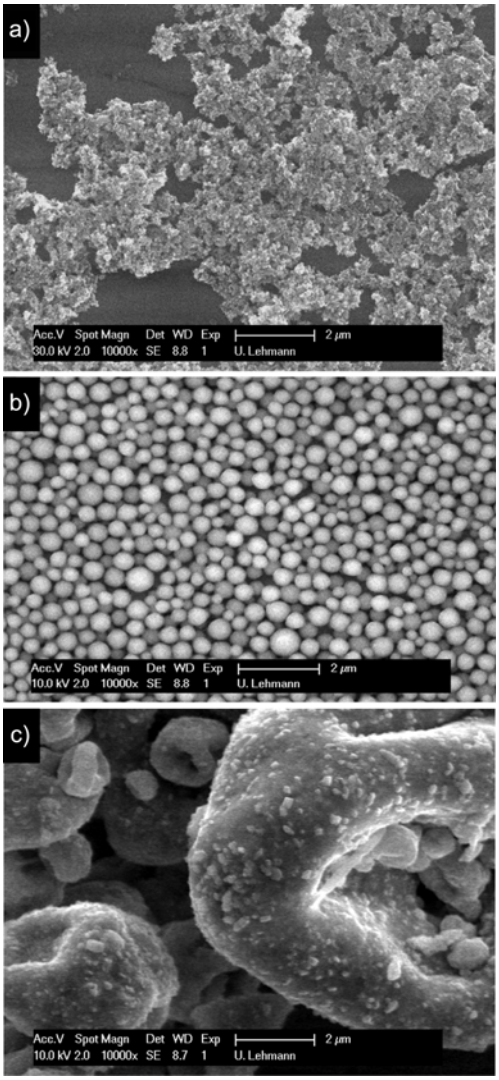

Figure 4.12 SEM images of the different particle types used for the droplet manipulation. a) Micromod Nanomag with 250 nm diameter, b) Ademtech Masterbeads with 500 nm diameter, c) Roche silica beads with an average diameter of 6 µm

The particles need to have a hydrophilic surface, a sufficiently high magnetic susceptibility and the ability to be biologically activated in order to capture biomolecules of interest. In general, a small diameter of the particles is advantageous, since it increases the active surface for the capture of molecules. On the other hand, a decrease in diameter results in

a strong reduction in volume, which again lowers the magnetic force on one single particle and also makes it more prone to entropic effects. For this reason, different types of magnetic microparticles, see Table 4.3, were considered and their suitability for the magnetic droplet manipulation was studied. Figure 4.12 presents Scanning Electron Microscope (SEM) images of three types of magnetic particles examined in the droplet manipulation system. It is obvious that the polymer particles are the most spherical with the smallest size distribution. The small SiO_2 particles cluster in the absence of water, which makes it difficult to distinguish between single particles.

Particle	**Diameter**	**Surface**	**Magnetism**
NanoMag (Micromod)	250 nm	SiO_2	superparamagnetic
Masterbeads (Ademtech)	500 nm	Polymer with COOH	superparamagnetic
Bangs Lab BioMag	1.5 µm	Polymer with biotin	superparamagnetic
Silica beads (Roche)	6 µm (large distribution)	SiO_2	ferrimagnetic

Table 4.3 Parameters of the particles examined for use in the droplet manipulation system.

Placed in the homogeneous magnetic field, the magnetic particles form column-like structures along the field lines, spanning the full droplet height [66, 203], as visible in Figure 4.13. The application of a magnetic field gradient leads to the displacement of an entire column in the direction of the gradient. Figure 4.13 also shows the influence of the shape of the droplet on the distribution of the height of the particle columns. They are highest at the coil center, where the magnetic force is large enough to deform the droplet, but are visibly shorter towards the droplet's rim, where the field is smaller as is the droplet's height.

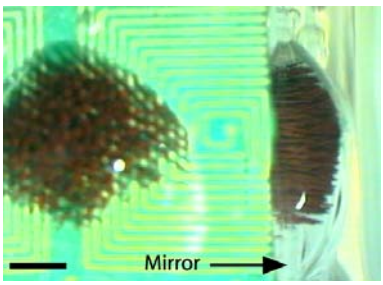

Figure 4.13 Photograph of a droplet sticking to the reservoir bottom next to an inclined mirror. The magnetic particles (Roche) form columns in the direction of the applied static magnetic field, as can be seen in the profile of the droplet visualized by placing a mirror at a 45° angle with the surface. (Dimension bar = 1mm)

4.3 Droplet Handling

In order to perform all necessary liquid handling steps in an automated fashion on the chip, a set of obligatory droplet manipulation steps had to be implemented. These are:

- the **transport** of the droplet for transferring liquid from one point of interest to another
- the **merging** and **mixing** of droplets for the different reaction steps of the bioanalytical protocol
- the **splitting** of droplets, necessary for the extraction of liquid fractions after the reactions.

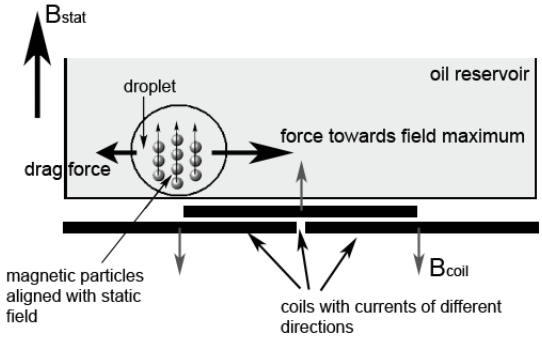

Figure 4.14 Schematics of the droplet transport. The magnetic particles in the submerged droplet are attracted towards the field maximum and drag the droplet along with them.

The main mechanism of the droplet handling, as schematically shown in Figure 4.14, is the transfer of the magnetic force onto the droplet via an interaction with the droplet surface. The interfacial tension σ between the droplet medium and the surrounding liquid plays hereby a crucial role, since it governs the behavior of the droplet during transport as well as during splitting.

4.3.1 Droplet Transport

A droplet can be transported, when the magnetic force is larger than the sum of the opposing forces generated by friction and drag (see Section 2.1.2). Figure 4.15 schematically summarizes the forces involved at the droplet surface during droplet transport. One sees that a successful droplet displacement requires a large magnetic force as well as small drag and friction. The latter is determined by the interaction of the droplet and the reservoir bottom. Since the droplet maintains its spherical shape and

slides over the surface, this interaction is reduced drastically. In addition, the reservoir floor is made of Teflon (FEP50, DuPont), whose friction coefficient α_r towards water is very low. In consequence, the drag force and therefore the droplet velocity is mainly dependent on the viscosity of the silicone oil, if the droplet diameter is kept constant (equation (2.10)). Thus, for the same applied magnetic force, a low viscosity will result in a high droplet velocity, whereas a highly viscous medium will slow the droplet down.

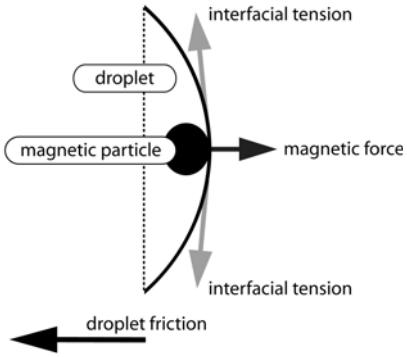

Figure 4.15 Schematics of the forces acting during the droplet transport.

When observing a droplet that is actuated out of a resting position, as presented in Figure 4.16, we clearly see the force transfer mechanism. The hydrophilic magnetic particles first move towards the droplet wall and upon contact start pushing against it. At that point, the opposing surface tension acts similar to a spring and translates the particle movement into a droplet movement.

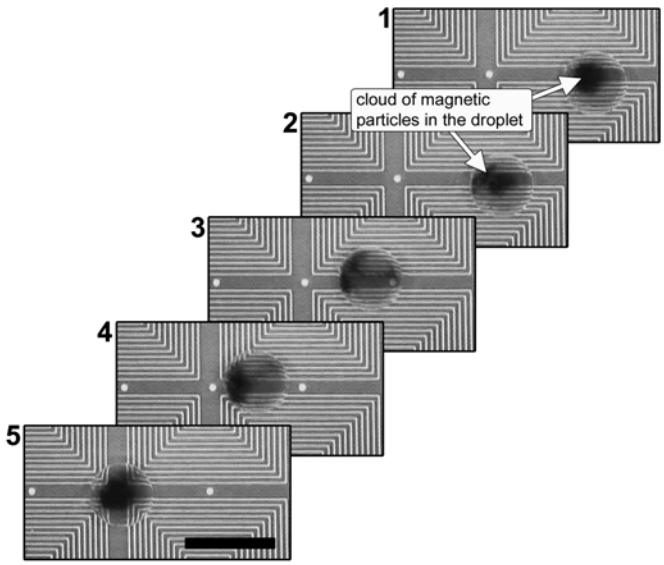

Figure 4.16 Sequence of photographs taken during droplet transport. The cloud of 250 nm large magnetic particles is moved towards the droplet wall and pushes the droplet towards the neighboring field maximum. (Dimension bar: 3 mm)

Any droplet deformation leads hereby to a loss in kinetic energy, because the latter will be converted into a change of droplet surface area, as discussed in Chapter 2.2. For a sufficiently large interfacial tension, the force on a droplet of constant volume depends therefore only on the magnetic particles enclosed in the droplet.

To study this relation, I measured the velocity of droplets containing varying amounts and also different types (see Table 4.3) of magnetic particles. In order to ensure a large interfacial tension, these experiments were performed in pure OMTS (σ = 40.5 mN/m). The obtained velocity was subsequently converted into the magnetic force via equation (2.14). Figure 4.17 summarizes the measured velocities and magnetic forces obtained for the different particle types and contents. The linear dependence on the enclosed particle amount and thus the total number of particles *N*, as expected from the theory (equation (2.16)), is clearly visible. The slope of the magnetic force amounts hereby to 1 nN per µg of magnetic particles.

Moreover, we see that the different particle types, especially with respect to their size, do not have an influence on the droplet transport behavior. Due to this observation we can assume that all examined particle volumes contain the same total amount of magnetic responsive material.

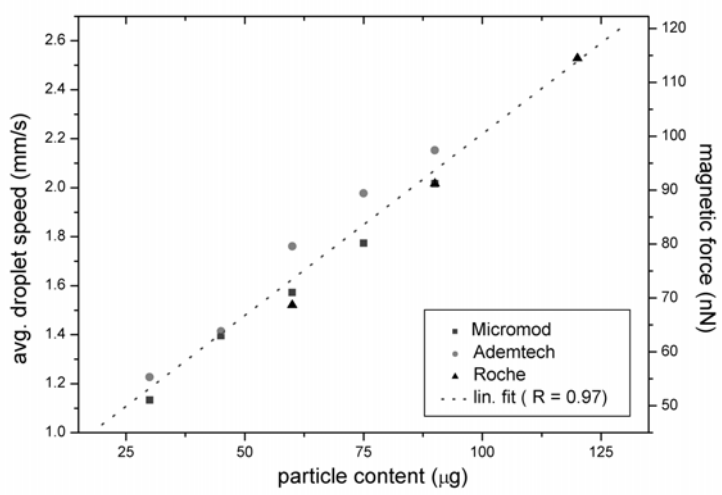

Figure 4.17 Measured speed of a 3 µl droplet for different types of magnetic microparticles at varying concentration. The right side of the graph shows the conversion into the magnetic force via the viscous drag.

When making use of the capability of the magnetic actuation platform, a small aqueous droplet can be transported along any chosen path on the

chip surface by simply varying the direction of the magnetic channels on the PCB as well as the position of the local maxima, as shown exemplarily in Figure 4.18.

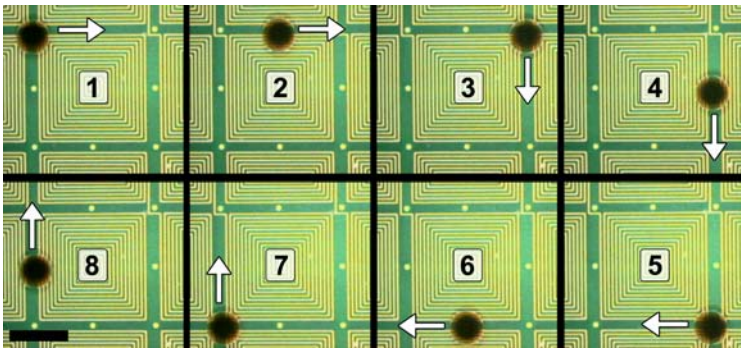

Figure 4.18 Transport of a three µl droplet around a square coil. (Dimension bar: 3 mm)

4.3.2 Droplet Merging and Mixing

The merging of two droplets that come into contact, is driven by the interfacial tension, since a joint droplet exhibits a lowered surface-to-volume ratio and thus a more favorable state of energy. The excess energy is translated into kinetic energy driving the droplet contents into each other, thus supporting the mixing process. Since, however, the interfacial tension is very low in the droplet manipulation system, the energy change will be small and thus does not accelerate the mixing significantly.

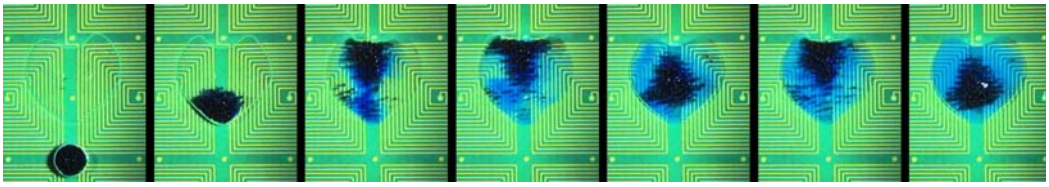

Figure 4.19 Snapshots of the droplet mixing. Blue ink is mixed with a clear water droplet via magnetic actuation of the merged droplet.

Thus mixing is performed via magnetic actuation, as demonstrated in Figure 4.19. The magnetic particles are agitated inside the droplet, which introduces convective flow inside the droplet, as demonstrated in Figure 4.20. This inner droplet flow accelerates the diffusion process and leads to mixing times in the range of seconds for a 10 µl droplet. Without magnetic stirring, the duration t of the droplet mixing has to rely on diffusion alone, and would be governed by:

Diffusion length

$$L_d = \sqrt{2Dt} \tag{4.3}$$

with the diffusion length L_d and the diffusion coefficient D. The latter can be expressed as:

Stokes-Einstein Equation

$$D = \frac{k_B T}{6\pi\eta r} \tag{4.4}$$

where k_B is the Boltzmann constant, T the absolute temperature, η the liquids viscosity and r the molecule's radius [69]. In consequence, with diffusion coefficients ranging from D = 2 10^{-9} m^2/s for small molecules to D = 10^{-11} m^2/s for large molecules, the droplet mixing via diffusion would take significantly longer than when supported by magnetic stirring. While the particle supported mixing takes on average t_{mix} = 20 s, the mixing via diffusion would take between t_{mix} = 280 s = 4 min 40 s (small molecules) and t_{mix} = 5600 s = 1 h 33 min 20 s (large molecules) and is therefore too long for a Lab-on-a-Chip application.

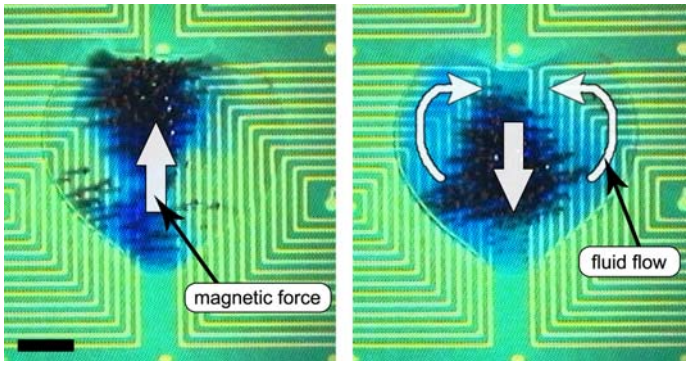

Figure 4.20 Droplet mixing via convection. The movement of the particles inside the droplet gives rise to a fluid flow in the opposite direction at the wings of the droplet. (Dimension bar: 1 mm)

4.3.3 Droplet Splitting

The splitting of a droplet requires two opposing forces. One is the magnetic force acting on the particles, whereas the second holds the larger droplet in place. The holding force can be obtained by either locally increasing the surface friction or by placing an obstacle in the droplet's path. For the droplet manipulation system, the local increase of surface friction was chosen, since it can be introduced easily and does not require elaborated additional patterning or molding steps. It can be achieved via **hydrophilic patterning** based on the effect of accelerated aging of Teflon in an oxygen plasma, which leads to a defluorination of the PFTE surface, an increase in the number of hydrocarbon moieties and an increase in the

yield of O^- and OH^- ions [192]. Since the treated Teflon exhibits a decreased hydrophobicity[4], a localized oxygen plasma treatment of the reservoir's Teflon bottom layer can generate areas of increased friction [78], which allows the immobilization of an aqueous droplet. The use of a metal mask with laser-cut openings of the desired droplet shapes, as demonstrated in Figure 4.21, permits hereby a very flexible design of the hydrophilic areas.

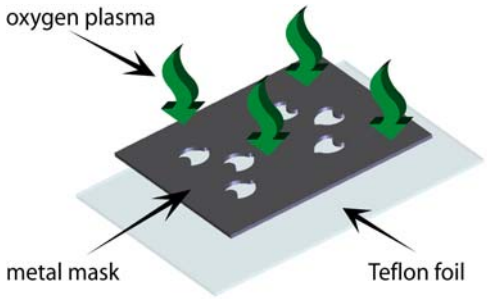

Figure 4.21 Schematic of the Teflon treatment. The foil is exposed to an oxygen plasma via openings in a metal mask. The exposed areas express a higher hydrophilicity than the unexposed areas.

Prior to the plasma treatment, the Teflon foil (FEP50, DuPont) is cut into a square of the appropriate size and sandwiched between a glass slide and the metal mask. The plasma (Scancoat six, Edwards SA) is set to:

Pressure	Current	Time
0.2 mbar	20 mA	60 s

Table 4.4 Plasma parameters for the hydrophilic Teflon patterning.

After the hydrophilization step, the Teflon foil is clamped into the reservoir frame, which results in a highly even surface and provides an obstacle-less pathway for the droplet transport. Thus only the hydrophilic/hydrophobic surface patterning will influence the droplet behavior.

Droplet Shaping

The low interfacial tension between the droplet and the oil medium, allows the deformation of a water droplet sitting on a hydrophilic area of a distinct shape. Instead of reclaiming the spherical form, the droplet accommodates to the outline of the hydrophilic area. This behavior enables the creation and study of immobilized droplets of various shapes.

4. The wetting angle decreases from 120° to 105°.

Figure 4.22 shows a selection of different mask openings used for the Teflon treatment.

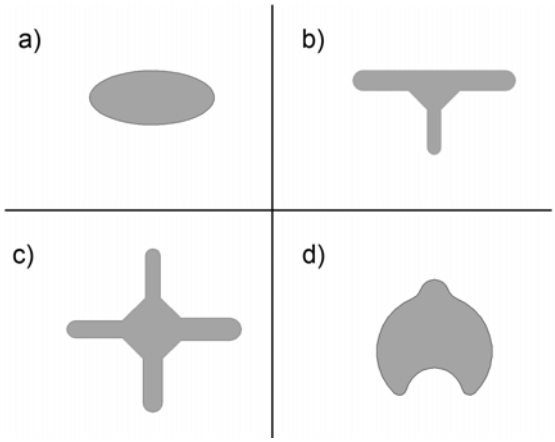

Figure 4.22 Mask design for the different immobilized droplet shapes (grey: mask opening). a) ellipse, b) triangle, c) cross and d) heart.

The shapes of the droplet achieved via the respective hydrophilic areas are presented in Figure 4.23. It can be seen, that the droplet follows the boundaries of the hydrophilic area, defined by the mask (Figure 4.22), very closely, as expected due to the low interfacial tension. The static deformation of the droplet has the advantage of facilitating the droplet splitting, since the additional change in surface area until the formation of a secondary droplet is smaller compared to a spherical or semispherical droplet.

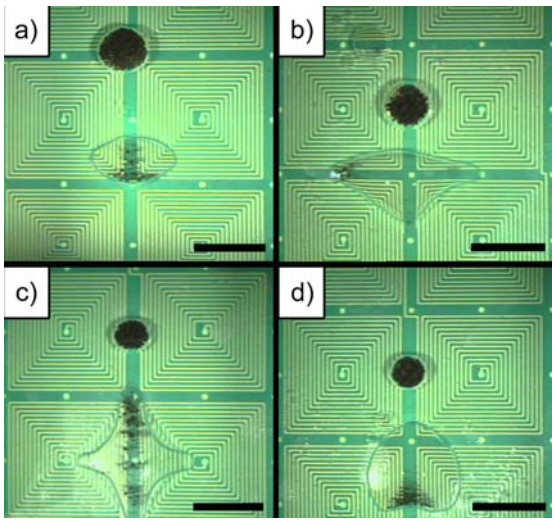

Figure 4.23 Photographs of different droplet shapes and the droplets separated from them. a) ellipse, b) triangle, c) cross and d) heart. (dimension bar: 3 mm)

An experimental comparison of the different proposed droplet shapes shows that the droplet splitting from the pointed end of an immobilized

droplet (shapes c and d) results in a smaller volume and also a better size control of the extracted droplet, as Figure 4.23 demonstrates. The extrusion of the droplet allows the magnetic particles to be assembled in a small volume before they start pushing against the droplet wall. This results in a larger pressure compared to a configuration, where the particles push against a flat inner surface. The droplet can therefore be more easily extended until the point, where the component of the capillary force defined by the local Laplace becomes negative and acts against the interfacial tension. This leads to a thinning and finally splitting of the droplet at the meniscus. Figure 4.24 shows a diagram of the forces acting on the extended droplet. The friction due to the local surface hydrophilization holds the main body of the droplet in place, while the magnetic force pulls a fraction of the droplet towards the neighboring field maximum. The competition between the magnetic pull and the capillary force, leads to a stretching and thinning of the meniscus.

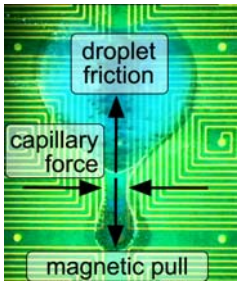

Figure 4.24 Schematics of the forces during droplet splitting. The initial droplet shape is overlaid with a picture of the extended droplet before breakup.

The heart-like shape was finally chosen for the droplet manipulation system, since only one droplet extrusion is needed for droplet splitting and the immobilized droplet's smaller dimensions permitted the placement of six microreservoirs on the chip surface. Figure 4.25 presents a sequence of pictures taken during the droplet splitting starting from the initial heart-like shape. The particles are first concentrated at the heart's tip and then pulled away. While the particles are held in place at the neighboring field maximum, the bridge between the droplets thins and finally breaks.

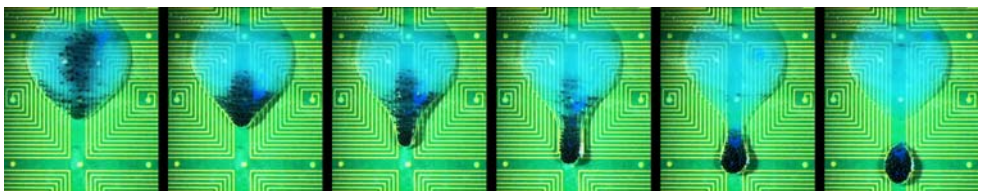

Figure 4.25 Steps of the droplet splitting. The droplet is extended towards the next field maximum and breaks at the meniscus due to capillary forces.

Droplet volume

Since on-chip bioanalysis requires a precise control of the handled liquid volumes, the dependence between the volume of an extracted droplet and the amount of magnetic material was examined. The droplet volume was hereby measured optically via a microscope mounted CCD camera and a MATLab algorithm based on a calibration measurement.

Figure 4.26, summarizing the measurements, shows that the volume of an extracted droplet is smaller than the initial droplet introduced into the system. Since the concentration of the magnetic particles inside the injected droplet is kept constant, the volume of the extracted droplet can be linked to the amount of magnetic material present in the system.

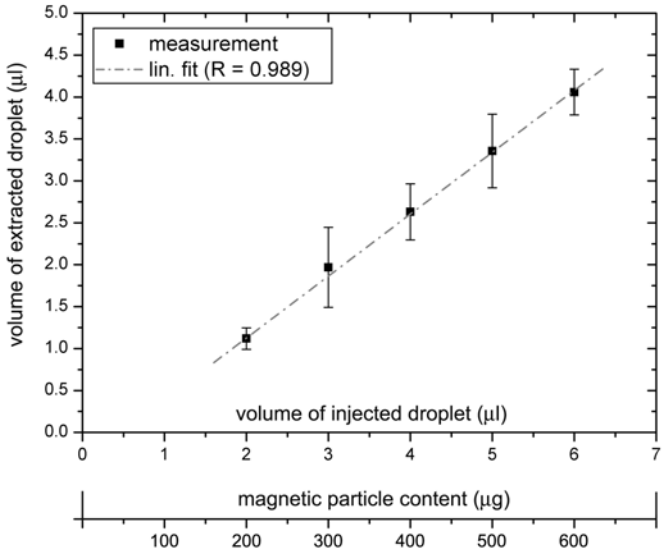

Figure 4.26 Measured volume change for droplets due to the splitting step. The concentration of the magnetic particles (Roche) is kept constant at 100 mg/ml.

Upon evaluation of the linear relation, we obtain a **liquid extraction capacity** of the silica coated Roche magnetic particles of about 7 nl per µg of magnetic particles. Thus, if we want to transfer a volume of 2 µl from one microreservoir to the next, we need to inject an amount of 300 µg of magnetic particles into the system. In addition, we learn from the droplet splitting experiments that the minimum amount of magnetic particles (Roche) necessary for the successful droplet splitting is 200 µg. However, when performing the droplet splitting step using magnetic microparticles of different size and composition, the minimum amount of particles required for successful droplet splitting varies significantly.

Particle size vs. Droplet Splitting

This behavior was further looked into and droplet splitting experiments were performed using varying amounts of the different particles

presented in Table 4.3. The droplet splitting capabilities of these particles are summarized in Table 4.5 and indicate clear differences between the particles' comportments. We see that larger particles (Roche) perform better than small particles (Micromod), because the latter require the injection of a larger amount into the droplet for a successful splitting. Since the forces obtained from equal amounts of different particle types should not vary, as measured previously (Figure 4.17), the reason for the differences in behavior must be related to particle size.

	particle content inside droplet			
particle type	**200 μg**	**250 μg**	**350 μg**	**500 μg**
Micromod Nanomag	n/a	-	-	+
Ademtech Masterbeads	+	+	++	+++
Bangs Lab BioMag	+	++	n/a	+++
Roche (DNA kit)	++	n/a	+++	+++

Table 4.5 Comparison of the droplet splitting properties for varying quantities of the different magnetic particles inside the droplets (- : splitting not possible, + : splitting possible, but performance is not stable, ++ : splitting ok, +++ : splitting works well and is repeatable)

Theory indicates (Table 2.3) that a sharp point deforming the droplet from the inside requires less force than a blunt point. In consequence, the concentration of the magnetic particles in a small volume facilitates droplet deformation and subsequent splitting.

Observation shows (Figure 4.27) that, for equal amounts, large particles occupy less volume than small particles and thus are more easily able to deform the droplet. For this reason, the pressure on the droplet surface exerted by the Roche particles is significantly larger than the pressure created by the Ademtech particles, which results in the less pronounced droplet deformation visible in Figure 4.27. Experiments indicate the required amount of injected magnetic particles of 500 nm diameter to be twice the amount of particles with 6 μm diameter in order to obtain a similar deformation. We also see that the small magnetic particles are spread over a larger volume, for the same weight fraction, than the larger particles. One reason is the lower density of a cloud of small particles with respect to a single large particles as described by the Kepler conjecture[5].

5. According to the Kepler conjecture about sphere packing in Euclidian space, the densest arrangement of equal sphere reaches 74 % of the density of the bulk material.

For example, a particle of 6 μm diameter has a volume of V = 1.13 10^{-16} m^3, whereas the same amount and type of material in the shape of 500 nm large spherical particles will occupy a volume of V = 1.52 10^{-16} m^3, which is an increase in volume of 34 %. In addition, the Roche particles have a very high size distribution (see Figure 4.12 c)), which leads to a better packing of a given volume than is the case for the highly monodisperse Ademtech particles (Figure 4.12 b)). In consequence, the same magnetic force will be distributed over a volume increased by one third, when using monodisperse particles with 500 nm instead of particle of large size distribution with an average diameter of 6 μm. As a result the pressure at the droplet surface will be smaller for the Ademtech particles. The increase in volume is easily visible when comparing the first row images of Figure 4.27 a) and b).

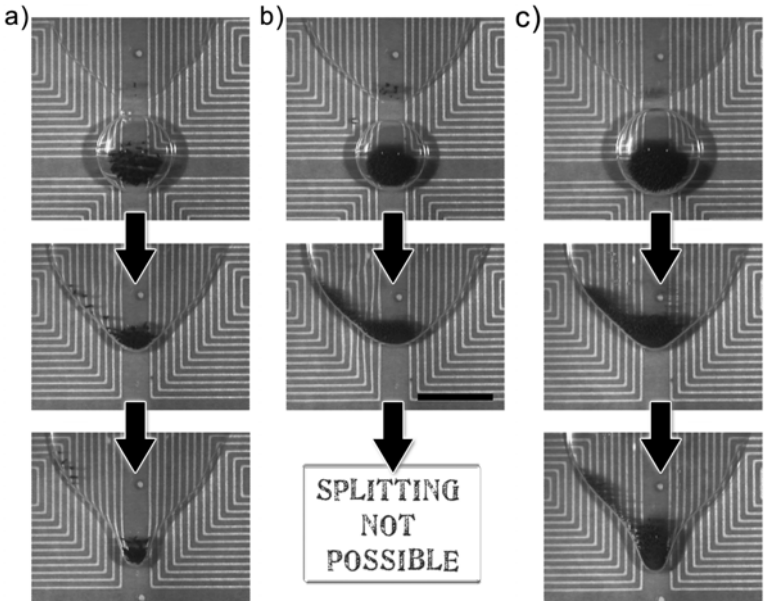

Figure 4.27 Droplet splitting using different particle types a concentration of at 50 mg/ml. The top row shows the injected droplet containing magnetic microparticles before merging with the immobilized droplet. The following rows show the droplet behavior during the splitting test. a) 3 μl of Roche magnetic particles (Ø = 6 μm), b) 3 μl of Ademtech magnetic particles (Ø = 500 nm), c) 6 μl of Ademtech magnetic particles (Ø = 500 nm). The difference in tip deformation is clearly visible. (Dimension bar = 2 mm)

Further parameters of influence are the choice of the shell material and the fill factor. Since the particle content in the droplet is related to the particle weight, the number of particles of low specific weight will be higher than the number of particles of higher specific weight, even if their size is identical. The specific weight of the particle, however, is dependent on the shell material used and the content of magnetic material inside the

particle. Therefore a low magnetite content results in a lowered specific weight and - as a result - a larger volume of the solid material present in the droplet. With the magnetic content of a particle generally given in weight percent (wt%), a change in shell material and thus total weight of the particle results in a changed magnetic volume content (v%), if the amount of enclosed magnetic material is kept constant. The volume of the enclosed magnetic material can hereby be calculated as follows:

$$V_{part} = \frac{m_{part}}{\rho_{part}} = V_m + V_{shell} \tag{4.5}$$

$$V_m = \frac{m_{part} \cdot FF}{\rho_m} \tag{4.6}$$

$$V_{shell} = \frac{m_{part} \cdot (1 - FF)}{\rho_{shell}} \tag{4.7}$$

with V_{part} the total volume, m_{part} the total weight and ρ_{part} the density of the magnetic particles, V_m the volume and ρ_{mag} the density of the enclosed magnetic material, V_{shell} the volume and ρ_{shell} the density of the shell material and FF the fill factor in weight percent. The different densities are summarized in Table 4.6.

material	**density [g/cm^3]**
silica	2.2
polysterene	1.05
magnetite	5.15

Table 4.6 Densities of the different particle materials

Thus, a magnetic silica particle containing the same amount of magnetic material as a polysterene particle will be significantly smaller than the latter due to the heavier particle shell.

Based on the information given by the particle suppliers we can estimate the different volumes occupied by the particles used in the droplet splitting experiments presented in Figure 4.27. According to the data sheet, the polysterene-based Ademtech particles have an average density of 2.2 g/cm^3 and a magnetite content of 65 - 70 wt%. When applying the values given in Table 4.6 to equations (4.5) to (4.7), we calculate a magnetite volume of $V_{mag} = 1.9\ 10^{-2}$ mm^3 contained in 150 µg of Ademtech

particles. The volume of the shell material amounts at the same time to $V_{shell} = 4.9\ 10^{-2}$ mm^3, which results in a total volume of $V_m = 6.8\ 10^{-2}$ mm^3. The magnetite volume in 150 µg of Roche particles is about the same value as calculated for the Ademtech particles, following the measurements presented in Figure 4.17. The silica shell has subsequently a volume of $V_{shell} = 2.4\ 10^{-2}$ mm^3. In consequence, the total amount of 150 µg of Roche silica particles is contained in a volume of $V_m = 4.3\ 10^{-2}$ mm^3, which is only 63 % of the volume taken up by the Ademtech particles. In combination with the less dense packing of the smaller Ademtech particles, the total volume of a group of these particles occupies twice the volume as the same weight of Roche particles. This results in a reduction of the pressure on the droplet wall by half, which is in accordance with the observation that the amount of Ademtech particles needs to be doubled in order to successfully perform the droplet splitting, as compared to the larger Roche particles. The increased spread of the cloud visible for the smaller particles additionally results in a higher probability of particles remaining in the immobilized droplet after the meniscus' constriction.

4.4 Conclusion

The combination of hydrophobic/hydrophilic surface patterning with carefully adjusted interfacial chemistry permits the transformation of a 2D magnetic manipulation platform, as described by A. Rida [150], into a droplet manipulation system. The enclosure of hydrophilic magnetic particles into a water droplet allows the transfer of the magnetic force, generated by the applied field gradient, onto the droplet. I demonstrated that a careful adjustment of the droplet environment's parameters, such as viscosity, density and interfacial tension, is the key to the implementation of all necessary droplet manipulation steps. Further on, I presented a design of hydrophilic areas on a hydrophobic Teflon sheet, which provides a very flexible and convenient way to create microreservoirs on the chip surface. The shape of the microreservoirs has an influence of the droplet splitting step and a comparison of different shapes led to the choice of heart-shaped microreservoirs. The transfer of sample fractions between these microreservoirs is performed via the magnetic actuation of droplets as summarized in Figure 4.28. A sequence of liquid extraction, transfer, merging and mixing takes hereby only

several minutes and can be fully automated, since no external moving parts are required.

Finally, the possibility of controlling the size of the extracted droplet was examined, since it is an important factor for the subsequent use of the droplet manipulation system for on-chip bioanalysis. In this context, the influence of the particle size was studied, with the result that - for identical amounts of magnetic responsive material inside the particles - the higher the magnetic volume content of a particle and also the larger the particles, the smaller the amount needed for successful droplet splitting.

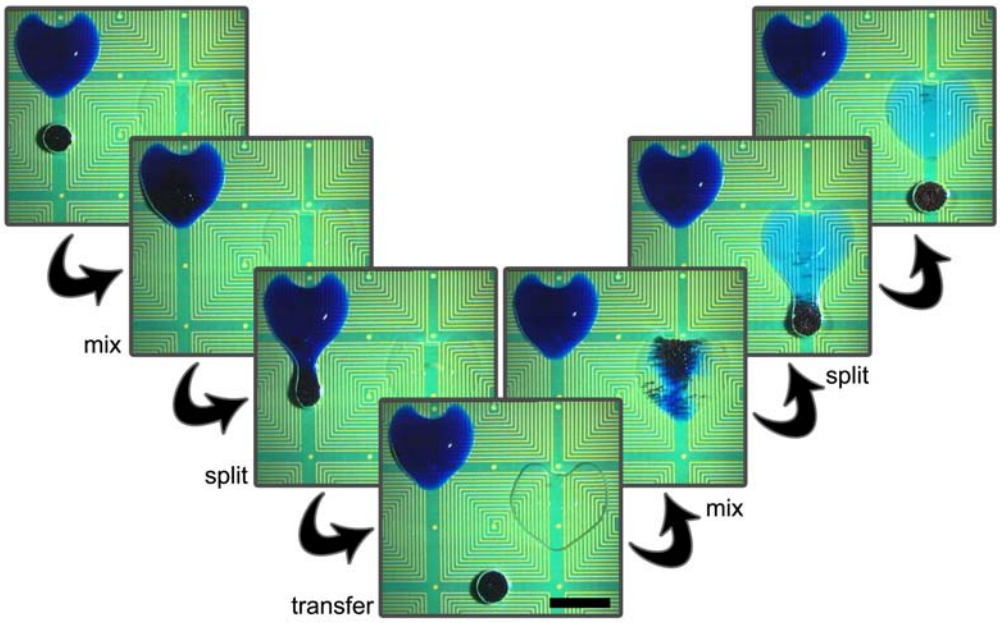

Figure 4.28 Sequence of on-chip droplet manipulation steps. The small fraction of the blue dye contained in the left-hand immobilized droplet is split and transferred to the neighboring clear droplet via magnetic particles. The initially clear droplet is tainted light blue after the merging and mixing with the extracted blue liquid fraction. (Dimension bar = 3 mm)

To put it all in a nutshell, this chapter described the design of a magnetic droplet manipulation system based on a matrix of electromagnets. The inventive hydrophilic/hydrophobic patterning of the liquid container's bottom permits the positioning and shaping of immobilized microreservoirs, between which liquid sample fractions are exchanged via the magnetic actuation of super-paramagnetic microparticles enclosed in the droplets.

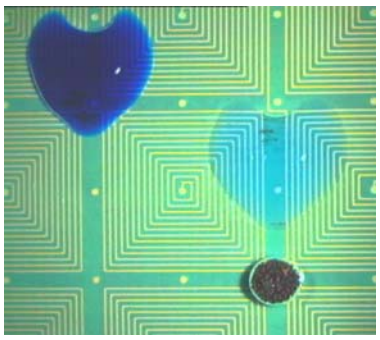

CHAPTER 5

DROPLET BASED LAB-ON-A-CHIP FOR MINIATURIZED BIOANALYSIS

In this chapter, I will examine the applicability of the droplet manipulation system, presented in the previous chapter, to bioanalytical procedures. Starting from standardized lab-bench protocols droplet based on-chip DNA extraction and purification will be studied, as well as the detection of enzyme-labeled antibodies.

5.1 Introduction

The specific binding of biomolecules to the surface of microparticles is of great interest for miniaturized bioanalytical systems [181]. Due to their small size, the particles offer a large surface-to-volume ratio, which increases the number of possible binding sites compared to bulk material of the same volume. New technologies allow hereby the synthesis of a large variety of microparticles adapted to the needs of the different bioanalytical procedures. In consequence, magnetic microparticles can be applied for DNA capture as well as antibody detection, depending on their surface chemistry and the reagents used.

5.1.1 Biology on a Bead

Specific binding via Immunoassay

A standard procedure to capture biomolecules via antibody-antigen links is shown in Figure 5.1. Such immuno-assays are usually performed in microtiterplates [90] but can similarly be conducted on the surface of a microparticle [68]. The latter is hereby grafted with specific binding sites prepared to selectively capture the biomolecules of choice. These can subsequently be detected via a third layer of labeled bioactive molecules

[40]. The capture efficiency of this approach is limited by the number of binding sites present at the particle surface as well as by the amount of particles in the solution. But since the main interest in bioanalysis is an ever increasing sensitivity of detection resulting in a continuously lowered limit of detection, this presents rather a challenge than a drawback.

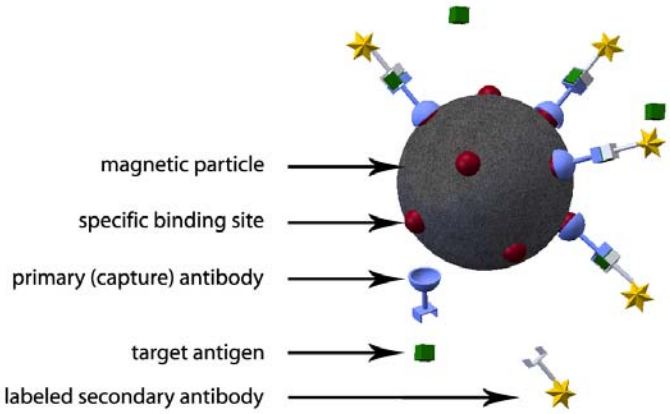

Figure 5.1 Sandwich immuno-sorbent assay on a microparticle. Fluorescent or chemoluminescent labels allows the quantification of the captured sample.

Binding via surface charges

In addition to the use of specifically functionalized microparticles, the temporary modification of the particles' surface properties due to changes of pH or surface charge can be used to capture biomolecules of choice. A well studied application is the binding of DNA molecules to a silica surface in the presence of chaotropic salts, such as guanidine or sodium iodine [14, 95, 175]. This binding mechanism is specific to nucleic acids, while other molecules present in a sample of lysed cells, e.g. proteins and lipids, remain free in solution. The main driving mechanisms of the DNA binding are hereby the shielding of intermolecular electrostatic forces, the dehydration of DNA and silica surfaces, and the formation of intermolecular hydrogen bonds in the DNA-silica contact layer. The advantage of this method is the possibility of releasing the captured biomolecules by simply changing the properties of the surrounding medium.

5.1.2 Bioanalysis in Droplets

Besides the capture of biomolecules, bioanalytical protocols require a range of other standardized steps, including sample processing and detection as presented in Figure 5.2. Furthermore, these steps need to be separated by washing stages in order to prevent cross-contamination and

carry-over effects. When transferring the steps of a bioanalytical protocol similar to the schematics of Figure 5.2 into the droplet manipulation system, the immobilized droplets will serve as microreservoirs for the solutions required in the different stages. Since the on-chip washing is an important issue, attention needs to be paid to its efficiency.

Figure 5.2 Schematics of the steps common to bioanalytical protocols.

Washing in the droplet manipulation system occurs via continued dilution of the liquid fraction transferred from one immobilized droplet to the next. In consequence, a 2 µl droplet will be diluted six-fold upon mixing with an immobilized droplet of 10 µl. In a second washing stage, the fraction of the six-fold diluted droplet is further thinned out at the same ratio. Figure 5.3 shows the effect of the washing procedure on the chip. We see that the blue dye is highly diluted after the third washing stage. For the subsequent experiments, the number washing steps is set to three, as a compromise between the cleanness of the sample and the number of washings steps the system can provide.

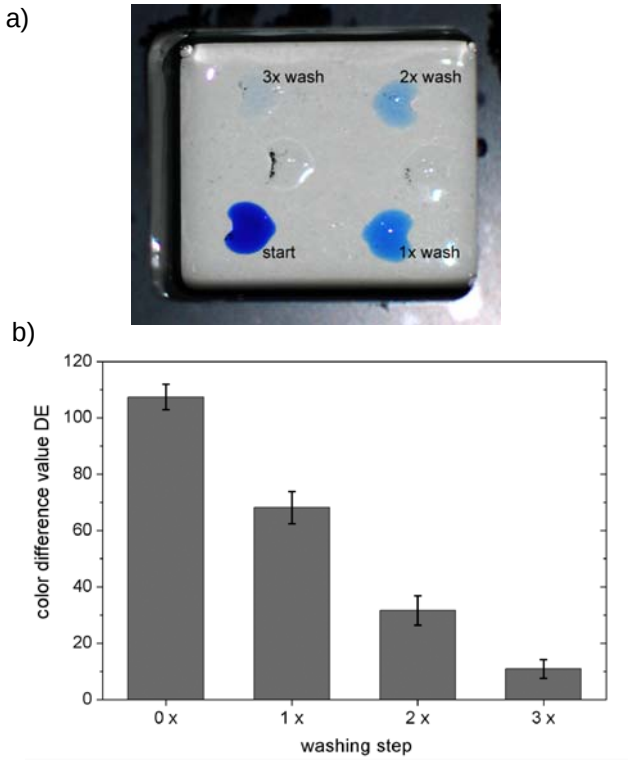

Figure 5.3 Effect of the on-chip washing via continued dilution. (a) The blue tint of the initial droplet (start) is diluted in the subsequent washing steps. (b) Color evaluation of the washing steps presented in (a).

5.2 DNA Purification and Extraction

adapted from the journal article: U. Lehmann, C. Vandevyver, V.K. Parashar and M.A.M. Gijs. Droplet-Based DNA Purification in a Magnetic Lab-on-a-Chip. Angewandte Chemie International Edition 45, 19 (2006), 3062-3067.

Integrated on-chip DNA purification - starting from raw cell samples - is of high interest for miniaturized bioanalysis applications, since current chip-based devices for Polymerase Chain Reaction (PCR) require pure DNA samples for a successful DNA amplification [30, 91]. In that context, several promising adsorption-based separation techniques employing the binding of DNA to silica surfaces have been reported recently [17, 175, 197]. Their application in on-chip systems offers an alternative to work-intensive traditional methods, such as phenol extraction procedures. However, the majority of these devices employ microfluidic channels for the handling of the various reagents, which limits their flexibility with respect to scalability and reconfigurability [73]. The combination of a particle-based adsorption technique with the manipulation of liquids in small discrete volumes (microdroplets) can provide an alternative solution.

In the following, a system is described, which enables the extraction and purification of DNA from a crude sample. The DNA is hereby bound temporarily to the surface of the magnetic particles via the chaotropic salt induced variation of the surface charges, and the magnetic actuation allows the transfer of the particle-and-DNA complex from one on-chip microreservoir to the next.

5.2.1 Protocol and Materials

The on-chip procedure for the extraction and purification of nucleic acids follows a standard protocol using silica coated magnetic beads and the reagents provided by a commercial kit (Roche MagNA Pure LC DNA Isolation Kit I) [154], with volumes and reaction times adapted to suit the chip-based droplet manipulation setup, described in Chapter 4. As a consequence of the geometric constraints determined by chip's dimensions, the procedure employs six stations for droplet merging, mixing and splitting. The different buffer solutions required for the binding, washing and elution steps are present on the chip in the form of immobilized droplets of 10 µl volume. Figure 5.4 summarizes the complete procedure schematically. It involves DNA-to-particle binding

(Figure 5.4 a), particle washing steps (Figure 5.4 b) and the elution of the DNA from the particles (Figure 5.4 c). Following the chosen protocol, the sample DNA is bound to the silica beads after chemical cell lysis in a colored guanidine thiocyanate (GuSCN) binding buffer (position 1).

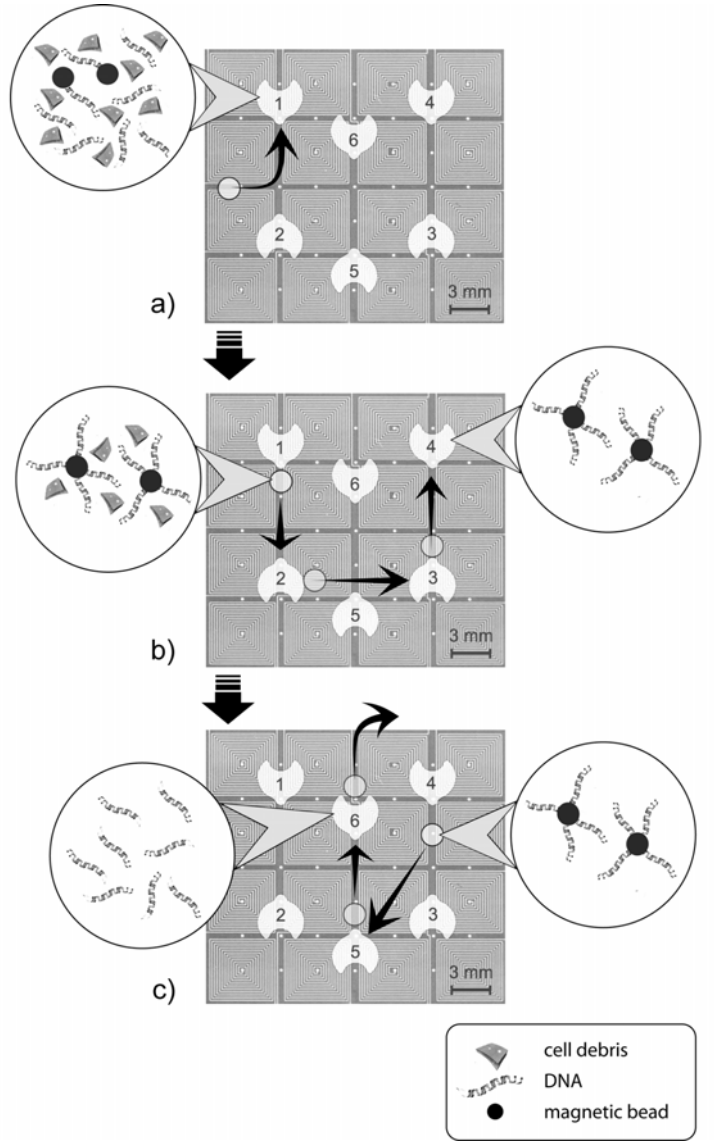

Figure 5.4 Schematics of the DNA purification from a lysed cell sample solution: (a) the binding of the DNA to the magnetic particles in the binding/lysis buffer (position 1) is followed by (b) a series of three washing steps to remove any transferred cell debris, proteins and lipids (positions 2-4). Finally, (c) the DNA is removed from the magnetic beads via magnetic agitation in two immobilized droplets of elution buffer (positions 5-6) and, subsequently, the magnetic particle droplet is extracted from the chip.

After binding, a small droplet containing the particle-and-DNA compound is extracted from the binding site and passed through a series of immobilized droplets of washing buffers (positions 2-4) to remove cellular debris, proteins and lipids. For that purpose, the first washing site

(position 2) contains ethanol (30 - 40 %) and guanidinium hydrochloride (1.5 %), while the following two sites hold only ethanol (50 %) (position 3-4). The composition of the oil medium surrounding the droplets prevents in this case the ethanol from diffusing out of the immobilized microreservoir.

Finally, the cleaned particle-bound DNA is mixed with droplets containing low-ionic strength elution buffer or water (positions 5-6), which leads to a separation of the DNA from the particles. After a final separation step, the magnetic particles are extracted from the system. The eluted DNA can be detected on- or off-chip via a fluorescent marker, or used for subsequent amplification.

5.2.2 Results and Discussion

The performance of the system is characterized with respect to its ability to successfully carry out the stages of the DNA extraction and purification protocol. Attention is hereby paid to the questions, if a sufficiently high fraction of the sample DNA is bound to the particles silica surface during the first step and if the bound DNA can be transported through the washing steps and afterwards be released in the elution buffers. These problems are studied using different types of DNA material of increasing complexity:

- ***Hind*III-digested λ-phage DNA** purchased from Gibco® Invitrogen Cell Culture (Carlsbad, CA)
- **Human Genomic DNA fragments** (> 50 kb) purchased from Promega (Madison, WI)
- Cell lysates prepared from **Jurkat cells** (ATCC TIB-152).

The eluates, obtained after the completion of the protocol (position 5-6 in Figure 5.4 c)), are either extracted from the chip subjected to further off-chip detection steps, or examined directly on-chip. The off-chip detection includes the DNA quantification via the PicoGreen® dsDNA Quantitation kit (Molecular Probes) with the help of a microplate fluorometer (Cytofluor® series 4000, Perceptive Biosystems) using wavelengths of 485 nm and 530 nm for excitation and emission respectively. For the genomic DNA and the Jurkat cell DNA an additional PCR is performed off-chip in order to examine the purity and intactness of the extracted DNA[6]. For on-

6. The preparation of the DNA and cell samples as well as the off-chip measurements (fluorometer and PCR) were performed by C. Vandevyver.

chip detection the PicoGreen® reagent is added to the immobilized elution droplets and examined via a fluorescent microscope setup (Zeiss Axiovert S100 with Hamamatsu Orca-ER digital camera).

Capture Efficiency

Capture efficiency

The binding step's performance is evaluated by quantifying the DNA bound to the magnetic particles during the initial binding step. For this measurement, magnetic particles are actively mixed with the binding buffer for three minutes and are extracted from the chip after the splitting step. Off-chip, the extracted particles are subjected to the remaining protocol steps, washing and elution - using the reagent volumes of the macroscopic procedure - and the obtained eluate is subsequently evaluated. The fluorometer measurements, summarized in Figure 5.5, show that more than 70 % of the initial DNA can be recovered from the particle surface, demonstrating the efficiency of the on-chip binding step driven by the presence of the chaotropic salt.

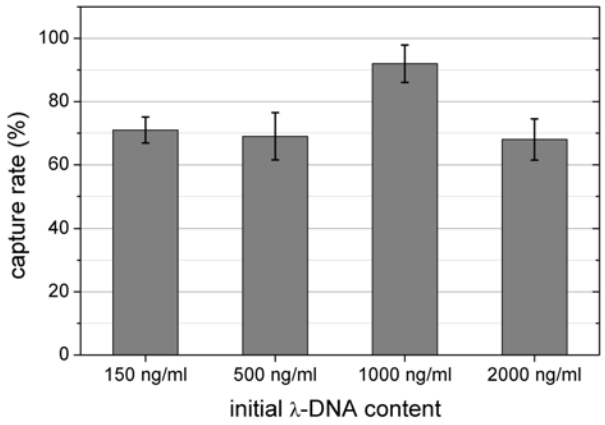

Figure 5.5 Capture efficiency of the binding step for different concentrations of *Hind*III-digested λ-phage DNA at a constant amount of magnetic particles (200 µg, Roche). The bound DNA is recovered off-chip and is quantified using PicoGreen reagent and a fluorometer.

The lower capture efficiency for the smaller DNA concentrations is explained by the decreased probability for contacts - and in consequence binding events - between the magnetic particles and the λ-DNA molecules [79]. For higher concentrations these contacts occur more often, but the probability for the binding sites being already occupied rises as well, which in total leads to a lowered capture efficiency. Thus there exists an optimum concentration, where the probability for the contact of biomolecules with free binding sites is highest. Our measurements

indicate that in the system, presented here, such an optimum occurs at a λ-DNA concentration of 1000 ng/ml.

Processing λ-DNA

λ-DNA

The next stage is the introduction of the full protocol into the droplet manipulation system. Since the successful capture of the λ-DNA in the first step had been shown, the same type of DNA is used in the first set of experiments. Different concentrations are subjected to subsequent steps of binding, washing and elution stages and the eluate is extracted from the chip and quantified in the microplate fluorometer. The off-chip quantification requires an additional dilution step, since the equipment cannot handle the small liquid quantities extracted from the chip. In consequence, 20 µl of PBS and 25 µl of PicoGreen reagent are added to the extracted eluate of 5 µl volume. Since the dilution factor is known, the measured DNA content on the microtiterplate can be converted into the DNA content of the eluate. The fluorescent signal detected by the fluorometer is hereby converted into the actual DNA content via a standard curve measured on the same titer plate. Due to the additional dilution and the small eluate volume, the signal obtained from the eluates is close to the fluorometer's lower limit of detection. This requires the use of comparatively high initial DNA concentrations in the sample droplet. The sum of the DNA contents measured in the extracted liquids of the two final elution steps (see Figure 5.4) is presented in Figure 5.6.

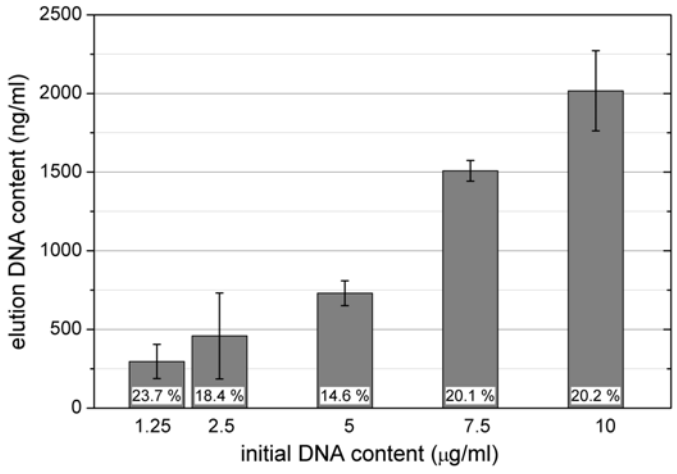

Figure 5.6 Off-chip measurement of the λ-DNA content in the eluates for different initial sample concentrations. The recovery rate (ratio between recovered and initial DNA) is indicated at the bottom of each column, which represent the average amount of recovered DNA while the error bars show the variation between the different measurements.

We see that the quantity of DNA recovered from the particles after washing and elution amounted to around 25 % of the initial DNA content in contrast to 70 - 90 % measured directly after the binding step. The loss of DNA results from an irreversible attachment of molecules to the particles as well as the loss of molecules during the washing steps. Moreover, the additional handling of the eluates can lead to an attachment of molecules to the plastic pipette tips, which further reduces the DNA content.

Complementary, an on-chip fluorescent quantification step is performed by adding 10 µl of the PicoGreen reagent to the eluates on the chip. After a reaction time of t = 5 min the signal is measured via a fluorescent microscope and is compared with a previously prepared reference curve (standard). The sum of the DNA contents of the two eluates (Figure 5.7) shows a recovery rate of nearly 50 %, which is significantly higher than the value measured off-chip. The high value of 78.7 % obtained for the lowest DNA content (1250 ng/ml) can be linked to the higher capture rate measured for this concentration range, as discussed above. However, also for the on-chip fluorescent detection the small sample volume and DNA content result in a signal close to the lower limit of detection determined by the technological limits of the camera.

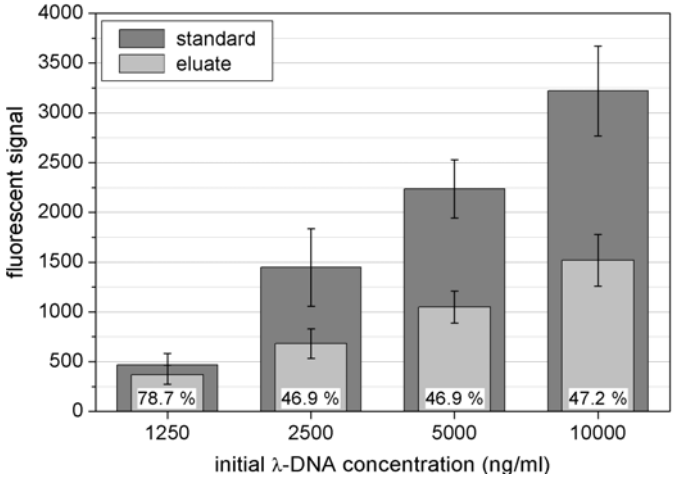

Figure 5.7 On-chip measured λ-DNA content in the eluates for different initial sample concentrations. The columns represent the average of at least five measurements with the error bars indicating the variation. The fluorescent signal is measured with reference to the background. The recovery rate is shown at the bottom of each column.

The better recovery rate demonstrates that the direct on-chip handling and evaluation of liquids containing biomolecules can lead to a higher

yield and sensitivity of the detection process, because the number of handling steps involving potentially absorbing surface is significantly reduced. The consequential improvement of the system's performance proves the advantage of a Lab-on-a-Chip system.

Processing human-genomic DNA

Human-genomic DNA

The subsequent step is the study of the performance of the on-chip DNA extraction and purification when using longer stranded human-genomic DNA. Following the procedure tested using λ-DNA, we perform the capturing, washing and elution steps using varying sample concentrations. Also in this case a fraction of the elution droplets is removed from the chip after the experiments and evaluated off-chip.

The fluorometric measurements, presented in Figure 5.8, show that we recover 25 % of the initial DNA in the elution buffers. This result is equal to the off-chip evaluation of the λ-DNA (Figure 5.6) and we can conclude that the system's performance is insensitive to the length of the DNA fragments.

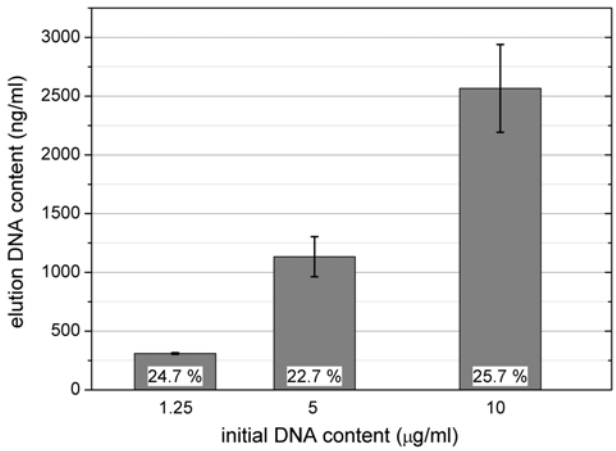

Figure 5.8 Off-chip fluorescent measurement of the DNA content of the eluates for different initial concentrations of human-genomic DNA. The recovery rate (ratio between recovered and initial DNA) is indicated at the bottom of each column, which represent the average amount of recovered DNA while the error bars show the variation between the different measurements.

The additional on-chip fluorescent measurements, presented in Figure 5.9, also show the improved DNA recovery observed during the λ-DNA experiments. As in the earlier measurements, we obtain a higher recovery for the lowest DNA concentration, which can be linked to the dependence of capture rate on the DNA concentration. The generally higher DNA content in the eluate as compared to the off-chip measurement

demonstrates afresh the system's increased efficiency as a consequence of the elimination of additional pipetting steps.

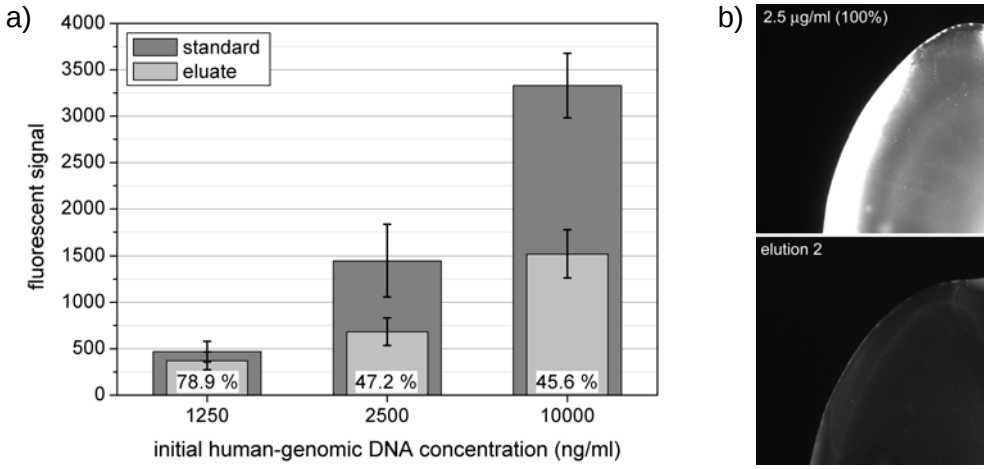

Figure 5.9 On-chip fluorescent detection. a) measured fluorescence of the eluates for different initial concentrations of human-genomic DNA (exposure time: 2.46 s). The columns represent the average of at least five measurements with the error bars indicating the variation. The fluorescent signal is measured with reference to the background. The recovery rate is shown at the bottom of each column. b) photographs of the fluorescent signal of the on-chip PicoGreen reaction for (top) a 20 µl droplet containing 10 µl of 2.5 µg/ml DNA solution and 10 µl PicoGreen reagent and (bottom) a 20 µl droplet containing 10 µl of the eluate E2 of initially 2.5 µg/ml DNA solution and 10 µl PicoGreen reagent.

Processing raw cell samples (Jurkat cells)

Jurkat cells

After the successful evaluation of the handling of human-genomic DNA, we examine the system's capability to extract DNA from raw cell samples. For this purpose, different amounts of Jurkat cells are added to the binding buffer solution, where they are chemically lysed in order to free the DNA from the cell compound. According to theory, the DNA is expected to selectively bind to the magnetic particles' silica surface as a result of the presence of the guanidine thiocyanate (GuSCN).

As done for the experiments using pure DNA, the eluate is extracted after the experiments and studied off-chip in the microplate fluorometer. The small sample volume processed on the chip allows hereby the examination of small numbers of cells. Starting with 1000 cells per 10 µl droplet, the number is subsequently decreased to 500 and finally to 100 cells per experiment. With a DNA content of 6 pg per cell[7], the DNA concentration in the droplet holding the lysed sample ranges therefore

7. http://www.medizin.uni-tuebingen.de/virologie/exp_viro/Exp_Viro_de/Forschung/Sonstiges/Useful_remarks.html

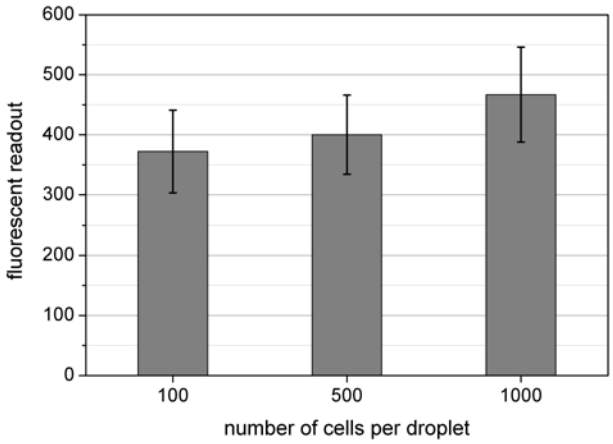

Figure 5.10 Off-chip fluorescent measurement of the DNA content of the eluates for different amount of Jurkat cells contained in the sample. The columns represent the average of several measurements at the same initial cell content, while the error bars show the variation between the different measurements.

from 60 ng/ml for 100 cells to 600 ng/ml for 1000 cells. The microplate fluorometer measurements indicate a visible difference for the three cell concentrations, as shown in Figure 5.10. Since, however, the fluorescent signals are very close to the lower limit of detection, the quantification of the DNA content for the smaller cell numbers is not entirely possible.

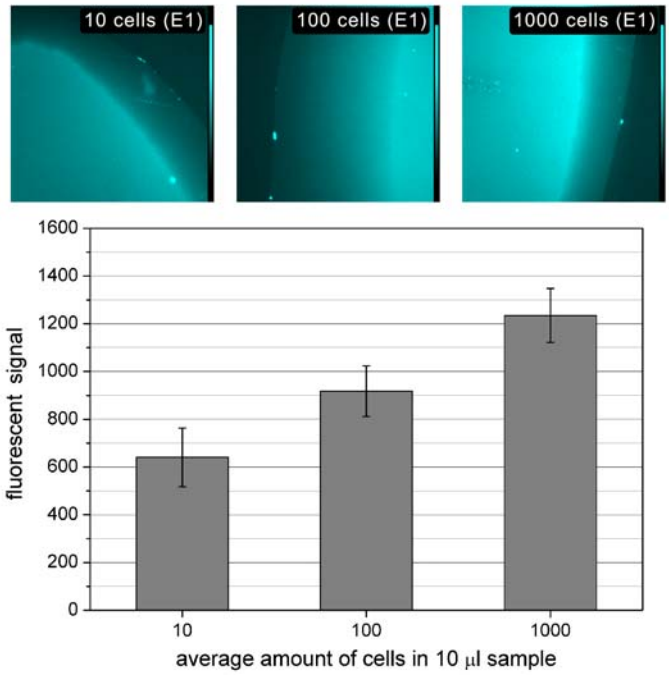

Figure 5.11 On-chip fluorescent detection of the DNA recovered from a raw cell sample containing different amount of Jurkat cells. (E1: first elution). The exposure time was set to 10 s. The columns represent the average of at least five measurements with the error bars indicating the variation. The fluorescent signal is measured with reference to the background. The top row presents fluorescent images of the first eluate for different initial cell contents.

Based on the measurements for pure cell samples, we examine the possibility of improving the detection limit, by evaluating the eluate's DNA content directly on the chip. For these measurements we lower the minimum number of cells in the sample droplet to 10, which amounts to a total DNA content in the sample droplet of 60 pg. The experiments demonstrate the increased sensitivity of this approach, since we can clearly distinguish the three different cell contents ranging from 10 to 1000 cells, as shown in Figure 5.11. However, the necessary long exposure time of 10 s indicates also in the case of on-chip detection the proximity to the lower detection limit of the fluorometric setup.

Testing the quality of the extracted DNA via PCR

The successful extraction and purification of DNA from raw cell samples is an important preliminary step for the amplification of DNA-fragments of interest. A common method for DNA amplification is PCR, which however is highly sensitive to contaminants such as proteins, cell debris or chaotropic salts. For this reason, PCR will be a suitable means for testing the purity of the sample obtained in the elution step, while at the same time verifying its quality.

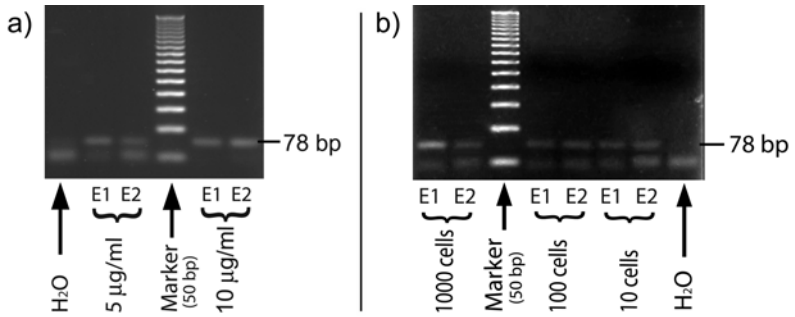

Figure 5.12 Agarose gel electropherograms of human β-actin after 35 cycles of PCR starting from 3 µl of eluate obtained from samples containing (a) human genomic DNA fragments (> 50 kb) and (b) Jurkat cells (ATCC TIB-152). (E1, E2: first and second elution, bp: basepairs).

Therefore, we perform an off-chip PCR procedure using 5 µl fractions of the eluates. Figure 5.12 presents the agarose gel electropherograms obtained after the PCR of the recovered human-genomic DNA and the DNA extracted from the Jurkat cells. The amplified fragment is human-β actin, which has a length of 78 basepairs (bp). We see, that in both cases the DNA was intact and also sufficiently clean to be successfully amplified. Even though PCR is a qualitative and not quantitative test, the small amount of DNA, used in the amplification, leads to differences in

the amounts of the primers consumed in the reaction. The larger DNA content in the experiments with human-genomic DNA consumed all primers during the amplification, which can be told by the absence of the lowest band in the electropherogram, see Figure 5.12 a). In the case of 10 Jurkat cells, the primer band is still clearly visible in Figure 5.12 b), since only a fraction of their volume has been consumed during the amplification.

5.2.3 Conclusion

The successful DNA amplification step demonstrates the capability of the droplet manipulation system to perform a standard DNA extraction and purification protocol in a miniaturized format. The modular setup allows hereby the transfer of the reaction unit to a fluorescent microscope, which permits the on-chip examination of the DNA in the eluates. We showed that the elimination of additional handling steps leads to a higher system effectivity, since less DNA is lost through the contact with plastic surfaces such as pipettes, vials and titerplates.

An advantage of the droplet manipulation system is its capability to use the same reagents as the standard protocol for the DNA extraction and purification, while strongly reducing the amount of reagents required. Thus non-specialists can easily apply the system for miniaturized bioanalysis and evaluate the results with respect to known macroscopic benchmarks. A comparison with the data sheets of the DNA extraction kit [154], used as a basis for the experiments, shows that the miniaturized system‘s sensitivity is 10^4 times higher. It is capable of detecting the DNA extracted from as little as 10 cells while the macroscopic system requires at least 10^5 cells for successful DNA recovery.

5.3 On-chip antibody binding and detection

adapted from the journal article (with permission from Elsevier): U. Lehmann, D. de Courten, C. Vandevyver, V.K. Parashar and M.A.M. Gijs. On-chip antibody handling and colorimetric detection in a magnetic droplet manipulation system. Microelectronic Engineering 84, 5-8 (2007), 1669-1672.

In bioanalysis, antibodies are generally detected via immuno-assays. Among those, the enzyme-linked immuno-sorbent assay (ELISA) is the most commonly used [40]. In a sandwich ELISA protocol (Figure 5.1), the target antigens in the sample bind to specific markers (capture antibodies), which are grafted to a surface. In a subsequent step, the bound sample molecules are used to capture labeled specific antibodies, whose labels allow the quantification of the complex [90]. The labels present in the third layer are either enzymes, which lead to a colorimetric or fluorescent reaction, or fluorescent markers or metallic labels, which can be directly measured. In a macroscopic approach the reaction takes place in a titer plate, whose surface serves as the binding site for the assay. In contrast to using a stationary binding platform, magnetic particles can be used as anchors for the assay and instead of changing the liquids in the reservoir, the particles are transported through the various reagents [68].

Since the processes for capturing the antibodies and building the assay are rather straightforward, the main challenge is the detection step. Based on standard protocols we chose to examine the feasibility of the on-chip colorimetric detection of the labeled antibodies as used in the final step of an ELISA procedure. Figure 5.13 shows the principle of the detection, where the presence of an enzyme labeled antibody leads to a color change of a specific chromogen.

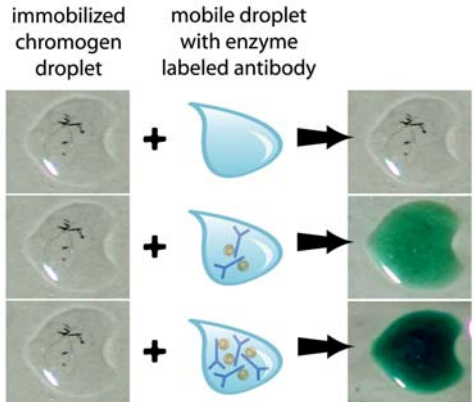

Figure 5.13 Principle of the on-chip antibody detection. Enzyme-labeled antibodies lead to a color reaction of a chromogen in the immobilized droplet, which is proportional to the concentration of the labeled antibody.

5.3.1 Protocol and Methods

Colorimetric Reaction

The reaction used to determine the amount of antibody is the enzyme induced color change of a chromogen. Such colorimetric reactions are widely used in enzyme-linked immuno-sorbent assays (ELISA) [40, 90], since they provide an easily readable optical signal.

For the experiments presented in this section, the 2,2'-Azino-bis[3-Ethylbenzthiazoline-6-Sulfonic acid] (ABTS) liquid substrate system for ELISA (SIGMA A3219) is used as the chromogen, which gives a blueish tint (absorbance maximum at 405 nm) upon reaction with peroxidase. Since the detection antibody needs to be labeled with the suitable enzyme, Rabbit Anti-Mouse Immunoglobulin coupled to Horseradish-Peroxidase (HRP) (DAKO PO260, 1.3 g/L) is chosen for the experiments. This antibody specifically binds to mouse antigens, e.g. antibodies produced by a mouse, and has been obtained from a rabbit, which makes it in turn express rabbit antigens.

Colorimetric Detection

The color change of the chromogen can be measured via colorimetry, which describes the numerical specification of the color as a physically defined stimulus in a way that:

- stimuli with the same specifications look alike to an observer with normal color vision, and vice versa
- the number comprising the specifications are continuous functions of the physical parameters defining the spectral radiant power distribution of the stimulus

Thus the color change of a chromogen arising from an enzymatic reaction can be colorimetrically quantified and related to the concentration of biomolecules in the solution. The color change can be determined via absorbance measurements, which require specialized equipment such as a spectrophotometer, or via the evaluation of the color of the reagent recorded by a CCD camera.

CIE Lab color space

The latter offers a higher flexibility with respect to the experimental setup, but requires a systematic approach to numerically represent and compare the color changes recorded during the experiment. A convenient method is the evaluation of the color coordinates in a suitable color space system.

Since illumination and background color can vary between experiments, a system needs to be chosen, where the influence of these variations can be easily eliminated. One such color system is the CIE Lab color space [200], which is up to now the most complete color model used conventionally to describe all the colors visible to the human eye. It was developed by the International Commission on Illumination (Commission Internationale d'Eclairage - CIE)[8].

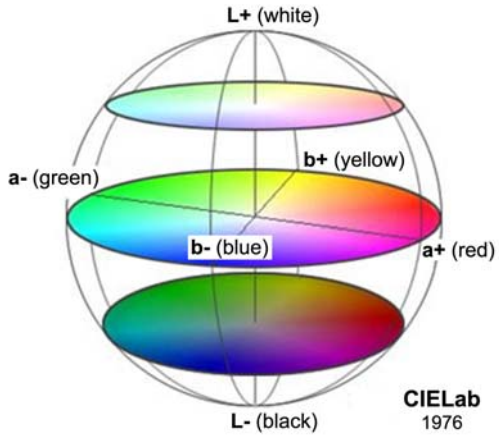

Figure 5.14 Schematic visualization of the CIE Lab color space as described by the Commission Internationale d'Eclairage (CIE)

Figure 5.14 shows the schematic structure of the color space, whose three basic coordinates represent the lightness of the color *L* (L = 0 yields black and L = 100 indicates white), its position between magenta and green *a* (negative values indicate green and positive values indicate magenta) and its position between yellow and blue *b* (negative values indicate blue and positive values indicate yellow). Thus the difference between two colors can be described by the euclidic distance of their corresponding positions in the CIE Lab color space.

Euklidic distance

$$DE = \sqrt{(a_1 - a_2)^2 + (b_1 - b_2)^2 + (L_1 - L_2)^2} \tag{5.1}$$

with the coordinates *a*, *b* and *L* of the respective colors (1) and (2).

Conversion from the RGB color space to the CIE Lab system

Since the photographs taken by a CCD camera are generally in the RGB format the color must be converted into the CIE Lab color space in order to apply equation (5.1). The conversion can be performed in two steps,

8. http://www.cie.co.at/index_ie.html

with the RGB colors firstly being translated into the CIE XYZ system[9] via a 3x3 matrix transform (equation (5.2)), and the CIE XYZ colors subsequently being converted into the CIE Lab coordinates, according to the algorithm given by equation (5.3) [200].

Conversion Matrix

$$\begin{pmatrix} X \\ Y \\ Z \end{pmatrix} = \begin{pmatrix} 0.412453 & 0.357580 & 0.180423 \\ 0.212671 & 0.715160 & 0.072169 \\ 0.019334 & 0.119193 & 0.950227 \end{pmatrix} \cdot \begin{pmatrix} R \\ G \\ B \end{pmatrix} \tag{5.2}$$

The conversion of CIE XYZ into CIE Lab requires the tri-stimulus values X_n, Y_n and Z_n of the nominally white object. Therefore a reference white spot in the image can be used to create an adaptable white point independent of environmental parameters. Upon the conversion of different images of a colorimetric reaction, the color of a region of interest can be compared by evaluating the euclidic distance DE. The mathematical approach to the color conversion and evaluation allows hereby the automatization of the detection process.

Conversion Factors

$$\begin{aligned} L &= 116 \cdot \left(\frac{Y}{Y_n}\right)^{\frac{1}{3}} - 16 && \text{for} \quad \frac{Y}{Y_n} > 0.008856 \\ L &= 903.3 \cdot \frac{Y}{Y_n} && \text{otherwise} \\ a &= 500 \cdot (f(X/X_n) - f(Y/Y_n)) \\ b &= 200 \cdot (f(Y/Y_n) - f(Z/Z_n)) \\ \text{where } f(t) &= t^{\frac{1}{3}} && \text{for} \quad t > 0.008856 \\ f(t) &= 7.787 \cdot t + \frac{16}{116} && \text{otherwise} \end{aligned} \tag{5.3}$$

Based on the above conversion algorithm a MatLab program is developed, which allows the automatic evaluation of multiple RGB images recorded during the reaction. The advantage of the conversion of the RGB images into the CIE Lab format is the inherent possibility of eliminating environmental influences such as variations of the illumination between experiments [200].

9. CIE XYZ color space is the cone-shaped space formed by (X, Y, Z)-weights, that when applied to the CIE primaries, match any visible color. The three standard primaries, defined by CIE in 1931 and called X, Y, Z, can be used to match, with only positive weights, all visible colors. The Y primary is intentionally defined to have a color-matching function that exactly matches the luminous-efficiency function of the human eye.

5.3.2 Results and Discussion

In order to study the feasibility of quantifying antibodies via a colorimetric reaction in the droplet manipulation system, the first set of experiments did not employ magnetic microparticles, but concentrated on the dependence between the color change and the antibody concentration. Figure 5.15 shows a photograph of six chromogen droplets after a reaction time of t = 15 minutes for different concentrations of the HRP labeled antibody. We can clearly observe the difference in the color intensity between the different antibody contents.

Figure 5.15 Photograph of the chromogen droplets after the reaction with different concentrations of enzyme-labeled antibody. The incubation time was 15 min. (The dilution ratio 1:1000 corresponds to a concentration of 1300 ng/ml).

We see that after a reaction time of only 15 minutes, a visual detection of an antibody concentration of as low as 3.6 ng/ml is easily possible. The conversion of the color change into the CIE Lab coordinates and the euclidic distance of each droplet color from the initially clear droplet leads to the reference curve for the antibody detection.

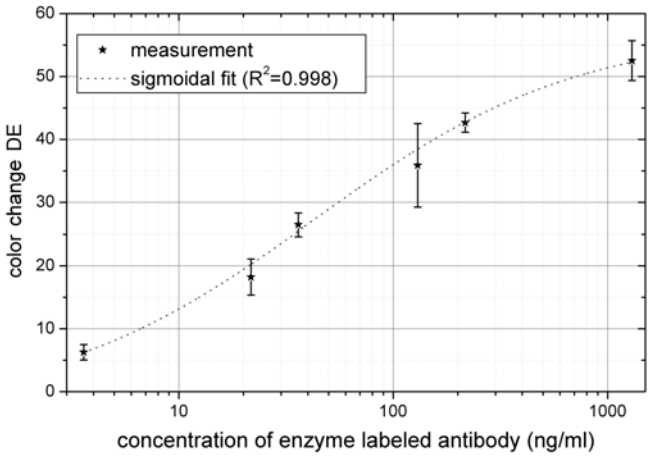

Figure 5.16 Reference curve for the colorimetric on-chip detection of enzyme labeled antibodies after a reaction time of 15 min.

The reference or standard curve presented in Figure 5.16 shows the sigmoidal behavior expected for this type of reaction [40]. The range of detection spans more than two orders of magnitude, which is in excellent agreement with literature [42, 179].

Due to the small sample volume of only 2 µl, which is injected into the detection droplets of 10 µl volume, the total amount of detected antibodies is very small. In the case of the lowest measured concentration of 3.6 ng/ml, the effective amount of labeled antibodies in the droplet is therefore only 7.2 pg. Since the use of magnetic particles allows a pre-concentration of the biomolecules via an incubation and capture step, a significantly lower concentration of the initial sample material could be easily measurable.

The high sensitivity of the detection also demonstrates the importance of an efficient washing procedure between the labeling step and the colorimetry step, because a non-specific transfer of the enzyme labeled antibodies will influence the measurement. In that respect, a set of experiments is conducted to study the non-specific antibody transfer via the extraction of a liquid fraction during the droplet splitting. The antibody concentration in the extracted fraction can be lowered via continued dilution, by passing the magnetic particles through a series of immobilized droplets containing PBS or distilled water. The effect of the continued dilution is shown in Figure 5.17, where the strength of the color change decreases with the increasing number of washing steps performed before the detection step.

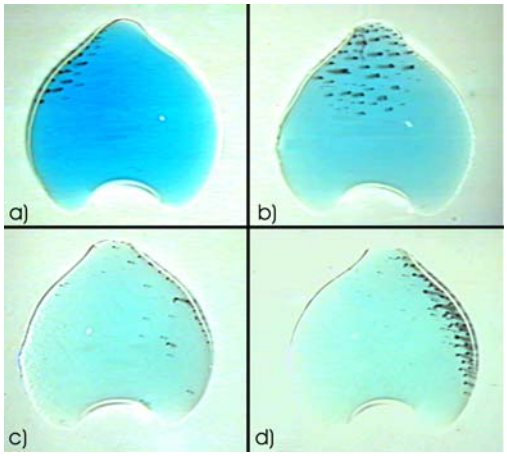

Figure 5.17 Photographs of the chromogen droplet for the detection of Rabbit Anti-Mouse Immunoglobulin-HRP showing the color reaction with increasing dilution due to a row of washing steps: a) initial concentration (0.13 µg/ml), b) after one dilution step, c) after two dilution steps, d) after three dilution steps. The reaction time was 15 min in each case.

The dilution factor can hereby be estimated according to the amount of magnetic material introduced into the system. Following the measurements of the droplet volume during droplet splitting, as presented in Chapter 4, we can determine the volume of an extracted droplet depending of the amount of magnetic material injected into the system. Based on this knowledge, the experiments presented in Figure 5.17 are conducted with 2 µl of sample solution containing 300 µg of magnetic particles (150 mg/ml). According to Figure 4.26, the volume of the extracted droplet is therefore 2 µl, which results in a dilution factor of 6 for each washing step. Based on the calculated dilution factor, we can evaluate the enzyme-induced color change of the chromogen droplet after different numbers of dilution steps and compare it with the reference presented above.

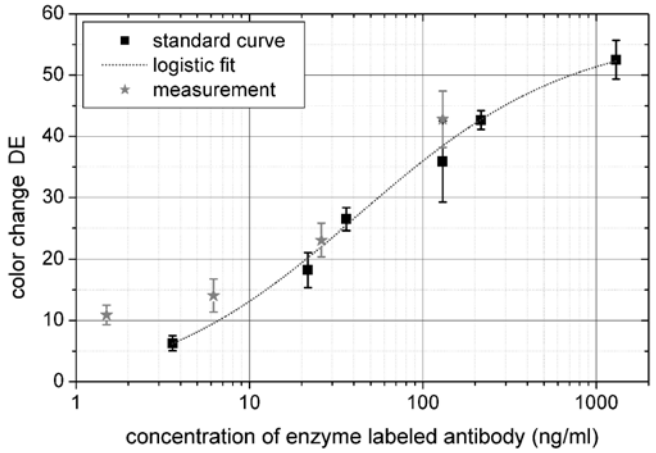

Figure 5.18 Color change of the chromogen for different concentration of enzyme labeled antibodies in solution obtained via continued dilution. The line represents a logistic fit of the reference measurement (standard).

The measurements are summarized in Figure 5.18 and plotted together with the reference curve. We see that both curves show a similar behavior, but we also note that for a higher number of washing steps, the measured color change is higher than expected. When compared with the reference, we can calculate a total offset of 9 pg of enzyme-labeled antibodies per measured sample droplet of 2 µl. The offsets may result from an unspecific binding of the antibodies to the particle‘s silica surface [57] at a ratio of 30 fg per µg of magnetic particles, since the particles had been mixed for a long time with the sample before the injection into the system. Additionally, the dilution factor might vary due to fluctuations in the size of the transferred droplet.

In order to study the influence of the mixing time on the unspecific carry-over of antibodies between different droplets due to unspecific binding, a set of experiments is prepared, where the particles are mixed with the sample solution on-chip (set 1) and also off-chip (set 2). Since the particles of set 1 are in contact with the sample for a significantly shorter time-span than the particles in set 2, we expect less difference to the reference curve and thus less unspecific binding for the measurements performed with the particles of set 1.

These experiments are performed with comparatively high concentrations (> 100 ng/ml), which allows a reduction of the reaction time [102]. A row of measurements, presented in Figure 5.19, indicates in that respect the dependence between reaction time and detection range. We additionally learn about the dynamics of the color reaction, which depend on the amount of bio-active molecules present in the solution. For a high concentration (1250 ng/ml) the color changes reaches its maximum value after two minutes, while a lower concentration (156 ng/ml) the color change still continues after five minutes. A reaction time of five minutes offers a sufficiently large range of detection and presents thus an acceptable compromise between detection delay and signal strength.

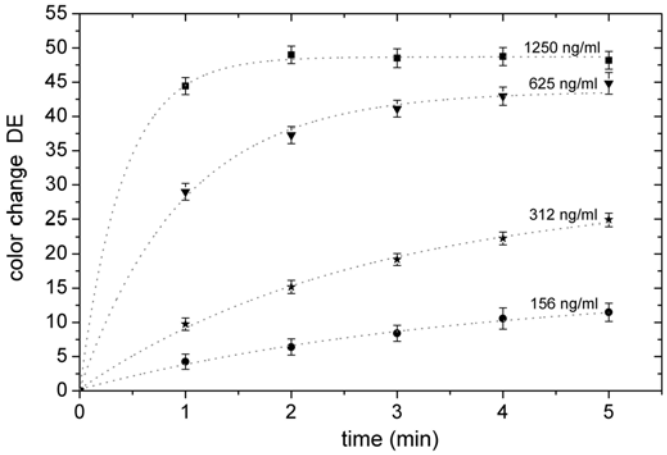

Figure 5.19 Color change due to transferred enzyme labeled antibodies depending on the reaction time and antibody concentration.

Based on a reaction time of five minutes a new standard curve is determined, which can be compared to the color changes measured for the differently treated particles. During the experiments, the particles of set 1 are injected onto the chip and merged with an immobilized sample droplets. After a short mixing step (t_{mix} = 1 min) a small liquid fraction is extracted, subjected to a washing step and transported to an immobilized

chromogen droplet, where the color reaction is studied. In contrast, the particles of set 2 are mixed with the sample solution for 15 minutes off-chip, and a 2 µl droplet containing 300 µg of magnetic particles is injected onto the chip. Here, the sample droplet is merged and mixed for a duration of t_{mix} = 1 min with an immobilized water droplet (washing step) and a subsequently extracted liquid fraction is transported to an immobilized chromogen droplet.

The results of the different measurements are summarized in Figure 5.20, where a clear difference between the short-time and long-time contact of the particles with the antibody solution can be seen. While the color change induced by set 1 (mixing of particles and sample for 1 min) is in very good agreement with the reference curve, the color change induced by set 2 (particles mixed with sample for 15 min) shows an off-set from the reference curve.

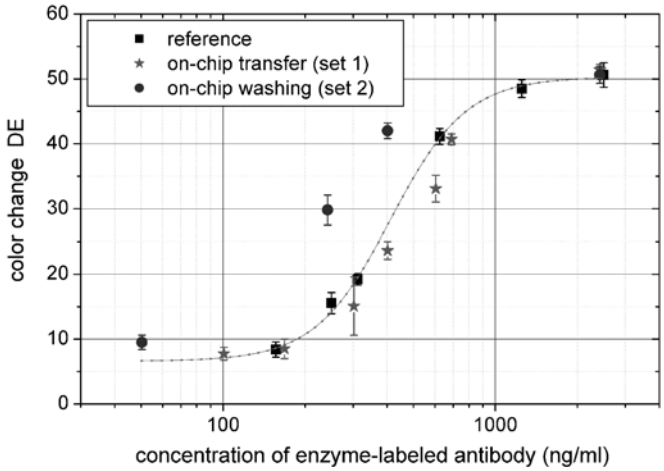

Figure 5.20 Comparison of the color change measured after a reaction time of 5 min for different sample transfer mechanisms. The line represents a logistic fit of the reference measurement (standard).

The measurements show that the comparatively short washing step suffices to dilute the liquid fraction of set 1, whereas the set 2 samples require a longer washing step. This indicates the importance of adjusting the ratio of incubation and washing times for the on-chip procedure.

On-chip ELISA

In consequence, upon implementing the labeling, washing and detection steps into the droplet manipulation system, the different reaction times are set to 3 min for the incubation, 1 min for each of the three washing steps and 10 min for the detection. This results in a duration of 20 min for the on-chip section of the ELISA protocol. The magnetic particles are in that case activated off-chip and incubated with the sample solution.

During the activation step, the magnetic particles (Masterbeads Carboxylic Acid, Ademtech) are covered with Rabbit Anti-Mouse Immunoglobulins (DAKO Z0109, 3 g/L), which allows capturing biomolecules expressing mouse antigens. In order to prevent unspecific binding of the sample molecules to the unoccupied binding sites at the particle surface, the particle-antibody compound is subjected to a solution of bovine serum albumin (BSA), which neutralizes all free carboxilic binding sites at the particle surface. The activated microparticles are afterwards washed and mixed for 5 min with different concentrations of Mouse Immunoglobulins (Roche, Mouse-IgG ELISA standard). Subsequently the particles are injected into the droplet manipulation system and mixed with a microreservoir containing Rabbit Anti-Mouse Immunoglobulins coupled to Horseradish-Peroxidase (concentration: 1.3 mg/L). These attach selectively to the remaining free binding sites of the Mouse IgGs[10] captured at by the Anti-Mouse Immunoglobulins bound to the particle surface. After the incubation step, the magnetic particles are split from the microreservoir, passed through three washing stages and are finally mixed with the immobilized chromogen droplet for 10 min.

Figure 5.21 shows the measured color change for initial sample concentrations of 1 μg/ml and 10 ng/ml. We see a clear difference between to two reactions, which indicates the capability of the droplet manipulation system to incubate and detect an immuno-sorbent assay.

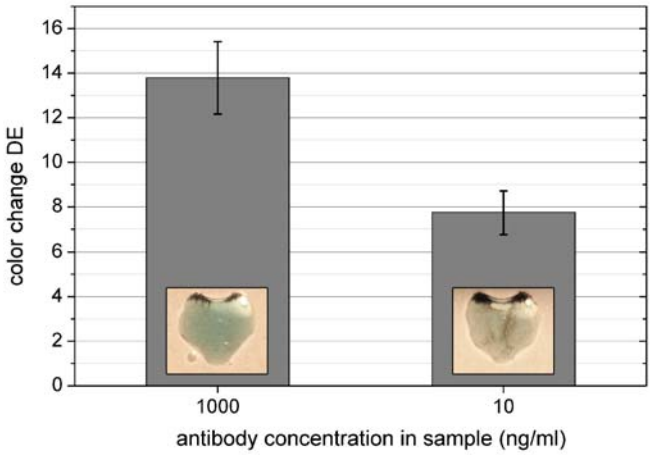

Figure 5.21 On-chip color change measurement after a full immuno-sorbent assay procedure. The columns represent the average of at least five measurements and the error bars indicate the variation of the detected color change. The photograph at the bottom of the column shows the immobilized chromogen droplet mixed with the magnetic particles after a reaction time of 10 min.

10. The Mouse IgGs used in the experiments are multivalent and have thus more than one binding site.

5.3.3 Conclusion

The possibility of performing on-chip colorimetric measurements of high sensitivity with a comparatively simple setup, demonstrates the potential of the droplet manipulation system to be used for on-chip immunosorbent assays. The current setup with only six immobilized microreservoirs, however, does not offer sufficient reactions steps to perform a full protocol on-chip. In consequence, I concentrated on the detection step, showing that the final labeling, washing and detection steps can be performed on-chip. Special attention was paid to the washing step, since a carry-over of the enzyme-labeled antibody from labeling to detection step will result in a false result. It was demonstrated, that the ratio between the durations of the labeling step and the washing step influences the carry-over. Preferably the washing steps should be as long as the labeling step, in order to successfully dilute molecules trapped loosely at the particles.

Moreover, the system's setup and the chosen protocol allow tuning the sensitivity by varying the detection time, which, in combination with the possibility of concentrating the sample molecules at the particle surface, permits the development of a highly performant ELISA Lab-on-a-Chip system. I demonstrated the system's capability to detect total amounts of enzyme labeled antibodies of as little as 7.2 pg in a 10 µl droplet, which compares very well to other recently presented ELISA based Lab-on-a-Chip systems [39, 64].

5.4 Conclusion

This chapter demonstrated the ability of the magnetic droplet manipulation system to perform standard bioanalytical procedures on a highly miniaturized level. Six small immobilized droplets of 10 µl volume hold the samples and reagents, while the magnetic microparticles are transferred from one stage of the protocol to the next. This approach is inverse to the majority of on-chip bioanalytical protocols, where the reagents are flushed over a zone of interest. The use of finite and also well-defined reagent volumes makes the down-scaling of the bioanalytical protocol an easy task. The largest challenge in that respect is the implementation of the washing steps, since these are usually performed using large amounts of liquids in order to obtain a high

dilution factor. This problem was solved by introducing a washing cascade, where the liquid fraction surrounding the mobile substrate is diluted repeatedly. Thus a dilution factor of more than 200 can be easily obtained by a cascade of three stages.

Subsequently two bioanalytical protocols were adapted to the system applying different binding and detection methods. In a first setup, the feasibility of on-chip capture and purification of DNA was examined. A standard kit (MagNa Pure DNA extraction kit 1, Roche) provided all reagents as well as the magnetic microparticles. The experiments showed that pure DNA (λ-DNA and human-genomic DNA) can be successfully captured and extracted from the binding buffer. The additional comparison of on- and off-chip fluorescent detection of the purified and eluted DNA demonstrated the improved sensitivity of the on-chip measurement. The eluate's significantly higher DNA content, when measured on-chip as compared to off-chip quantification, can be linked to a loss of biomaterial during transfer due to DNA absorption to plastic vials and pipettes.

Another set of experiments, performed in this context, examined the extraction and purification of DNA from a raw cell sample. We were able to capture, wash and detect the DNA extracted from a sample containing only 10 lysed Jurkat cells. The cells were obtained from a centrifuged pellet, which allows the concentration of a small number of cells in a 10 µl droplet. The experiments examining Jurkat cells and human-genomic DNA also included off-chip PCR as an additional detection step, which allowed to examine the purity and intactness of the recovered DNA. In consequence, the successful PCR, represented in an agarose electropherogram (Figure 5.12), demonstrates that we achieved our goal of extracting and purifying DNA from a raw cell sample, containing as little as 10 cells, without damaging the DNA. Thus the droplet-based procedure improved the protocol's sensitivity by a factor of 10000, while reducing the total reagent consumption by a factor of 36, as a comparison with the kit's manual [154] and related publications [191] show.

A second bioanalytical protocol implemented into the droplet manipulation system aims at examining the potential of on-chip ELISA using the magnetic microparticles as mobile substrate. After a thorough study of the enzymatic detection step in combination with on-chip washing, I was able to show that the colorimetric detection scheme devised for the system allows the detection of an enzyme-labeled

antibody content of as low as 7.2 pg per 10 µl droplet. However, I also observed a drawback of the detection system, where the signal strength decreases due to the small sample volumes. The chosen colorimetric scheme can correct for that decreased signal strength by increasing the reaction time. In consequence, the time required for the protocol will equal the macroscopic protocols process time [90], but the sample consumption can be decreased significantly, which in combination with the concentration of the biomolecules at the magnetic particles surface enables highly sensitive antibody detection.

In summary, I was able to show the applicability of the magnetic droplet manipulation system as a Lab-on-a-Chip. The small sample and reagent volumes, present as immobilized 10 µl droplets, as well as the magnetic particles, which serve as mobile substrates and concentrate the biomolecules of interest at their surface, allow to enhance the sensitivity and efficiency of known bioanalytical protocols.

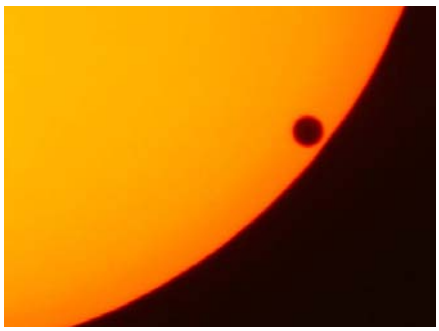

CHAPTER

6

MANIPULATION AND INTEGRATED OPTICAL DETECTION OF SINGLE MAGNETIC PARTICLES

This chapter describes a miniaturized magnetic manipulation system based on the magnetic transport via overlapping coils, which contain integrated optical detection elements. In the following, the system will be characterized with an emphasis on the optical detection principle.

adapted from the journal article: U. Lehmann, M. Sergio, S. Pietrocola, E. Dupont, C. Niclass, M.A.M. Gijs and E. Carbon. Microparticle photometry in a CMOS microsystem combining magnetic actuation and *in-situ* optical detection, Sensors and Actuators B: Chem. (2007), doi:10.1016/j.snb2007.10.021 (*in press*).

6.1 Introduction

An approach towards the further miniaturization of the magnetic manipulation system led to the design of a CMOS chip[11], which integrates a multilayer of square coils with optical detection elements. The combination of magnetic actuation and optical detection profits from the advantages of both principles. Magnetic actuation offers long ranging and large forces, while optical detection will permit measurements of high sensitivity, supported by the absence of an interaction with the actuating principle. In consequence, the manipulation and detection of single particles - and in the following the detection of single cells - will be possible, which is of increasing interest for miniaturized bioanalysis [99, 141]. Additionally, the optical elements chosen for the CMOS chip provide the possibility to perform on-chip fluorescent measurements, which will further enlargen the applicability of the proposed system.

11. The CMOS chip was designed in collaboration with M. Sergio and E. Charbon (EPFL, AQUA).

6.1. System Setup

The CMOS chip contains four metal layers, with the upper two forming the overlapping square coils, fabricated in 0.35 μm 2P4M CMOS technology. The coil double-layer is responsible for the actuation of the magnetic microparticles contained in a microcapillary placed on top of the CMOS chip (Figure 6.1). Each coil has five windings of 37.5 μm width, resulting in an inductance of L = 6 nH and a resistance of R = 16 Ω for each coil.

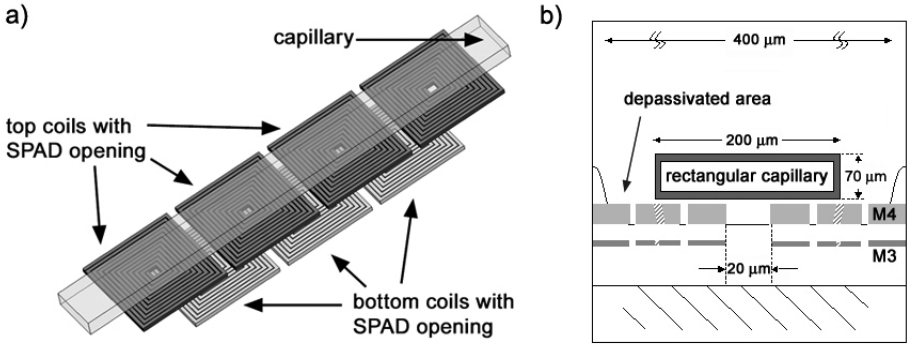

Figure 6.1 Schematics of the CMOS based magnetic particle manipulation system. a) explosion view, b) side-view.

Underneath the square opening of each coil, a Single Photon Avalanche Diode (SPAD) [56] is positioned, thus making the coil centers the detection sites. Figure 6.2 shows a top view of the CMOS chip, with a coil and a SPAD in greater detail. The rectangular glass capillary on top of the chip contains the liquid medium and is used as a model for the envisioned microfluidic system.

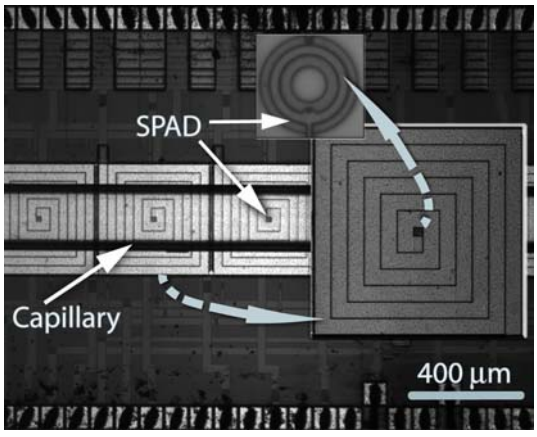

Figure 6.2 Photograph of the CMOS based magnetic particle manipulation system with integrated optical detection elements (Single Photon Avalanche Diodes = SPADs). The insets show a coil and a SPAD in greater detail.

A large circular coil (∅ = 3 cm) is placed over the CMOS and generates the static magnetic field for magnetizing the magnetic particles perpendicular to the chip surface. The coil's magnetic field perpendicular to the chip amounts to B_{ext} = 7 mT at the CMOS surface.

For the experiments the CMOS chip is connected to a custom-made PCB[12] (see Figure 6.3 and 6.4) and placed underneath a microscope (AxioImager.A1m, Zeiss). Thus the magnetic particles can be directly observed using the microscope and a CCD camera, while the microscope's focused lightsource (HAL 100, Zeiss) serves simultaneously as the photon source for the SPAD illumination. When using the first generation PCB (Figure 6.3), the pulses emitted by a SPAD circuit are counted using a LabView controlled computer interface (NI TB-2715, National Instruments), while the second generation PCB (Figure 6.4) counts the SPADs' pulses on-board in a scanner-like fashion and transfers the count of all SPADs to a PC via the serial connection.

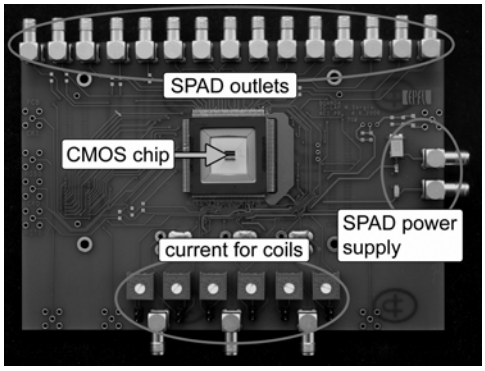

Figure 6.3 Photograph of the first generation PCB housing the CMOS chip. The PCB has three connections for the coil currents, two connections to set the SPAD's voltage and one connection for the outlet of each of the 15 SPADs.

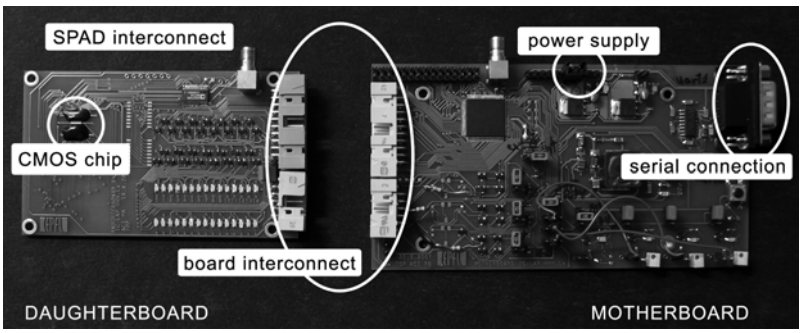

Figure 6.4 Photograph of the second generation PCB. For reasons of flexibility, the circuit is split into daughter- and motherboards, with the latter housing all control units and the former housing the CMOS chip and the current indicators (LEDs).

12. The PCB were designed in collaboration with S. Pietrocola and H.H. Hoang Le during their respective master projects.

The first generation PCB permits the reading of only one SPAD at a time but allowed a very flexible testing of the chip. The second generation PCB has a higher degree of integration and allows a parallel readout of all SPADs via a microchip on the board. It, furthermore, requires only a single power supply and is entirely computer-controlled via a serial connection.

6.1.1 Magnetic Actuation

The magnetic transport follows a three-phase current scheme [151], where an attractive coil is flanked by repulsive coils. The resulting magnetic field gradient creates a force that is sufficiently large for moving a magnetized particle to the center of the nearest attractive coil. The amplitude of the DC currents driving the coils are determined by the dimensions of the wires. In the present case, the coils were designed to sustain a DC current of up to I_{max} = 50 mA. The power consumption of each coil amounts therefore to 40 mW, which adds up to 600 mW for the whole chip containing 15 coils. The small size of the chip and its good heat conductivity permit hereby higher current densities, than is the case for the PCB, without the need for cooling.

Figure 6.5 presents a sequence of the coils' states and the corresponding particle behavior during particle transport. In the first step, the particles are assembled around the center of the attractive coil. In the subsequent step, a neighboring coil is also changed to the attractive state, which leads to a widened but lowered magnetic field maximum resulting in a spreading of the particle cloud over the maximum. In the third step, the first coil is changed to the repulsive state, resulting in an assembly of the magnetic particles over the neighboring, now solely attractive coil.

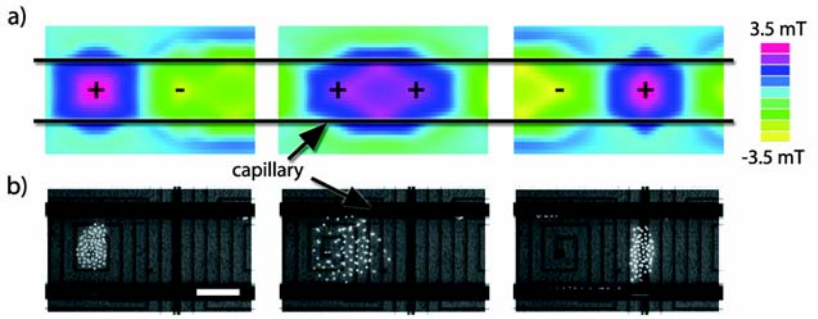

Figure 6.5 Magnetic particle transport. a) Simulation of the magnetic field generated by the CMOS. The "+" sign demonstrates a coil in attractive mode while "-" denotes a coil in repulsive state. b) Behavior of a group of magnetic particles of 5 µm diameter according to the respective topology of the magnetic field. (Dimension bar = 100 µm)

The optical observation of the moving cloud of particles shows that the particles follow a multitude of paths between the two coil centers, with the majority moving along a straight line. The path a particle describes between the two coil centers depends hereby on its position at the coil's center opening upon departure.

The magnetic actuation is additionally influenced by the thickness of the capillary's bottom-wall, which determines the distance between the particle and the coils. Figure 6.6 shows analytical simulations for the shape of the magnetic field over one square coils of five windings at different distances. We see that a thin capillary wall (z = 2 µm) results in a strong magnetic field. At that distance however, the field variations and in consequence local field minima induced by the spacing between the windings can hinder the magnetic transport of particles, since they might be trapped between windings. For very large distances (z = 100 µm) the field is very smooth but of low strength, thus resulting in a small magnetic force.

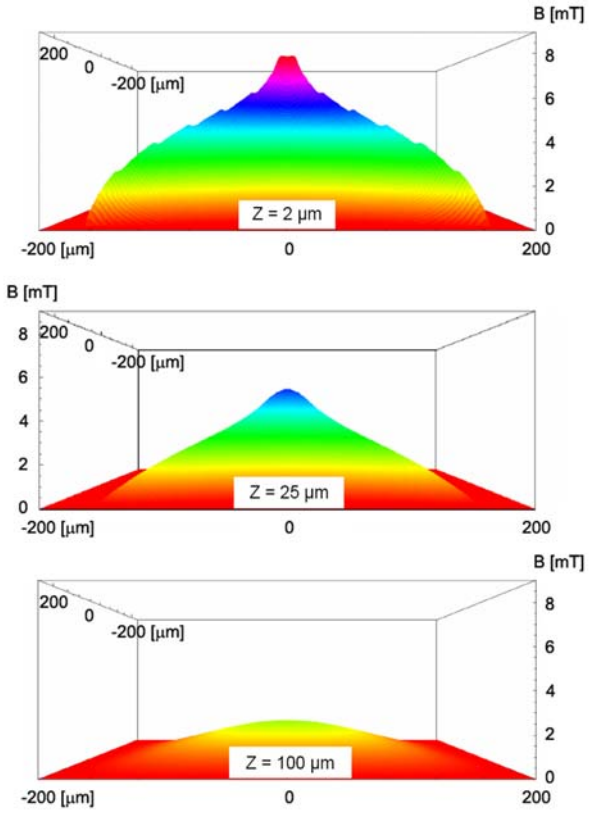

Figure 6.6 Simulation of the magnetic field over one square coil for three different distances.

In consequence capillaries were used, whose wall thickness did not exceed 100 µm. All experiments with small particles (∅ < 15 µm) were

performed in capillaries with 25 μm sidewalls, resulting in a smooth and comparatively strong magnetic field.

6.1.2 Optical Detection Elements

For the integrated optical detection, Single Photon Avalanche Diodes [131] are chosen due to their high sensitivity, very good signal to noise ratio and wide dynamic range [56]. A SPAD is basically a p-n-junction that is reverse biased above breakdown by the excess bias voltage *Ve*. Thus, for a SPAD in Geiger mode, every electron-creating event will trigger an avalanche and subsequently generate a countable signal. To achieve this, the voltage pulse generated during a detection cycle is regenerated and converted to a digital pulse by an inverter. Figure 6.7 shows a schematics of the SPAD and its surrounding circuit. The diameter of the active region (Anode) is hereby ∅ = 8.4 μm. In case an avalanche is triggered in this region, the resistance placed in series to the p-n junction lets the reverse bias temporarily drop below breakdown and thus quenches the avalanche. In the present design, avalanche quenching, which in combination with the recharge time determines the dead time and thus the detection cycle of a SPAD, is achieved through a passive method. The measured dead time of 40 ns results in a maximum detectable frequency of 25 MHz. Thus an incident flux of 25 10^6 photons per second can be detected by the SPAD.

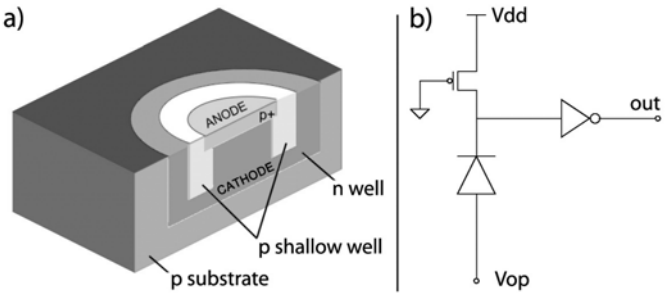

Figure 6.7 Schematics of the Single Photon Avalanche Diode. a) 3D visualization of the CMOS structure, b) electrical circuit for the SPAD in Geiger mode.

Wavelength Dependence

Wavelength Dependence

The probability that a digital pulse is generated upon impinging photons, the photon detection probability (PDP), is plotted in Figure 6.8 as a function of excess bias voltage *Ve* and wavelength. It can be seen that the PDP is highest (> 25 %) for wavelengths between 400 and 520 nm. For longer as well as shorter wavelengths the probability of detection

decreases, which leads to a lowered sensitivity as well as an increased influence of noise. The SPAD's background noise determines hereby the minimum detectable photon flux and is characterized by the frequency of spurious pulses. Since it is measured in the absence of incident light, it is known as dark count rate (DCR). In the current CMOS chip the DCR is 1150 Hz for an excess bias voltage of Ve = 3.3 V at room temperature. Since the detection elements are illuminated with a photon flux generating a count of 8 MHz, the DCR is less than one promille of the measured signal.

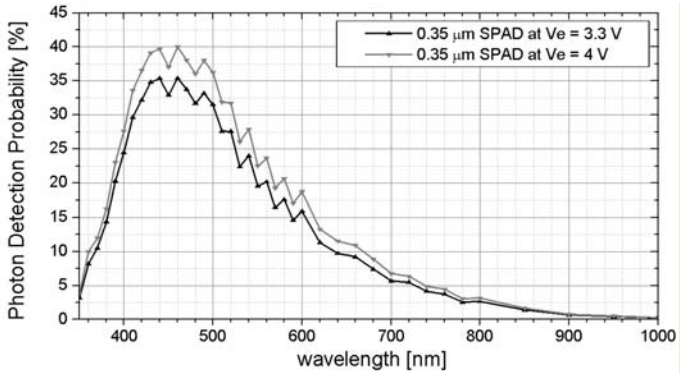

Figure 6.8 Photon detection probability (PDP) for different excess bias voltages as a function of the wavelength of impinging photons.

Temperature Dependence

Temperature Dependence

A further factor influencing the stability of the measured photon count is the temperature. Since the chip is driven with currents close to the technological limit, the produced ohmic heat will have an effect on the SPAD behavior. Measurements (Figure 6.9) show that the temperature in the chip can rise up to 34 °C for 50 mA.

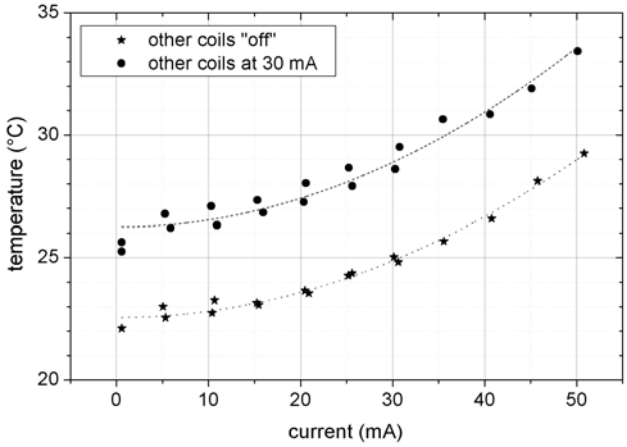

Figure 6.9 Coil temperature depending on the currents in the CMOS chip. The temperature is determined via the change in resistance of a single coil. The dotted lines are parabolic fits of the measured points.

Since a rising temperature leads to an increasing breakdown voltage of the SPAD, the excess bias voltage will be reduced (see Figure 6.7). Subsequently the PDP and, in consequence, the SPAD's sensitivity are lowered as indicated in Figure 6.8. This effect results in a decreasing photon count with increasing temperature, as clearly visible in Figure 6.10, where each activated coil leads to a further increase in temperature.

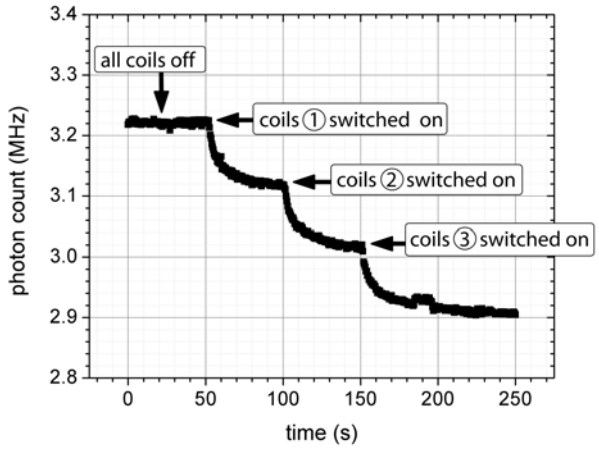

Figure 6.10 Photon count variation due to ohmic heating of the CMOS coils for switched DC currents of 40 mA.

The measurements also indicate a fairly high thermal time constant in the range of more than 10 s, which necessitates either a time delay between the switching steps and the optical measurements or a fast coil switching, depending on the velocity of the particles.

6.1.3 Optical Detection - Theory and Model

The evaluation of the signal obtained from the SPAD is based on a technique known from astronomy, where **transit photometry** is applied to detect and characterize extrasolar planets [15]. This measurement principle allows the evaluation of the transiting object's properties, such as its size and the composition of its atmosphere via optical effects.

Micro-Eclipse

In the present case, the dimensions are significantly smaller, but the ratios and observed effects are comparable. Figure 6.11 a) and b) present the events expected during a particle's transit. Due to the numerical aperture of the microscope's objective and the circular detection area, the lightsource appears as a large disc. Any particle passing between the SPAD and the lightsource will block a fraction of the incoming light, therefore creating a transiting dark spot or "micro-eclipse". Such events are known from astronomy, when planets cross between an earthbound

telescope or an observing satellite and a distant star, as Figure 6.11 c) shows.

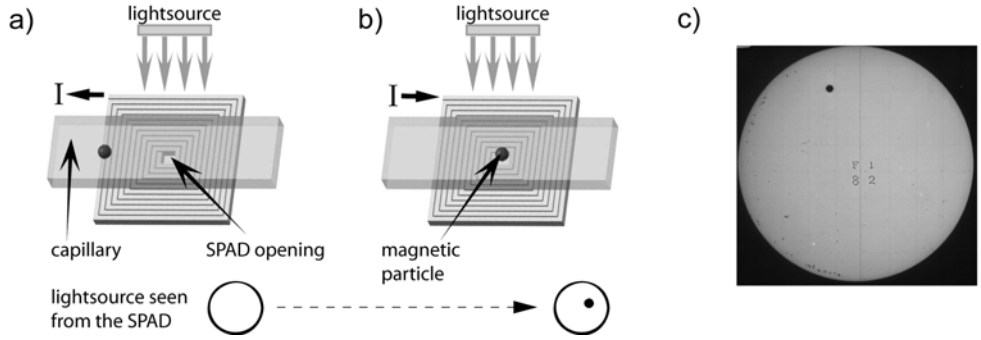

Figure 6.11 Principle of the micro-eclipse. (a) in the absence of a particle, the Single Photon Avalanche Diode (SPAD) is fully illuminated, (b) in the presence of a particle over the SPAD, the incident light is partly obstructed. (c) Transit of the planet Venus on Dec. 6th 1882. This picture taken by the American Transit-expedition is probably the oldest photograph of Venus.

Transit photometry exploits hereby the effect that the passage of an object (radius *r)* in front of a lightsource (radius $R >> r$) results in a lowered light intensity measured at a detector directed towards the respective lightsource. Thus, the photon count of a SPAD drops during the passage of a magnetic particle between the active area and the microscope's lightsource, as demonstrated in Figure 6.12 a) and b).

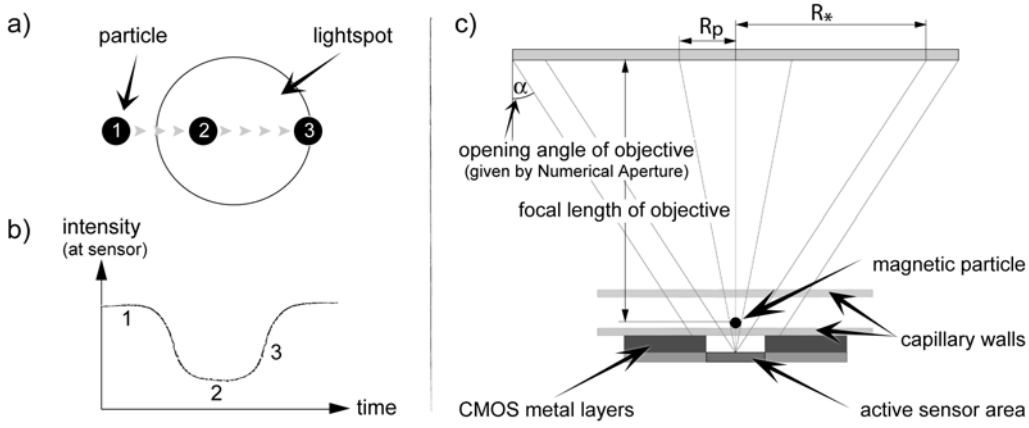

Figure 6.12 Principle of the SPAD based optical detection. The passage of a magnetic particle over the SPAD blocks a part of the incident light seen by the SPAD (a). The measured intensity drops accordingly (b). c) The optical setup shows that only a part (R_s) of the incident light of the microscope arrives at the SPAD.

It is also known that the intensity drop ΔI is dependent on the cross-section of the passing object [157].

Intensity drop

$$\frac{\Delta I}{I_0} = \left(\frac{R_p}{R_*}\right)^2 \tag{6.1}$$

with I_0 the light intensity in the absence of the obstructing object and the projected radii R_p and R_* as defined in Figure 6.12 c).

Since the geometry of the microscope and chip setup differ slightly from the astronomical circumstances, some of the dimensions need to be converted in order to adhere to the photometry theory. In that respect, the optical path (see Figure 6.12 c)) needs be taken into account. The latter includes the capillary walls, the liquid inside the capillary and the silicon oxide on top of the SPAD (Table 6.1). These elements determine the optical distance $dist_{SPAD}$ between the particle and the SPAD, whereas they can be neglected when determining the distance between the particle and the light source, since the focal length $f >> dist_{SPAD}$.

	thickness [μm]	**refractive index**
capillary wall (glass)	25, 50 and 100	1.5
capillary height	20 and 100	1.3
airgap	4	1
oxide (SiO_2)	6	1.5

Table 6.1 Elements of the optical stack between the particle and the SPAD.

Extracting the passing object's radius from the intensity measurement of transit photometry relies on the assumption that the distance between the light and the transiting object is smaller than the distance between the object and the observer. In order to adhere with this assumption, one can project the particle onto the light source as demonstrated in Figure 6.12 c). In consequence, we obtain the radius of the projected particle R_p and the radius R_* of the light spot "seen" by the SPAD via:

$$\begin{aligned} R_p &= \frac{r}{dist_{SPAD}} \cdot f + r \\ R_* &= (f + dist_{SPAD}) \cdot tan(\alpha) \end{aligned} \tag{6.2}$$

with the particle radius r, the objective's focal length f and the distance between particle and SPAD $dist_{SPAD}$. The numerical aperture NA of the objective is expressed in the angle α = arcsin(NA/n), with the refractive

index n = 1 for air. However, the distance $dist_{SPAD}$ needs to be much smaller than the focal length f, assured by the use of suitable objectives.

6.2 Experiments and Results

A first range of experiments is performed in order to study the system's behavior with respect to the magnetic transport and optical detection capabilities. Magnetic particles of 30 μm diameter (Micromod) are introduced into a square glass capillary (Vitrotubes) with a bottom wall thickness of 100 μm. The capillary is then sealed and placed on the chip. The sealing of the capillary prevents the evaporation of the liquid and suppresses thus liquid motion within the channel.

Figure 6.13 shows the successful displacement of the magnetic microparticles in the system and demonstrates in addition the capability of the system to detect the presence of the particle over the SPAD at the coil center via the micro-eclipse effect discussed previously. Even though the particle is larger than the coil's center opening, the incident light is not fully blocked, which is in agreement with the projection model presented in Figure 6.12 c).

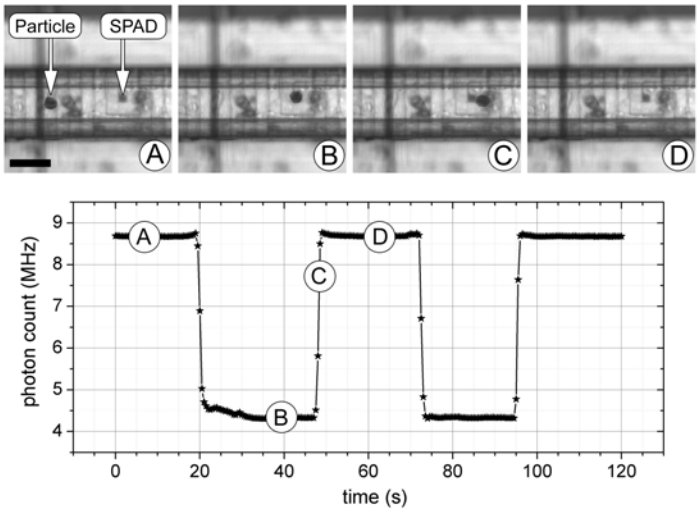

Figure 6.13 Transport of a particle of 30 μm diameter in a glass capillary of 50 μm sidewall thickness and the corresponding photon count of the indicated SPAD. The particle is held immobile over the coil center during the measurements. (dimension bar = 100 μm).

Particle size measurement

Particle size measurement

In a second step, smaller particles (Table 6.2) are introduced into the system in order to examine the system's ability to distinguish between the

different particles sizes. The glass capillary, used to hold the highly diluted solutions of particles, has a sidewall thickness of 25 μm, which will allow larger magnetic forces (see Figure 6.6) and a better resolution according to equations (6.1) and (6.2) than the capillary used in the first experiments.

∅ [μm]	magnetite [wt%]	brand	properties
1	63.4	BangsLabs	fluorescent: 480/520
3	12.5	BangsLabs (COMPEL)	fluorescent: 660/690
5		Spherotech (Nile Red)	fluorescent: 559/637
6	5.5	BangsLabs (COMPEL)	fluorescent: 480/520

Table 6.2 Particle properties as given by the suppliers.

Since the experiments are performed using a broad-band halogen microscope lightsource (HAL 100, Zeiss) and top illumination, the fluorescence of the opaque particles will be overlaid with the general illumination.

Figure 6.14 shows the signal obtained from a SPAD during the transit of the different magnetic particles. The signals for particles of different sizes can be clearly distinguished and we see that particles with a diameter as low as ∅ = 1 μm can be easily detected by the system. The measurements show an additional effect, which is related to the non-collimated character of the light source. Even though it varies between the particle types, we observe the phenomenon that, when a particle approaches the SPAD's field of vision, the photon count increases before the expected drop in intensity occurs.

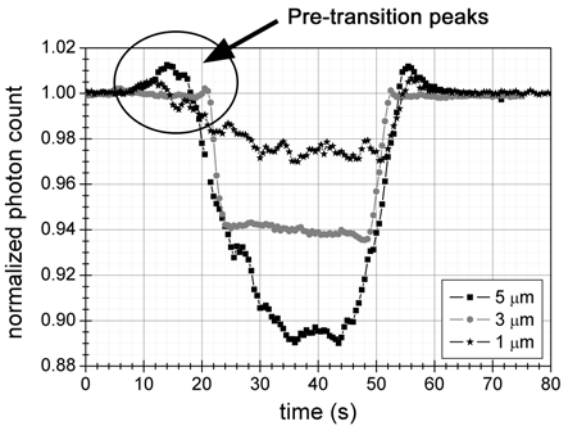

Figure 6.14 Normalized photon count of a SPAD during the transit of single particles with 1, 3 and 5 μm diameter.

This pre-transition peak results from the microscope‘s lightsource‘s emission of light of broad bandwidth and of various angles forming the objective‘s light-cone (Figure 6.12 c)) in combination with the reflection of light falling onto the opaque particle. Thus some photons, which would normally arrive outside the SPAD‘s sensitive area, are diverted towards the active region and increase the measured photon flux, as schematically shown in Figure 6.15. The probability for the redirection of photons towards the SPAD center increases the closer a particle gets to the detection area.

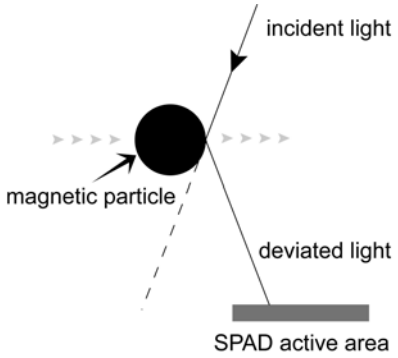

Figure 6.15 Schematic of the origin of the pre-transition peak. The incoming magnetic microparticle deviates incident light, arriving out of bounds, towards the SPAD‘s sensitive area.

However, once a particle fully enters the SPAD‘s fields of vision, light is no longer diverted towards the SPAD‘s sensitive area, but away, which leads to the previously described effect of the micro-eclipse. In consequence, the number of photons arriving at the sensor surface is reduced. The evaluation of the measurements for the different particle sizes and their comparison with the model is presented in Figure 6.16.

We see that the measurements agree well with the expected values and that, as predicted by the model, a small distance between the particles and the sensors favors the resolution. However, observation shows that for the measurement of larger particles or cells an increased distance is advantageous, since the upper limit of detection will increase as well. As an example, the calculated maximum diameter of a particle that can be detected in a capillary with 25 µm sidewall thickness is ∅ = 17 µm, while a capillary with a 100 µm thick side wall can detect particles up to 60 µm diameter. But, we also see that the minimum size of particles that can be detected depends on the width of the capillary wall. While a capillary with 25 µm sidewall thickness allows the detection of particles with 1 µm

diameter, a capillary of 100 μm sidewall thickness will yield the same signal for particles of 5 μm diameter. Thus the "working distance", defined by the channel bottom, needs to be chosen as a function of the required resolution and detection limits.

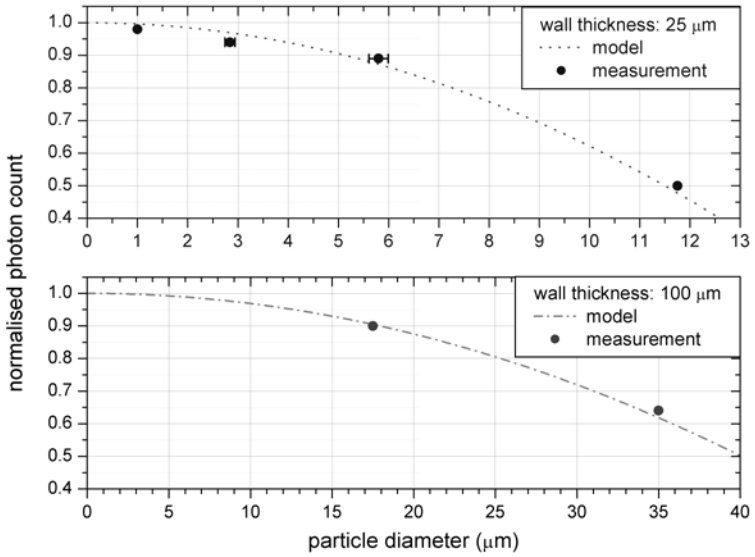

Figure 6.16 Comparison of the measured and expected values for different particle diameters and varying capillary wall thicknesses.

Particle velocity measurement

Particle velocity measurement

When recording the signals of two adjacent SPADs simultaneously, we are able to determine the average particle velocity as Figure 6.17 demonstrates. During the time elapsed between the intensity drops of two adjacent SPADs, the magnetic particle travels the distance of 200 μm.

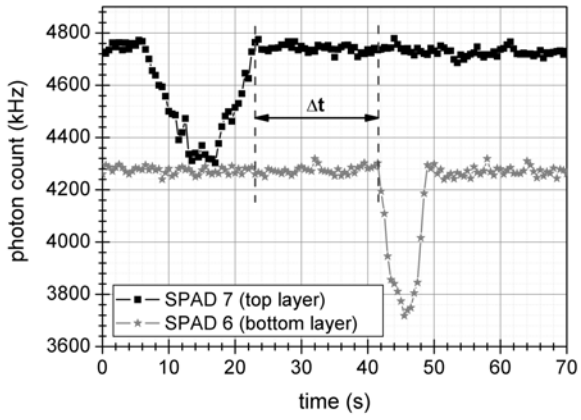

Figure 6.17 Photon count of two adjacent SPADs during particle transport for a particle of 5 μm diameter showing the successive intensity drops. During the time difference Δt the particle moved in a straight line from SPAD 7 to the neighboring SPAD 8.

The measured average velocity can be translated into the magnetophoretic mobility of the particles based on the theoretical value of the magnetophoretic driving force S in the direction of the particle displacement. Figure 6.18 shows the result of a analytical simulation of the forces along the coils center-line generated by the magnetic actuation. We see that the particles experience a force in x-direction directed from the repulsive (-) coils to the closest attractive (+) coil, while the force in the y-direction is close to zero. Additionally, the particles experience a repulsive force in z-direction at the position of coils carrying negative currents (-) but are attracted towards the chip when reaching the position of coils carrying positive currents (+). Thus the particles are lifted from the capillary surface and, in consequence, experience only a viscous drag during the transport. When reaching the center of the next attractive coil, the particles are again pulled towards the capillary bottom, which ensures a constant distance between particle and SPAD for all optical measurements, depending only on the thickness of the capillary wall.

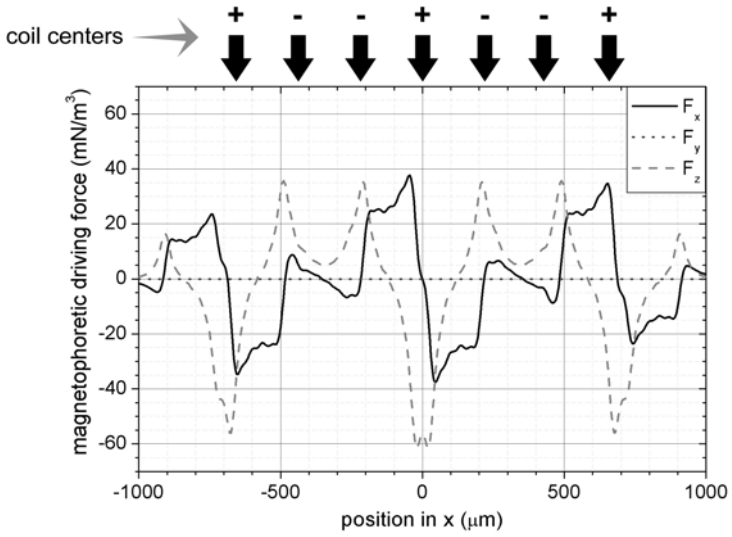

Figure 6.18 Analytical simulation of the magnetophoretic driving forces in the capillary. The arrows indicate the positions of the coil centers, with the algebraic signs identifying the orientation of the local magnetic field.

The comparison of the measured velocities, summarized in Table 6.3, shows a higher average velocity for the larger particles, even though their content of magnetically active material is lowest. The particle velocity can be translated into the viscous drag force F_{drag} acting on the particle during transport via equation (2.10). The obtained values are presented in Table 6.3 together with the drag force per unit volume F_{norm}.

Ø [μm]	magnetite [wt%]	v [μm/s]	F_{drag} [fN]	F_{norm} [kN/m^3]	$\Delta\chi_r$
1	63.4	1.6	13.6	35.6	3.3
1.6	42.5	2.9	43.7	20.4	1.9
3	12.5	4.7	124.0	10.8	1.0
6	5.5	5.9	322.5	3.2	0.3

Table 6.3 Summary of the average particle velocities for the magnetic particles examined in the system.

We see that, while the velocity, and thus the magnetic force acting on the particle, increases with the diameter, the force per unit volume decreases relative to the magnetite content of the particle.

Using the relation for the magnetophoretic mobility (equation (2.15)), it is furthermore possible to determine the relative magnetic susceptibility $\Delta\chi_r$ of a particle. With the viscosity of the liquid of $\eta = 1$ mPa s and the average magnetophoretic driving force $S = 27$ mN/m^3 we obtain the susceptibility values listed in the last column of Table 6.3.

When plotting the calculated relative magnetic susceptibility over the given magnetite content, we see that the magnetic susceptibility of the particles is related to the magnetite content via an exponential function, as expected from theory [49, 198]. The measured values also show the superparamagnetic character of the particles, since their relative susceptibility is significantly higher than the values known for paramagnetic materials (see Table 2.1).

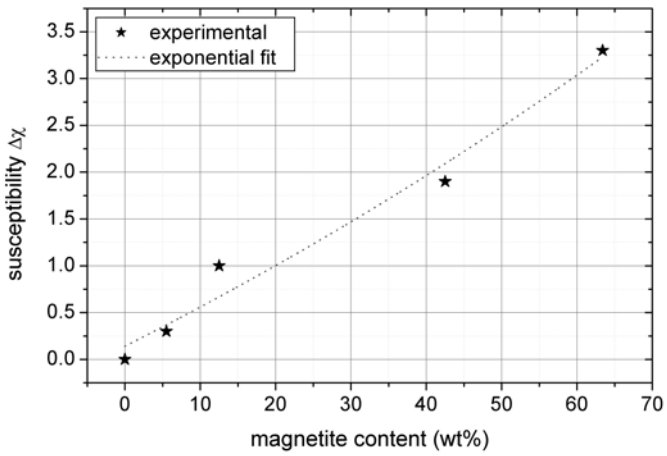

Figure 6.19 Magnetic susceptibility $\Delta\chi$ as obtained from the velocity measurements for known particle sizes.

Table 6.3 also shows that the forces obtained by the magnetic actuation are in the fN range. For this reason, the particles can only be held against very low flow rates - at the order of μm/s, which makes the current system unsuitable for flow through bioanalytical protocols [92]. The introduction of an additional retention system, e.g. via dedicated coils, can solve this problem and thus opens the way towards stop-flow bioanalytical protocols using single magnetic particles or magnetically labeled cells.

The system's capability for the optical measurement of particle size and particle velocity will permit the determination of further magnetic parameters of particles or cells. Especially in the case of magnetically labeled cells, the magnetophoretic mobility can be used as a measure for the number of magnetic particles attached to the cell surface, which are in turn an indicator for the number of specific binding sites expressed by the cell [120].

6.3 Towards a Lab-on-a-Chip

The ability of the hybrid CMOS system to manipulate single magnetic microparticles and to optically detect their position and size, makes the system a promising device for a Lab-on-a-Chip application. A first challenge towards such a system is the introduction of a microfluidic network of higher complexity, since a single glass microcapillary does not offer the flexibility needed for performing on-chip bioanalysis.

6.3.1 Microfluidic Network

The requirements for the microfluidic network placed on top of the CMOS chip are:

- thin bottom layer
- easy alignment with the chip
- connectivity to reservoirs and pumps
- channel height suitable for large particles and cells
- optically transparent material
- biocompatibility.

A material that offers suitable properties for the fabrication of such networks is the epoxy-based negative photoresist SU-8 [98, 164]. A multitude of recent studies demonstrate the increasing interest in this material, including its use for the fabrication of fluidic networks or

structural elements in MEMS as well as for the preparation of masters for replication molding.

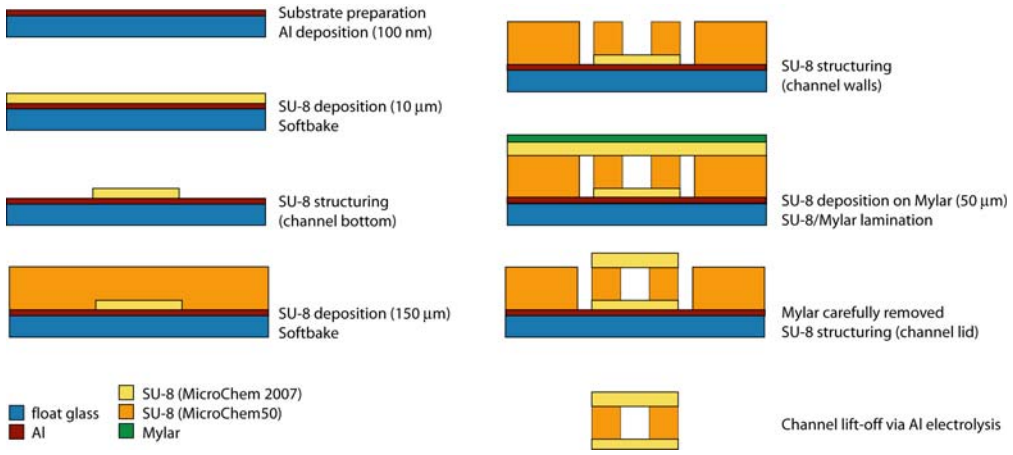

Figure 6.20 Process flow for the fabrication of the SU-8 capillary network.

For the fabrication of the microfluidic capillary network one can profit from the characteristics of SU-8, which permit to create deep channels with straight side-walls, to perform multi-layer processing and to obtain closed channels via a lamination step [2, 38]. Following the process flow presented in Figure 6.20, I fabricated capillaries in SU-8 with a bottom layer of 10 µm thickness and a channel height of 150 µm, as shown in Figure 6.21. The channel width of 400 µm allows an easy alignment with the CMOS coils by simply placing the capillary by hand. The magnetic particles inside the channels are positioned over the SPADs via magnetic force and in consequence an alignment of the channel is not required.

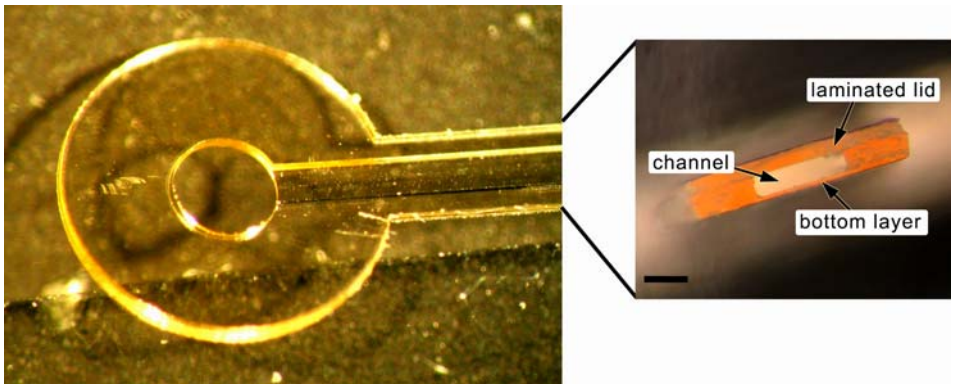

Figure 6.21 Photographs of the SU-8 capillary. The bottom layer has a thickness of 10 µm. (Side view dimension bar: 200 µm).

The SU-8 capillary is optically transparent (n = 1.8) as Figure 6.22 demonstrates and allows therefore optical detection via photometry.

However, its optical characteristics for the different wavelengths and its autofluorescence need to be taken into account, when using the SU-8 microfluidic network for on-chip fluorescent measurements [164].

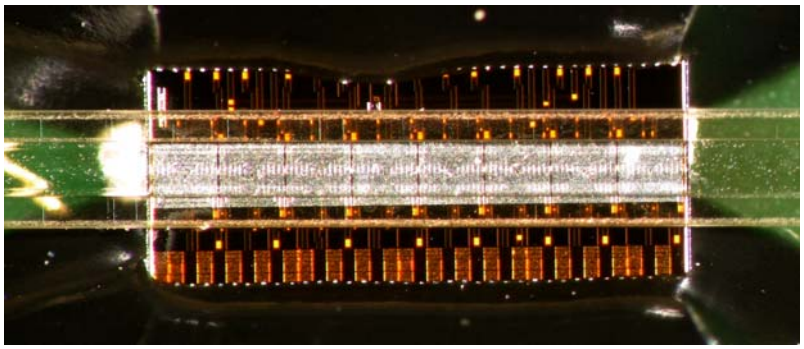

Figure 6.22 Photograph of the SU-8 capillary on the CMOS chip. The bonding wires are covered with epoxy for protection.

The microfabrication of the fluidic network also offers the possibility to directly introduce additional magnetic components for the retention or separation of the magnetic particles before or after detection.

6.3.2 Fluorescent Detection

The particle size measurements demonstrated the high sensitivity of the optical detection system, which is capable to detect the intensity drop created by the passage of a particle with a diameter of 1 μm. Additionally it is known that SPADs are able to perform fluorescent measurements. Thus by replacing the broad-band lightsource with a UV-lamp (X-Cite series 120, Zeiss), the system can be easily changed into a configuration for on-chip fluorescent detection. In reference to the PDP of the detection element (see Figure 6.8), a suitable filter (Fs 10, Zeiss)[13] as well as a fluorescent marker (FITC)[14] are chosen. In consequence, the additional photons due to fluorescent emission have a wavelength that matches the maximum sensitivity of the SPAD.

Based on known immuno-assays (see Figure 5.1) we can therefore envision a Lab-on-a-Chip that allows the detection of a fluorescent label captured at the surface of a single magnetic particle. In order to test the fluorescent detection principle, we use non-fluorescent streptavidin-

13. The filter has the following wavelength configuration: Excitation bandpass of 450-490 nm, Beamsplitter at 510 nm and Emission bandpass of 515-565 nm.

14. Fluoresceinisothiocyanat: fluorescein derivative with absorption maximum at 494 nm and emission maximum of 521 nm.

coated magnetic particles (BangsLabs) of 3 μm diameter, to whose surface we bind biotinylated antibodies with an FITC label[15]. An estimation of the particles loading capacity, according to the information given by the supplier, yields the amount of 2.6 10^6 antibodies that can be bound to the particle surface. In consequence, the total weight of a fully covered particle will increase by 2 % at maximum load (from 30 pg to 30.6 pg).

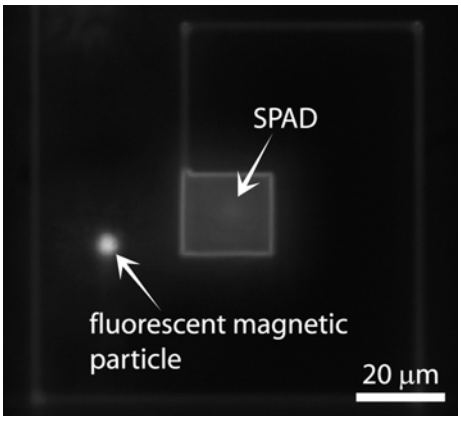

Figure 6.23 Top-view photograph of a fluorescently labeled particle of ∅ = 3 μm approaching a SPAD at the coil center.

When a particle, which carries fluorescent molecules at its surface, approaches the coil center, as presented in Figure 6.23, the photon count at the sensor will drop due to the micro-eclipse effect, but additionally the fluorescent circumference will influence the signal at the suitable light conditions. Figure 6.24 demonstrates the events, when the system is set to the fluorescence mode. Due to the light emission at the particle's circumference, the photon count of the SPAD will be higher than in the case of a non-fluorescent particle.

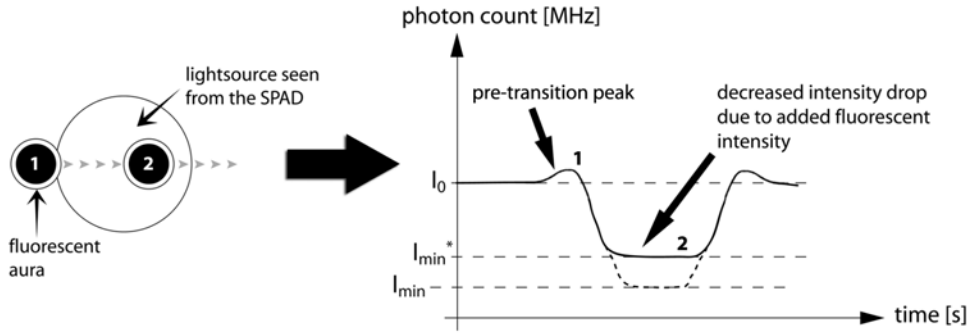

Figure 6.24 Principle of the fluorescent detection. The fluorescent aura around the particle leads to an increase of the light intensity measured during the micro-eclipse.

15. The experiments involving fluorescently labeled magnetic microparticles were performed with the help of M. Lombardini.

The difference between the two signals is the indication for the presence of fluorescent molecules at the particle surface. Such a differential measurement can be performed by varying the wavelength of the light between two measurements on the same particle, which allows to record the micro-eclipse signal of the same particle with and without the fluorescent component.

The origin of the fluorescent circumference is schematically presented in Figure 6.25. An incident lightwave is reflected at the particle surface and is deviated from its path towards the sensor surface. While passing the zone of the fluorescent molecules at the particle surface, the incident or reflected light excites a molecule, which will emit light in any possible direction. Thus a certain fraction of the light emitted in the fluorescently active zone at the particle surface will arrive at the sensor and increase the amount of counted photons. The part of the light emitting zone, "seen" by the SPAD, is limited to a stripe along the particle circumference, since the opaque particle body blocks the light emitted at the upper particle hemisphere and prevents the lower hemisphere from being illuminated. In consequence, the measured fluorescent signal does not correspond directly to the total amount of the captured fluorescent molecules but is an indicator for the density of the fluorescent molecules at the particle surface, since a decrease in density will result in a smaller number of active molecules at the particle's circumference.

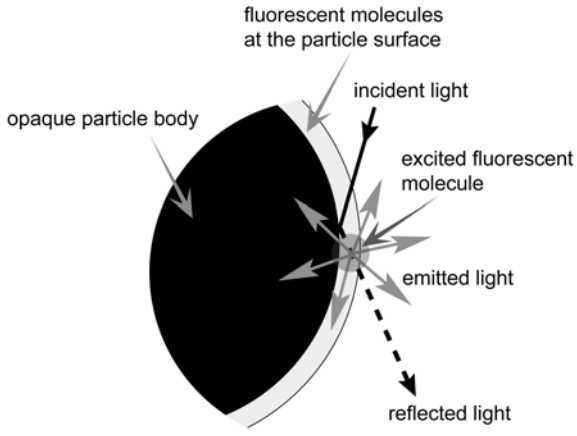

Figure 6.25 Schematics of the formation of the fluorescent aura. The undirected emission of light from molecules excited by blocked or deviated light waves creates an additional light source at the particle circumference.

Since the fluorescent aura is generated by light that would otherwise not reach the sensor surface, it adds photons to the incident light arriving at

the SPAD's detection area. Figure 6.26 shows the SPAD signals of a fluorescently labeled particle and a non-fluorescent particle of the same size. The drop in the photon count is significantly smaller for the particle with a fluorescent aura, which indicates the presence of an additional photon source. We further notice that the pre-transition peaks observed for the broad-band light source also occur during the fluorescent measurements, but are clearly smaller than the signal change observed in the experiments employing a broad-band lightsource.

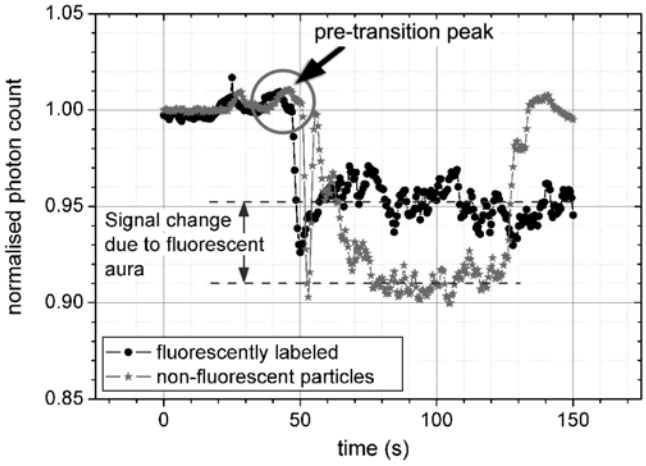

Figure 6.26 Measured SPAD signal for a 3 μm particle with and without fluorescent label.

Measurements show that the difference between the non-fluorescent particle and the particle fully covered with fluorescent molecules is on average 44 % of the total signal change. The micro-eclipse of a non-fluorescent particle leads hereby to a decrease in photon count of 9 %, while a fluorescently labeled particle decreases the measured photon flux by only 5 %. This difference in photon count is related to a fluorescent density of $8.6\ 10^4$ molecules per μm^2, for $2.6\ 10^6$ molecules at the surface of a particle of 3 μm diameter. Because all binding sites at the particle surface are occupied, this molecule density presents at the same time the upper limit of detection.

6.3.3 Conclusion

First experiments demonstrated the system's ability to extend its functionality towards bioanalytical applications. The introduction of a microfluidic network of increased complexity will permit the connection to external reservoirs, which hold reagents for on-chip bioassays. The assay itself can be quantified using fluorescent detection, based on the

measurement of the fluorescent aura. One of the largest challenges will be the retention of a single particle against the reagent's flow, since the forces exerted by the system itself are very small, as Table 6.3 shows.

6.4 Conclusion

This chapter described a CMOS-based system, where the magnetic actuation of single magnetic microparticles is combined with integrated optical detection. Since both principles do not require a direct contact between the object of interest and the actuator or sensor, a modular setup of the system is possible. The choice of the microfluidic component guides the performance of the system, since its dimensions control the distance between the magnetic particles and the chip surface. We demonstrated that a small distance improves the resolution, but limits the range of detectable particle sizes, while a large distance allows the detection of larger objects, but with a trade-off in sensitivity.

The simultaneous measurement of the particle speed, possible due to the parallel observation of multiple sensors, enables the determination of further particle properties such as its magnetophoretic mobility and its magnetic susceptibility. In consequence, we can envision the observation of magnetically labeled cells, whose transport velocity with respect to their size will be an indication for the number of magnetic particles attached to the surface and thus the number of specific binding sites.

In addition, I presented a path towards the design of a Lab-on-a-Chip based on the hybrid CMOS system. The introduction of a more complex SU-8 microfluidic network and the possibility of fluorescent detection, as described above, demonstrate the bioanalytical potential of a system combining long ranging magnetic actuation with high sensitivity optical detection elements. Since the system can handle single magnetic particles, only the amount of biomolecules bound to such a particle is subjected to the measurement, which allows to reduce the detection limits drastically.

CHAPTER 7

CONCLUSION AND OUTLOOK

The increasing interest in magnetic microparticles and their application in bioanalysis fuels the development of Lab-on-a-Chip systems employing them as active components. This thesis work looked into potential means of designing such systems, resulting in the in-depth study of two concepts. The first approach examined the applicability of magnetic microparticles for the handling of small liquid volumes and led to the development of a magnetic droplet manipulation system. Here, the interplay of magnetic forces, interfacial tensions and hydrophilic/ hydrophobic surface properties allows the transfer of small liquid fractions and clusters of magnetic particles from one immobilized microreservoir to another and, in consequence, permits the direct implementation of bioanalytical procedures onto the chip.
The second approach studied the performance and potential of the direct integration of optical detection elements into a CMOS system designed for magnetic particle actuation. The small dimensions enable the detection of single magnetic particles and ultimately the performance of a bioanalysis sequence on their surface.

7.1 Magnetic Droplet Manipulation

In Chapter 4, a magnetic droplet manipulation system was developed, which allows to perform all droplet handling steps on a small chip without requiring external moving magnets or complex surface structuring. I successfully demonstrated that the interaction between a magnetic field of variable topology, as generated by a multilayer-PCB, and magnetic particles inside an aqueous droplet creates sufficient magnetic force to overcome the friction present in the system and to move

droplets over a planar surface. The introduction of hydrophilic pattern on the hydrophobic chip surface furthermore permits the immobilization of liquid micoreservoirs on the chip. On that basis, droplets can be merged and mixed, supported by the actuation of the magnetic particles. The droplet splitting is achieved via the careful adjustment of the interfacial tensions between the different liquid phases to fit the available magnetic forces and completes the set of droplet manipulation steps.

An important feature of the droplet manipulation system is the immobilization and simultaneous deformation of small liquid volumes on hydrophilic areas of distinct shape. The local hydrophilization of the usually hydrophobic Teflon layer provides a simple but very effective solution for creating the force opposing the magnetic pull during the droplet splitting step. The innovative approach of passively determining the shape of the immobilized droplet adds a further handle for elegantly tuning the splitting behavior of the droplet.

In consequence, it is possible to transfer macroscopic bioanalytical procedures into a Lab-on-a-Chip setup and to study the influence of the miniaturization. The examination of two different protocols demonstrates the ability of the magnetic droplet manipulation system to use the same reagents and to perform the same steps as required in bench-top bioanalysis, but with a drastic reduction of reagent consumption and reaction time. In addition, the sensitivity of the system is improved, which is a result of the low sample volumes as well as the use of magnetic microparticles as mobile substrates. In that context, chapter 5 presents experiments, which employ the magnetic droplet manipulation system for miniaturized bioanalytical procedures. A first setup studies a miniaturized protocol for the extraction and purification of DNA from a raw cell sample employing silica magnetic microparticles and demonstrates the droplet manipulation system‘s capability to recover the DNA from as little as 10 cells. With such a small number of required cells, the magnetic droplet manipulation system is of high interest for the analysis of precious cell cultures, such as stem cells or cells lines with a high mutation rate. A second setup looks into a microparticle-based ELISA protocol and demonstrates the feasibility of particle-based sample concentration and the performance of on-chip colorimetric detection. Also in this case, miniature total amounts of biomolecules can be detected, but due to the small sample volumes, a pre-concentration of the molecules at the particle surface is necessary.

The main challenge in both cases is the detection of a weak optical signal, which is a consequence of the small sample volumes. One possible solution is the amplification of the biomolecules, either before (ELISA) or after (PCR) the reaction steps. Another solution is the improvement of the optical detection system, e.g. via the use of stronger biomolecule markers, the direct integration of the sensor elements or the use of highly sensitive detectors, as was examined in the second part of this thesis work.

7.2 Magnetic Particle Manipulation with Integrated Optical Detection

When miniaturizing the magnetic actuation system further, the complete manipulation of small droplets is no longer possible, since the decreased droplet volume, leading to a smaller amount of enclosed magnetic material, is accompanied by increased capillary force. Therefore the splitting step will require more force, which however has to be achieved with less magnetic material. For this reason, we shifted our focus to the manipulation of single magnetic microparticles in a system, whose dimensions are reduced by a factor of ten compared to the droplet manipulation system. These small dimensions permit a system realization using CMOS technologies, which makes the integration of further functionalities into the chip possible. In that context, we chose to include Single Photon Avalanche Diodes into the CMOS system, opening the way to in-situ optical detection of single magnetic microparticles.

Experiments demonstrated the capability of the system to manipulate single magnetic particles of different sizes and to detect them optically on-chip. Based on an optical measurement principle used for elements of much larger dimensions, I developed a photometric detection scheme, which allows to link the optical signal to the size of the detected particle. The optical setup requires hereby only a microscope light source, which permits the observation of the particle movement at the same time. In combination with velocity measurements, made possible by the simultaneous readout of multiple detection elements, the particle can be characterized in terms of its magnetic properties. Moreover, the possibility of performing fluorescent measurements on a single magnetic particle was examined. The successful detection of fluorescent molecules bound to the particle surface demonstrates hereby the system‘s usability for on-chip bioanalysis of high sensitivity.

7.3 Summary

To put it all in a nutshell, the following table summarizes the performances of the two proposed systems, when applied to bioanalytical procedures. The comparison with literature shows that:

- the droplet-based DNA extraction and purification system can handle significantly smaller samples than macroscopic systems and performs as well as other Lab-on-a-Chip systems, while being easier to handle.
- the on-chip colorimetry permits the detection of 7.2 pg of captured HRP labeled antibodies and in combination with on-chip incubation allows to obtain a signal from a sample solution of a concentration of 10 ng/ml, which is comparable to other Lab-on-a-Chip approaches applying the colorimetric ELISA principle.
- the combination of magnetic particle manipulation and optical detection in a CMOS system allows the size-sensitive detection of magnetically actuated single microparticles, as well as the measurement of their magnetophoretic mobility. The highly sensitive optical element also permits the in-situ fluorescent measurement of biomolecules at surface of a single particle.

	reagent volumes	**duration**	**performance**
DNA capture and purification in the droplet manipulation system	10 µl of sample 3 x 10 µl of washing solution 2 x 10 µl of elution buffer 200 µg of magnetic particles	20 min	Extraction of DNA from raw cell sample of **10 lysed cells**.
Colorimetric detection of enzyme labeled antibodies in the droplet manipulation system	10 µl of antibody solution 3 x 10 µl of washing solution 10 µl of chromogen 200 - 400 µg of magnetic particles	10 min + detection step	An total amount of 7.2 pg of HRP-labeled antibodies can be detected.
Fluorescent detection of biomolecules on the surface of a magnetic microparticle in a CMOS system	comparatively large volumes for off-chip preparation, only **one particle** needed for detection step.	n.a.	Upper limit of detection: $3\ 10^6$ molecules (= 0.6 pg for antibodies)

Table 7.1 Summary of the Lab-on-a-Chip applications examined during this thesis.

7.4 Going Forward

Starting from the concepts presented in this thesis work, a series of μTAS applications can be envisioned employing magnetic particle manipulation as a central element. Since the detection of small volumes and, in consequence, small total amounts of the biomolecules is one of the largest challenges in a Lab-on-a-Chip system, the possibility of concentrating these molecules via actuated microparticles, offers a new perspective for their detection on a chip.

The droplet manipulation system shows in that respect the potential of a fully enclosed and automated μTAS, employing standardized bioanalytical procedures. Since our experiments demonstrated the negative influence of additional off-chip handling steps, the next stage should be the improvement of the on-chip injection and detection. With the possibility to perform PCR or fluorescent quantification directly on the chip, the efficiency and sensitivity of the system can be improved further. For on-chip PCR one can profit from the effect of Joules-heating observed in the system. A dedicated design of heating coils will provide the required temperature zones, between which the sample droplet is cycled.

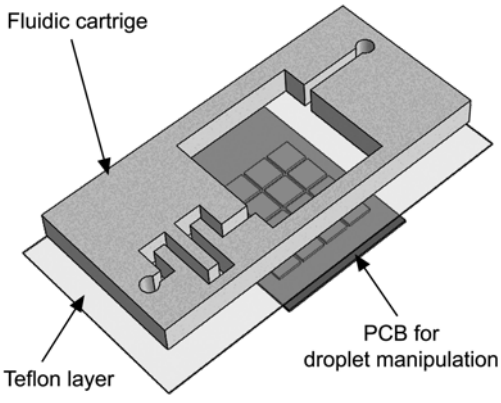

Figure 7.1 Schematic explosion view of a modular system for digital microfluidics containing multiple stages of droplet manipulation. The magnetic particles are pre-mixed with the sample in a meandering channel before being injected into the magnetic actuation chamber. After the reaction, the extracted droplet is transferred to the outlet or to further reaction stages.

In consequence, it will be possible to detect the DNA of a single cell, as well as to further lower the detection limit for captured antigens in an

ELISA-like procedure. Figure 7.1 shows a schematic setup of a fully enclosed droplet manipulation system combining magnetic actuation and continuous flow digital microfluidics. Such a combination allows the automated creation and injection of microdroplets of the different reagents as well as their controlled magnetic manipulation. The reagents can be guided to their respective position and the magnetic particles are passed through the different stages of the protocol, before being transferred to a channel-based detection section. Thus the sample can be processed in a fully enclosed system, which allows the safe examination of potentially dangerous samples, such as HIV, Anthrax or Malaria, or samples highly sensitive to contamination, such as RNA, in an easy-to-use setup.

Following the μTAs toolbox idea introduced in the beginning, the fully enclosed system can, in addition to combining magnetic microparticles and digital microfluidics, contain the third component studied in this thesis work. The integration of the in-situ optical detection will provide hereby a highly sensitive measurement stage. Especially the capability to perform fluorescent measurements offers a wide range of applications, when combined with other optical elements. Recent studies show the possibility of adding lenses [134] and filtering layers [88] to a SPAD, thus improving its optical performance with respect to detection area and wavelength dependence. In consequence, a detection area can be envisaged, where SPADs with different filters allow the examination of multiple markers attached to a magnetic particle or incorporated by a magnetically labeled cell. Further-on, the possibility to perform fluorescence lifetime imaging (FLIM) using SPADs offers another detection mechanism that can be applied in a Lab-on-a-Chip system. The main challenge in that respect is the generation of the localized excitation impulse, which at the moment requires an external laser.

All in all, magnetic microparticles, which present the central element in this thesis work, prove more and more to be a highly versatile tool for miniaturized bioanalysis. Their combination with other elements of the μTAS toolbox can yield interesting combinations, as has been demonstrated by the last chapters. Thus their further teaming with dielectrophoretic particle handling [178] or cytometry [71] might lead to new Lab-on-a-Chip systems.

"**MAGNET**, n. something acted upon by magnetism."
"**MAGNETISM**, n. something acting upon a magnet. The two definitions immediately foregoing are condensed from the works of one thousand eminent scientists, who have illuminated the subject with a great white light, to the inexpressible advancement of human knowledge."

Ambrose Bierce quotes (American Writer, Journalist and Editor, 1842-1914)

NOMENCLATURE

Abbreviations, Acronyms and Methods

2P4M	double polysilicon four metal
ABTS	2,2'-Azino-bis[3- Ethylbenzthiazoline-6-Sulfonic acid]
Agarose Electro-phero-gram	An agarose gel electropherogram is used to visualize the molecules size-separated by gel electrophoresis, where an electrical current is applied to a gel matrix in order to move and separate molecules. Molecules of similar size and charge move at the same speed and present themselves therefore as bands in the electropherogram. The distance a band travels is approximately inversely proportional to the logarithm of the size of the molecule.
BSA	Bovine Serum Albumin
CMOS	Complementary Metal Oxide Semiconductor
DNA	Deoxyribonucleic acid
DOP	Dioctylphtalat
ELISA	Enzyme-Linked Immuno-Sorbent Assay
FITC	Fluoresceinisothiocyanat
FLIM	Florescence lifetime imaging
GuSCN	Guanidine Thiocyanate
HRP	Horseradish-Peroxidase
IgG	Immunoglobulin G
LOC	Lab-on-a-Chip
MEMS	Micro Electro Mechanical System
µTAS	Micro Total Analysis System
OMTS	Octamethyltrisiloxane
PCB	Printed Circuit Board
PCR	The **Polymerase Chain Reaction** [30] is a common method for DNA amplification, which was developed in 1983 by Kary Mullis [129]. PCR amplifies a specific DNA target by copying the strands present in the sample and in repeated temperature cycles. Each cycle consists of a denaturation step, an annealing step and a synthesis step. In the first step, the DNA is denaturized and the double helix is split into two single strands. In the second step, primers, fitting either the end or the start of the sequence of interest, are attached to the respective position on the

	DNA strands. In the third step the respective complementary DNA strand is synthesized by adding the suitable nucleic-acids to the present DNA-and-primer complex. After each cycle the amount of initial DNA is doubled. Since the synthesis step is highly sensitive to contaminants such as proteins, cell debris or chaotropic salts, it is important to obtain a sufficiently clean sample from the initial sample solution.
PDMS	Polymethyltrisiloxane
PolyMPS	Poly-Dimethyl-Co-Methyl-Phenyl Siloxane
SEM	Scanning Electron Microscope
SPAD	Single Photon Avalanche Diode
SU-8	Negative photoresist on epoxy basis

Constants

μ_0	magnetic permeability of vacuum: $\mu_0 = 4\pi\ 10^{-7}$ H/m
μ_B	Bohr magneton: $\mu_B = 9.274\ 10^{-24}$ J/T
k_B	Boltzmann constant: $k_B = 1.3806504\ 10^{-23}$ J/K

Symbols

A	area [m^2]
B	magnetic flux density [T = Vs/m^2]
C	particle concentration [mg/ml]
Ca	capillary number
D	diffusion coefficient [m^2/s]
DE	Euclidic Distance in CIE Lab Color Space L, a, b: coordinates in the CIE Lab color space R,G,B: coordinates in the RGB color space X,Y,Z: coordinates in the XYZ color space X_n,Y_n,Z_n: white reference point for the XYZ -> Lab conversion
D_h	hydraulic diameter [m]

Symbols

F	force [N] F_{mag}: magnetic force F_{drag}: viscous drag force F_{line}: line tension F_x, F_y, F_z: force components with respect to the cartesian coordinates F_g: graviational force
FF	fill factor [wt%]
G	shear stress [Pa]
H	intensity of the magnetic field [A/m]
I	current [A]
I_L	intensity of illumination (photon count) [Hz]
J	total angular momentum [Nms] **S**: spin angular momentum **L**: orbital angular momentum
L_D	diffusion length [m]
M	magnetization [A/m]
N	number of particles
NA	numerical aperture
N_d	demagnetization factor (N_d = 1/3 for a sphere)
P	pressure [Pa] P1: pressure inside the droplet P2: pressure outside the droplet
R	Reynolds number
R_p	projected particle radius (photometry) [m]
R_*	projected radius of the illumination source (photometry) [m]
S	magnetophoretic driving force [N/m^3]
T	temperature [K]
U	circumference [m]
V	volume [m^3] V_m: volume of magnetic material V_{part}: particle volume V_{shell}: volume of non-magnetic particle material V_{drop}: droplet volume
W_{surf}	surface energy [J]

Symbols

$dist_{SPAD}$	distance between SPAD and particle [m]
dl	wire section [m]
f	focal distance [m]
g_L	Landè factor
Δh	height of droplet extrusion [m]
m_p	dipole magnetic moment [A/m^2]
m_{part}	particle mass (single particle or cluster) [kg]
m_s	magnetophoretic mobility
n	refractive index
r	particle radius [m] r_1, r_2: radii of curvature at the droplet surface
s	droplet outline [m]
t	time [s]
v	velocity [m/s] v_s: average velocity difference between two media/elements
α	opening angle of objective [°]
α_r	friction coefficient
η	(dynamic) viscosity [Pa s]
θ_{eq}	equilibrium angle (wetting) [°]
μ	electron magnetic dipole moment [J/T]
μ_r	relative magnetic permeability
ν	kinematic viscosity [m^2/s]
ρ	density [kg/m^3] ρ_m: density of magnetic material ρ_{shell}: density of non-magnetic particle material ρ_{part}: average particle density
σ	interfacial tension [N/m]
χ	magnetic susceptibility
χ_r	relative susceptibility χ_{eff}: effective relative magnetic susceptibility

Symbols

$\varnothing$	diameter
Δ	difference operator, Laplace operator
∇	Nabla operator

REFERENCES

[1] P. Abgrall and A. M. Gue, "Lab-on-chip technologies: making a microfluidic network and coupling it into a complete microsystem - a review," Journal of Micromechanics and Microengineering, vol. 17, pp. R15-R49, 2007.

[2] P. Abgrall, C. Lattes, V. Conederal, X. Dollat, S. Colin, and A. M. Gue, "A novel fabrication method of flexible and monolithic 3D microfluidic structures using lamination of SU-8 films," Journal of Micromechanics and Microengineering, vol. 16, pp. 113-121, 2006.

[3] A. W. Adamson and A. P. Gast, Physical Chemistry of Surfaces, 6th ed.: Wiley Interscience, 1997.

[4] C. H. Ahn, M. G. Allen, W. Trimmer, Y. N. Jun, and S. Erramilli, "A fully integrated micromachined magnetic particle separator," Journal of Microelectromechanical Systems, vol. 5, pp. 151-158, 1996.

[5] J.-I. Akutsu, Y. Tojo, O. Segawa, K. Obata, M. Okochi, H. Tajima, and M. Yohda, "Development of an integrated automation system with a magnetic bead-mediated nucleic acid purification device for genetic analysis and gene manipulation," Biotechnology And Bioengineering, vol. 86, pp. 667-671, 2004.

[6] J. Atencia and D. J. Beebe, "Controlled microfluidic interfaces," Nature, vol. 437, pp. 648-655, 2005.

[7] P. A. Auroux, D. Iossifidis, D. R. Reyes, and A. Manz, "Micro total analysis systems. 2. Analytical standard operations and applications," Analytical Chemistry, vol. 74, pp. 2637-2652, 2002.

[8] D. P. J. Barz and P. Ehrhard, "Model and verification of electrokinetic flow and transport in a micro-electrophoresis device," Lab on a Chip, vol. 5, pp. 949-958, 2005.

[9] J. Baudry, E. Bertrand, N. Lequeux, and J. Bibette, "Bio-specific recognition and applications: from molecular to colloidal scales," Journal of Physics-Condensed Matter, vol. 16, pp. R469-R480, 2004.

[10] T. Bayraktar and S. B. Pidugu, "Characterization of liquid flows in microfluidic systems," International Journal of Heat and Mass Transfer, vol. 49, pp. 815-824, 2006.

[11] D. J. Beebe, G. A. Mensing, and G. M. Walker, "Physics and Applications of Microfluidics in Biology," Annu. Rev. Biomed. Eng., vol. 4, pp. 261-286, 2002.

[12] A. S. E. Belloy, M.A.M. Gijs, "Olique powder basting for three-dimensional micromachining of brittle materials," Sensors and Actuators A, vol. 92, pp. 358-363, 2001.

[13] D. Beyssen, L. Le Brizoual, O. Elmazria, and P. Alnot, "Microfluidic device based on surface acoustic wave," Sensors and Actuators B-Chemical, vol. 118, pp. 380-385, 2006 (DOI: 10.1016/j.snb.2006.04.084).

[14] R. Boom, C. J. A. Sol, M. M. M. Salimans, C. L. Jansen, P. M. E. Wertheimvandillen, and J. Vandernoordaa, "Rapid and Simple Method for Purification of Nucleic-Acids," Journal of Clinical Microbiology, vol. 28, pp. 495-503, 1990.

[15] W. J. Borucki and A. L. Summers, "The photometric method of detecting other planetary systems," Icarus, vol. 58, pp. 121-134, 1984.

[16] A. Bourlinos, A. Simopoulos, D. Petridis, H. Okumura, and G. Hadjipanayis, "Silica-maghemite nanocomposites," Advanced Materials, vol. 13, pp. 289, 2001.

[17] M. C. Breadmore, K. A. Wolfe, I. G. Arcibal, W. K. Leung, D. Dickson, B. C. Giordano, M. E. Power, J. P. Ferrance, S. H. Feldman, P. M. Norris, and J. P. Landers, "Microchip-based purification of DNA from biological samples," Analytical Chemistry, vol. 75, pp. 1880-1886, 2003.

[18] M. R. Bringer, C. J. Gerdts, H. Song, J. D. Tice, and R. F. Ismagilov, "Microfluidic systems for chemical kinetics that rely on chaotic mixing in droplets," Philosophical Transactions of the Royal Society of London Series a-Mathematical Physical and Engineering Sciences, vol. 362, pp. 1087-1104, 2004 (DOI: 10.1098/rsta.2003.1364).

[19] B. J. Briscoe, C. J. Lawrence, and W. G. P. Mietus, "A review of immiscible fluid mixing," Advances in Colloid and Interface Science, vol. 81, pp. 1-17, 1999.

[20] F. Brochard, "Motions of Droplets on Solid Surfaces Induced by Chemical or Thermal Gradients," Langmuir, vol. 5, pp. 432-438, 1989.

[21] M. Brzeska, M. Panhorst, P. B. Kamp, J. Schotter, G. Reiss, A. Puhler, A. Becker, and H. Bruckl, "Detection and manipulation of biomolecules by magnetic carriers," Journal Of Biotechnology, vol. 112, pp. 25-33, 2004.

[22] A. Buguin, L. Talini, and P. Silberzan, "Ratchet-like topological structures for the control of microdrops," Applied Physics A, vol. 75, pp. 207-212, 2002.

[23] C. Burger and W. Ruland, "Analysis of chord-length distributions," Acta Crystallographoca Section A - Foundations of Crystallography, vol. 57, pp. 482-491, 2001.

[24] J. M. Buriak, "Magnetic chaperones for droplets," Nature Materials, vol. 3, pp. 847-849, 2004.

[25] M. Chabert, K. D. Dorfman, and J. L. Viovy, "Using droplet microfluidics to design a continuous flow PCR system," Houille Blanche-Revue Internationale De L'Eau, pp. 51-56, 2006.

[26] M. L. Chabinyc, D. T. Chiu, J. C. McDonald, A. D. Stroock, J. F. Christian, A. M. Karger, and G. M. Whitesides, "An integrated fluorescence detection system in poly(dimethylsiloxane) for microfluidic applications," Analytical Chemistry, vol. 73, pp. 4491-4498, 2001 (DOI: 10.1021/ac010423z).

[27] D. Chatterjee, B. Hetayothin, A. R. Wheeler, D. J. King, and R. L. Garrell, "Droplet-based microfluidics with nonaqueous solvents and solutions," Lab on a Chip, vol. 6, pp. 199-206, 2006.

[28] A. Chau, S. Rignier, A. Delchambre, and P. Lambert, "Three-dimensional model for capillary nanobridges and capillary forces," Modelling and Simulation in Materials Science and Engineering, vol. 15, pp. 305-317, Apr 2007.

[29] M. K. Chaudhury and G. M. Whitesides, "How to make water run uphill," Science, vol. 256, pp. 1539-1541, 1992.

[30] S. Cheng, C. Fockler, W. M. Barnes, and R. Higuchi, "Effective Amplification of Long Targets from Cloned Inserts and Human Genomic DNA," Proceedings of the National Academy of Sciences, vol. 91, pp. 5695-5699, 1994.

[31] S. Chikazumi, Physics of Magnetism, 1964.

[32] S. K. Cho, H. Moon, and C.-J. Kim, "Creating, Transporting, Cutting, and Merging Liquid Droplets by Electrowetting-Based Actuation for Digital Microfluidic Circuits," Journal of Microelectromechanical Systems, vol. 12, pp. 70-80, 2003 (DOI: 10.1109/JMEMS.2002.807467).

[33] J. W. Choi, C. H. Ahn, S. Bhansali, and H. T. Henderson, "A new magnetic bead-based, filterless bio-separator with planar electromagnet surfaces for integrated bio-detection systems," Sensors and Actuators B, vol. 68, pp. 34-39, 2000.

[34] J. W. Choi, T. M. Liakopoulos, and C. H. Ahn, "An on-chip magnetic bead separator using spiral electromagnets with semi-encapsulated permalloy," Biosensors & Bioelectronics, vol. 16, pp. 409-416, 2001 (DOI: 10.1016/S0956-5663(01)00154-3).

[35] J. W. Choi, K. W. Oh, J. H. Thomas, W. R. Heineman, H. B. Halsall, J. H. Nevin, A. J. Helmicki, H. T. Henderson, and C. H. Ahn, "An integrated microfluidic biochemical detection system for protein analysis with magnetic bead-based sampling capabilities," Lab on a Chip, vol. 2, pp. 27-30, 2002 (DOI: 10.1039/b107540n).

[36] L. A. Christel, K. Petersen, W. McMillan, and M. A. Northrup, "Rapid, automated nucleic acid probe assays using silicon microstructures for nucleic acid concentration," Journal of Biomechanical Engineering-Transactions of the Asme, vol. 121, pp. 22-27, 1999.

[37] H. G. Chun, T. D. Chung, and H. C. Kim, "Cytometry and velocimetry on a microfluidic chip using polyelectrolytic salt bridges," Analytical Chemistry, vol. 77, pp. 2490-2495, 2005.

[38] E. H. Conradie and D. F. Moore, "SU-8 thick photoresist processing as a functional material for MEMS applications," Journal of Micromechanics and Microengineering, vol. 12, pp. 368-374, 2002.

[39] A. G. Crevillen, M. Hervas, M. A. Lopez, M. C. Gonzalez, and A. Escarpa, "Real sample analysis on microfluidic devices," Talanta, vol. 74, pp. 342-357, 2007.

[40] J. R. Crowther, ELISA Theory and Practice, vol. 42: Humana Press, 1995.

[41] A. A. Darhuber, J. P. Valentino, J. M. Davis, S. M. Troian, and S. Wagner, "Microfluidic actuation by modulation of surface stresses," Applied Physics Letters, vol. 82, pp. 657-659, 2003.

[42] J. Dasso, J. Lee, H. Bach, and R. G. Mage, "A comparison of ELISA and flow micro sphere-based assays for quantification of immunoglobulins," Journal of Immunological Methods, vol. 263, pp. 23-33, 2002.

[43] T. Deng, G. M. Whitesides, and M. Radhakrishnan, "Manipulation of magnetic microbeads in suspension using micromagnetic systems fabricated with soft lithography," Applied Physics Letters, vol. 78, pp. 1775-1777, 2001 (DOI:10.1063/1.1356728).

[44] J. R. Dorvee, A. M. Derfus, S. N. Bhatia, and M. J. Sailor, "Manipulation of liquid droplets using amphiphilic, magnetic one-dimensional photonic crystal chaperones," Nature Materials, vol. 3, pp. 896-899, 2004.

[45] P. S. Doyle, J. Bibette, A. Bancaud, and J. L. Viovy, "Self-assembled magnetic matrices for DNA separation chips," Science, vol. 295, pp. 2237-2237, 2002.

[46] P. A. Dunne, J. Hilton, and J. M. D. Coey, "Levitation in paramagnetic liquids," Journal of Magnetism and Magnetic Materials, vol. 316, pp. 273-276, 2007.

[47] J. El-Ali, P. K. Sorger, and K. F. Jensen, "Cells on chips," Nature, vol. 442, pp. 403-411, 2006.

[48] R. B. Fair, "Digital microfluidics: is a true lab-on-a-chip possible?," Microfluidics and Nanofluidics, vol. 3, pp. 245-281, 2007.

[49] P. C. Fannin, B. K. P. Scaife, and S. W. Charles, "An Experimental Study of the Magnetic Susceptibility of Colloidal Suspensions of Magnetite as a Function of Particle-Volume Fraction," Journal of Physics D-Applied Physics, vol. 23, pp. 1711-1714, 1990.

[50] R. A. Fisher, "On the Capillary Forces in an Ideal Soil: Correction of Formulae given by W. B. Haines," Journal Agricultural Science, vol. 16, pp. 492-505, 1926.

[51] V. I. Furdui and D. J. Harrison, "Immunomagnetic T cell capture from blood for PCR analysis using microfluidic systems," Lab on a Chip, vol. 4, pp. 614-618, 2004.

[52] C. Fütterer, N. Minc, V. Bormuth, J.-H. Codarbox, P. Laval, J. Rossierb, and J.-L. Viovya, "Injection and flow control system for microchannels," Lab on a Chip, vol. 4, pp. 351-356, 2004.

[53] K. P. Galvin, "A conceptually simple derivation of the Kelvin equation," Chemical Engineering Science, vol. 60, pp. 4659-4660, 2005.

[54] J. Gantelius, C. Hamsten, A. Perrson, M. Uhlen, and H. Andersson-Svahn, "Biomagnetic Bead Based Microfluidic Device for Rapid Naked Eye Field Diagnostics of Cattle Pneumonia," in MicroTAS 2007 Paris, France, 2007.

[55] A. Garcia, J. A. Carrasco, J. F. Soto, F. Maganto, and C. Moron, "A method for calculating the magnetic field produced by a coil of any shape," Sensors and Actuators A, vol. 91, pp. 230-232, 2001.

[56] M. Ghioni, A. Gulinatti, I. Rech, F. Zappa, and S. Cova, "Progress in silicon single-photon avalanche diodes," Ieee Journal of Selected Topics in Quantum Electronics, vol. 13, pp. 852-862, 2007.

[57] C. E. Giacomelli, M. Bremer, and W. Norde, "ATR-FTIR study of IgG adsorbed on different silica surfaces," Journal of Colloid and Interface Science, vol. 220, pp. 13-23, 1999.

[58] M. A. M. Gijs, "Magnetic bead handling on-chip: new opportunities for analytical applications," Microfluidics and Nanofluidics, vol. 1, pp. 22-40, 2004.

[59] C. Gruttner, S. Rudershausen, and J. Teller, "Improved properties of magnetic particles by combination of different polymer materials as particle matrix," Journal of Magnetism and Magnetic Materials, vol. 225, pp. 1-7, 2001.

[60] S. C. Gu, T. Shiratori, and M. Konno, "Synthesis of monodisperse, magnetic latex particles with polystyrene core," Colloid and Polymer Science, vol. 281, pp. 1076-1081, 2003.

[61] J. L. Guesdon and S. Avrameas, "Magnetic Solid-Phase Enzyme-Immunoassay," Immunochemistry, vol. 14, pp. 443-447, 1977.

[62] Z. Guttenberg, H. Muller, H. Habermuller, A. Geisbauer, J. Pipper, J. Felbel, M. Kielpinski, J. Scriba, and A. Wixforth, "Planar chip device for PCR and hybridization with surface acoustic wave pump," Lab on a Chip, vol. 5, pp. 308-317, 2005 (DOI: 10.1039/b412712a).

[63] S. Haeberle and R. Zengerle, "Microfluidic platforms for lab-on-a-chip applications," Lab on a Chip, vol. 7, pp. 1094-1110, 2007.

[64] S. M. Han, J. H. Cho, I. H. Cho, E. H. Paek, H. B. Oh, B. S. Kim, C. Ryu, K. Lee, Y. K. Kim, and S. H. Paek, "Plastic enzyme-linked immunosorbent assays (ELISA)-on-a-chip biosensor for botulinum neurotoxin A," Analytica Chimica Acta, vol. 587, pp. 1-8, 2007.

[65] G. P. Hatch and R. E. Stelter, "Magnetic design considerations for devices and particles used for biological high-gradient magnetic separation (HGMS) systems," Journal of Magnetism and Magnetic Materials, vol. 225, pp. 262-276, 2001.

[66] M. A. Hayes, "Active control of dynamic supraparticle structures in microchannels," Langmuir, vol. 17, pp. 2866-2871, 2001

[67] W. Heisenberg, "Zur Theorie des Ferromagnetismus," Zeitschrift für Physik A Hadrons and Nuclei, vol. 49, pp. 619-636, 1928.

[68] M. Herrmann, E. Roy, T. Veres, and M. Tabrizian, "Microfluidic ELISA on non-passivated PDMS chip using magnetic bead transfer inside dual networks of channels," Lab on a Chip, vol. 7, pp. 1546-1552, 2007 (DOI: 10.1039/b707883h).

[69] P. C. Hiemenz and R. Rajagopalan, Principles of Colloids and Surface Chemistry, 3rd ed. New York: Marcel Dekker, 1997.

[70] C.-M. Ho and Y.-C. Tai, "Micro-electro-mechanical-systems (MEMS) and fluid flows," Ann. Rev. Fluid. Mech., vol. 30, pp. 579-612, 1998.

[71] D. Holmes, J. K. She, P. L. Roach, and H. Morgan, "Bead-based immunoassays using a micro-chip flow cytometer," Lab on a Chip, vol. 7, pp. 1048-1056, 2007.

[72] K. Honda, "Über die ferromagnetischen Theorien von P. Weiss und W. Heisenberg," Zeitschrift für Physik A Hadrons and Nuclei, vol. 63, pp. 141-148, 1930.

[73] J. W. Hong, V. Studer, G. Hang, W. F. Anderson, and S. R. Quake, "A nanoliter-scale nucleic acid processor with parallel architecture," Nature Biotechnology, vol. 22, pp. 435-439, 2004.

[74] D. Horak, M. Babic, H. Mackova, and M. J. Benes, "Preparation and properties of magnetic nano- and microsized particles for biological and environmental separations," Journal of Separation Science, vol. 30, pp. 1751-1772, 2007.

[75] L. H. Hung, K. M. Choi, W. Y. Tseng, Y. C. Tan, K. J. Shea, and A. P. Lee, "Alternating droplet generation and controlled dynamic droplet fusion in microfluidic device for CdS nanoparticle synthesis," Lab on a Chip, vol. 6, pp. 174-178, 2006.

[76] T. P. Hunt, D. Issadore, and R. M. Westervelt, "Integrated circuit/ microfluidic chip to programmably trap and move cells and droplets with dielectrophoresis," Lab on a Chip, vol. 8, pp. 81-87, 2007.

[77] V. Hynek, L. Hnedkovsky, and I. Cibulka, "A new design of a vibrating-tube densimeter and partial molar volumes of phenol(aq) at temperatures from 298 K to 573 K," Journal of Chemical Thermodynamics, vol. 29, pp. 1237-1252, 1997.

[78] N. Inagaki, K. Narushim, N. Tuchida, and K. Miyazak, "Surface characterization of plasma-modified poly(ethylene terephthalate) film surfaces," Journal of Polymer Science Part B-Polymer Physics, vol. 42, pp. 3727-3740, 2004.

[79] P. Irwin, W. Dalmert, J. Brewster, A. Gehring, and S.-I. Tu, "Immuno-Magnetic Bead Mass Transport and Capture Efficiency at Low Target Cell Densities in Phosphate-Buffered Saline," Journal of Rapid Methods and Automation in Microbiology, vol. 10, pp. 129-147, 2002.

[80] R. F. Ismagilov, "Integrated microfluidic systems," Angewandte Chemie-International Edition, vol. 42, pp. 4130-4132, 2003.

[81] N. Jaffrezic-Renault, C. Martelet, Y. Chevolot, and J. P. Cloarec, "Biosensors and bio-bar code assays based on biofunctionalized magnetic microbeads," Sensors, vol. 7, pp. 589-614, 2007.

[82] B. Janczuk, T. Bialopiotrowicz, and A. Zdziennicka, "Some Remarks on the Components of the Liquid Surface Free Energy," Journal of Colloid and Interface Science, vol. 211, pp. 96-103, 1999.

[83] K. Jensen and A. Lee, "The science & applications of droplets in microfluidic devices - Foreword," Lab on a Chip, vol. 4, pp. 31N-32N, 2004.

[84] M. Joanicot and A. Ajdari, "Droplet Control for Microfluidics," Science, vol. 309, pp. 887-888, 2005.

[85] J. W. Judy, "Microelectromechanical Systems (MEMS): fabrication, design and applications," Smart Materials and Structures, vol. 10, pp. 1115-1134, 2001.

[86] K. S. Kim and J.-K. Park, "Magnetic force-based multiplexed immunoassay using superparamagnetic nanoparticles in microfluidic channel," Lab Chip, vol. 5, pp. 657-664, 2005.

[87] E. Kneller, "Superparamagnetism: Classical Theory and Experimental Situation," Zeitschrift Für Angewandte Physik, vol. 21, pp. 16, 1966.

[88] H.-S. Koo, M. Chen, and P.-C. Pan, "LCD-based color filter films fabricated by a pigment-based colorant photo resist inks and printing technology," Thin Solid Films, vol. 515, pp. 896-901, 2006.

[89] S. Kostner and M. J. Vellekoop, "Low Cost Cytometer Based on a DVD Pickup Head," in MicroTAS 2007 Paris, France, 2007.

[90] KPL, Technical Guide for ELISA - Protocols and Troubleshooting: KPL (www.klp.com).

[91] L. J. Kricka and P. Wilding, "Microchip PCR," Analytical and Bioanalytical Chemistry, vol. 377, pp. 820-825, 2003.

[92] F. Lacharme, C. Vandevyver, and M. A. M. Gijs, "Magnetic bead retention device for full on-chip sandwich immuno-assay," in IEEE MEMS 2008 Tuscon (AZ), USA, 2008.

[93] L. Lagae, R. Wirix-Speetjens, J. Das, D. Graham, H. Ferreira, P. P. F. Freitas, G. Borghs, and J. De Boeck, "On-chip manipulation and magnetization assessment of magnetic bead ensembles by integrated spin-valve sensors," Journal of Applied Physics, vol. 91, pp. 7445-7447, 2002.

[94] L. Lagae, R. Wirix-Speetjens, C. X. Liu, W. Laureyn, G. Borghs, S. Harvey, P. Galvin, H. A. Ferreira, D. L. Graham, P. P. Freitas, L. A. Clarke, and M. D. Amaral, "Magnetic biosensors for genetic screening of cystic fibrosis," Iee Proceedings-Circuits Devices and Systems, vol. 152, pp. 393-400, 2005.

[95] R. Lakshmi, V. Baskar, and U. Ranga, "Extraction of superior-quality plasmid DNA by a combination of modified alkaline lysis and silica matrix," Analytical Biochemistry, vol. 272, pp. 109-112, 1999.

[96] A. Lande, "Term structure and Zeeman effect of multipletts," Zeitschrift für Physik, vol. 15, pp. 189-205, 1923.

[97] C. S. Lee, H. Lee, and R. M. Westervelt, "Microelectromagnets for the control of magnetic nanoparticles," Applied Physics Letters, vol. 79, pp. 3308-3310, 2001 (DOI:10.1063/1.1419049).

[98] G.-B. Lee, C.-H. Lin, and G.-L. Chang, "Micro flow cytometers with buried SU-8/SOG optical waveguides," Sensors and Actuators A: Physical, vol. 103, pp. 165-170, 2003.

[99] H. Lee, Y. Liu, R. M. Westervelt, and D. Ham, "IC/Microfluidic hybrid system for magnetic manipulation of biological cells," IEEE Journal of Solid-State Circuits, vol. 41, pp. 1471-1480, 2006 (DOI: 10.1109/JSSC.2006.874331).

[100] K. B. Lee, S. Park, and C. A. Mirkin, "Multicomponent magnetic nanorods for biomolecular separations," Angewandte Chemie-International Edition, vol. 43, pp. 3048-3050, 2004.

[101] D. L. Leslie-Pelecky and R. D. Rieke, "Magnetic Properties of Nanostructured Materials" Chemistry of Materials, vol. 8, pp. 1770-1783, 1996.

[102] I. P. Lewkowich, J. D. Campbell, and K. T. HayGlass, "Comparison of chemiluminescent assays and colorimetric ELISAs for quantification of murine IL-12, human IL-4 and murine IL-4: chemiluminescent substrates provide markedly enhanced sensitivity," Journal of Immunological Methods, vol. 247, pp. 111-118, 2001.

[103] G. X. Li, V. Joshi, R. L. White, S. X. Wang, J. T. Kemp, C. Webb, R. W. Davis, and S. H. Sun, "Detection of single micron-sized magnetic bead and magnetic nanoparticles using spin valve sensors for biological applications," Journal of Applied Physics, vol. 93, pp. 7557-7559, 2003 (DOI: 10.1063/ 1.1540176).

[104] G. X. Li, S. H. Sun, and S. X. Wang, "Spin valve biosensors: Signal dependence on nanoparticle position," Journal of Applied Physics, vol. 99, 2006.

[105] K. Y. Lien, J. L. Lin, C. Y. Liu, H. Y. Lei, and G. B. Lee, "Purification and enrichment of virus samples utilizing magnetic beads on a microfluidic system," Lab on a Chip, vol. 7, pp. 868-875, 2007.

[106] Q. Liu, Y. Q. Li, F. Tang, L. Ding, and S. Z. Yao, "Cationic gemini surfactant as dynamic coating in CE for the control of EOF and wall adsorption," Electrophoresis, vol. 28, pp. 2275-2282, 2007.

[107] X. Q. Liu, Y. P. Guan, Y. Yang, Z. Y. Ma, X. B. Wu, and H. Z. Liu, "Preparation of superparamagnetic immunomicrospheres and application for antibody purification," Journal of Applied Polymer Science, vol. 94, pp. 2205-2211, 2004.

[108] L. E. Locascio, C. E. Perso, and C. S. Lee, "Measurement of electroosmotic flow in plastic imprinted microfluid devices and the effect of protein adsorption on flow rate," Journal of Chromatography A, vol. 857, pp. 275-284, 1999.

[109] T. A. Louis, G. Ripamonti, and A. Lacaita, "Photoluminescence lifetime microscope spectrometer based on time-correlated single-photon counting with an avalanche diode detector," Review of Scientific Instruments, vol. 61, pp. 11-22, 1990.

[110] H. Lomas, "A method for the calculation of surface and interfacial tensions from the shape of pendent drops," Canadian Journal of Chemistry, vol. 46, pp. 3918-3919, 1968.

[111] T. Lommatzsch, M. Megharfi, E. Mahe, and E. Devin, "Conceptual study of an absolute falling-ball viscometer," Metrologia, vol. 38, pp. 531-534, 2001.

[112] A. H. Lu, E. L. Salabas, and F. Schuth, "Magnetic nanoparticles: Synthesis, protection, functionalization, and application," Angewandte Chemie-International Edition, vol. 46, pp. 1222-1244, 2007.

[113] J. Lu, C. Lau, and M. Kai, "Magnetic bead-based label-free chemiluminescence detection of telomeres," Chemical Communications (Cambridge, England), pp. 2888-2889, 2003.

[114] Y. Lu, Y. D. Yin, B. T. Mayers, and Y. N. Xia, "Modifying the surface properties of superparamagnetic iron oxide nanoparticles through a sol-gel approach," Nano Letters, vol. 2, pp. 183-186, 2002.

[115] M. J. Madou, Fundamentals of microfabrication: the science of miniaturization, 2nd edition. Boca Raton, USA: CRC Press, 2002.

[116] E. Mansfield, E. E. Ross, and C. A. Aspinwall, "Preparation and characterization of cross-linked phospholipid bilayer capillary coatings for protein separations," Analytical Chemistry, vol. 79, pp. 3135-3141, 2007.

[117] A. Manz, C. S. Effenhauser, N. Burggraf, D. J. Harrison, K. Seiler, and K. Fluri, "Electroosmotic Pumping and Electrophoretic Separations for Miniaturized Chemical-Analysis Systems," Journal of Micromechanics and Microengineering, vol. 4, pp. 257-265, 1994.

[118] A. Manz, N. Graber, and H. M. Widmer, "Miniaturized Total Analysis Systems: a Novel Concept for Chemical Sensing," Sensors and Actuators B, vol. 1, pp. 244-248, 1990.

[119] K. E. McCloskey and J. J. Chalmers, "Magnetic Cell Separation: Characterization of magnetophoretic mobility," Analytical Chemistry, vol. 75, pp. 6868-6874, 2003.

[120] K. E. McCloskey, J. J. Chalmers, and M. Zborowski, "Magnetophoretic Mobilities Correlate to Antibody Binding Capacities," Cytometry, vol. 40, pp. 307-315, 2000.

[121] M. Megens and M. Prins, "Magnetic biochips: a new option for sensitive diagnostics," Journal of Magnetism and Magnetic Materials, vol. 293, pp. 702-708, 2005.

[122] D. Meyers, Surfaces, Interfaces and Colloid - Principles and Applications, 2nd ed.: Wiley-VCH, 1999.

[123] M. M. Miller and P. E. Sheehan, "A DNA array sensor utilizing magnetic microbeads and magnetoelectronic detection," Journal of Magnetism and Magnetic Materials, vol. 225, pp. 138-144, 2001.

[124] R. S. Molday, S. P. S. Yen, and A. Rembaum, "Application of Magnetic Microspheres in Labeling and Separation of Cells," Nature, vol. 268, pp. 437-438, 1977.

[125] I. Moon and J. Kim, "Using EWOD (Electrowetting-on-Dielectric) Actuation in a Micro Conveyor System," in Transducers'05 Seoul, Korea, 2005.

[126] F. Mugele and J. C. Baret, "Electrowetting: From basics to applications," Journal of Physics-Condensed Matter, vol. 17, pp. R705-R774, 2005.

[127] R. Mukhopadhyay, "Magnetic dust mobilizes droplets," Analytical Chemistry, vol. 77, pp. 55A-55A, 2005.

[128] R. Mukhopadhyay, "Diving into droplets," Analytical Chemistry, vol. 78, pp. 1401-1404, 2006.

[129] K. B. Mullis and F. A. Faloona, "Specific Synthesis of DNA Invitro via a Polymerase-Catalyzed Chain-Reaction," Methods in Enzymology, vol. 155, pp. 335-350, 1987.

[130] N. Nam-Trung and S. T. Wereley, Fundamentals and Applications of Microfluidics: Artech House, 2002.

[131] C. Niclass, A. Rochas, P.-A. Besse, R. Popovic, and E. Charbon, "A 4 [mu]s integration time imager based on CMOS single photon avalanche diode technology," Sensors and Actuators A: Physical, vol. 130-131, pp. 273-281, 2006.

[132] V. Nittis, R. Fortt, C. H. Legge, and A. J. de Mello, "A high-pressure interconnect for chemical microsystem applications," Lab on a Chip, vol. 1, pp. 148-152, 2001.

[133] R. C. O'Handley, Modern Magnetic Materials: Principles and Applications. New Yourk: John Wiley, 2000.

[134] J. B. Orhan, V. K. Parashar, A. Sayah, and M. A. M. Gijs, "Fabrication and characterization of three-dimensional microlens arrays in sol-gel glass," Journal of Microelectromechanical Systems, vol. 15, pp. 1159-1164, 2006.

[135] Z. Osawa, K. Kawauchi, M. Itawa, and H. Harada, "Effect of polymer matrices on magnetic properties of plastic magnets," Journal of Materials Science, vol. 23, pp. 2637-2644, 1988.

[136] P. Y. Paik, D. J. Allen, A. E. Eckhardt, V. K. Pamula, and M. G. Pollack, "Programmable Flow-Through Real-Time PCR Using Digital Microfluidics," in MicroTAS 2007 Paris, France, 2007.

[137] N. Pamme, "Magnetism and microfluidics," Lab Chip, vol. 6, pp. 24-38, 2006.

[138] N. Pamme and A. Manz, "On-chip free-flow magnetophoresis: Continuous flow separation of magnetic particles and agglomerates," Analytical Chemistry, vol. 76, pp. 7250-7256, 2004.

[139] N. Pamme and C. Wilhelm, "Continuous sorting of magnetic cells via on-chip free-flow magnetophoresis," Lab on a Chip, vol. 6, pp. 974-980, 2006.

[140] J. Park, E. Lee, N. M. Hwang, M. Kang, S. C. Kim, Y. Hwang, J. G. Park, H. J. Noh, J. Y. Kim, J. H. Park, and T. Hyeon, "One-Nanometer-Scale Size-Controlled Synthesis of Monodisperse Magnetic Iron Oxide Nanoparticles," Angewandte Chemie-International Edition, vol. 44, pp. 2872-2877, 2005.

[141] S. Peyman, A. Iles, and N. Pamme, "Parallel Multi-Reagent Streams for a Bioassay on Single Magnetic Particles in Continuous Flow," in MicroTAS 2007 Paris, France, 2007.

[142] J. Pipper, M. Inoue, L. F.-P. Ng, P. Neuzil, Y. Zhang, and L. Novak, "Catching Bird Flu in a Droplet," Nature Medicine, vol. 13, pp. 1259-1263, 2007.

[143] M. G. Pollack, A. D. Shenderov, and R. B. Fair, "Electrowetting-based actuation of droplets for integrated microfluidics," Lab on a Chip, vol. 2, pp. 96-101, 2002 (DOI: 10.1039/b110474h).

[144] E. M. Purcell, "Life at Low Reynolds-Number," American Journal of Physics, vol. 45, pp. 3-11, 1977.

[145] Q. Ramadan, V. Samper, D. Poenar, and C. Yu, "On-chip micro-electromagnets for magnetic-based bio-molecules separation," Journal of Magnetism and Magnetic Materials, vol. 281, pp. 150-172, 2004.

[146] Q. Ramadan, C. Yu, V. Samper, and D. P. Poenar, "Microcoils for transport of magnetic beads," Applied Physics Letters, vol. 88, 2006.

[147] I. Rech, A. Restelli, S. Cova, M. Ghioni, M. Chiari, and M. Cretich, "Microelectronic photosensors for genetic diagnostic microsystems," Sensors and Actuators B-Chemical, vol. 100, pp. 158-162, 2004.

[148] G. Reekmans, C. Liu, R. De Palma, R. Wirix-Speetjens, W. Laureyn, and L. Lagae, "Ultra-Sensitive Magnetic Immunosensing Platform Based on the Combined Manipulation and Detection of Magnetic Particles," in MicroTAS 2007 Paris, France, 2007.

[149] D. R. Reyes, D. Iossifidis, P. A. Auroux, and A. Manz, "Micro total analysis systems. 1. Introduction, theory, and technology," Analytical Chemistry, vol. 74, pp. 2623-2636, 2002.

[150] A. Rida, "Microfluidic magnetic particles manipulation: concepts and devices," Lausanne: EPFL, 2004.

[151] A. Rida, V. Fernandez, and M. A. M. Gijs, "Long-range transport of magnetic microbeads using simple planar coils placed in a uniform magnetostatic field," Applied Physics Letters, vol. 83, p. 2396, 2003 (DOI: 10.1063/1.1613038).

[152] J. C. Rife and M. M. Miller, "Design and performance of GMR sensors for the detection of magnetic microbeads in biosensors," Sensors and Actuators A, vol. 107, pp. 209-218, 2003.

[153] L. S. Roach, H. Song, and R. F. Ismagilov, "Controlling nonspecific protein adsorption in a plug-based microfluidic system by controlling interfacial chemistry using fluorous-phase surfactants," Analytical Chemistry, vol. 77, pp. 785-796, 2005.

[154] Roche Applied Science, "MagNA Pure LC DNA Isolation Kit I: Instruction Manual", 2004.

[155] R. Rong, J. W. Choi, and C. H. Ahn, "An on-chip magnetic bead separator for biocell sorting," Journal of Micromechanics and Microengineering, vol. 16, pp. 2783-2790, 2006.

[156] A. E. Saliba, E. Psichari, L. Saias, N. Minc, V. Studer, and J. L. Viovy, "Ferrofluid Pattern for Guiding Magnetic Beads Self-Organisation: Application to Affinity Cell Separation and on Chip Cell Culture," in MicroTAS 2007 Paris, France, 2007.

[157] P. Sartoretti and J. Schneider, "On the detection of satellites of extrasolar planets with the method of transits," Astronomy & Astrophysics Supplement Series, vol. 134, pp. 553-560, 1999.

[158] J. A. Schwartz, J. V. Vykoukal, and P. R. C. Gascoyne, "Droplet-based chemistry on a programmable micro-chip," Lab on a Chip, vol. 4, pp. 11-17, 2004.

[159] S. S. Shevkoplyas, A. C. Siegel, R. M. Westervelt, M. G. Prentiss, and G. M. Whitesides, "The force acting on a superparamagnetic bead due to an applied magnetic field," Lab Chip, vol. 7, pp. 1294 - 1302, 2007.

[160] M. Shikida, K. Inouchi, H. Honda, and K. Sato, "Magnetic handling of droplet in micro chemical analysis system utilizing surface tension and wettability," in 17th IEEE International Conference on Micro Electro Mechanical Systems (MEMS 2004), Maastricht, The Netherlands, 2004, pp. 359-362.

[161] M. Shikida, K. Takayanagi, K. Inouchi, H. Honda, and K. Sato, "Using wettability and interfacial tension to handle droplets of magnetic beads in a micro-chemical-analysis system," Sensors and Actuators B-Chemical, vol. 113, pp. 563-569, 2006.

[162] M. Shikida, K. Takayanagi, H. Honda, H. Ito, and K. Sato, "Development of an enzymatic reaction device using magnetic bead-cluster handling," Journal of Micromechanics and Microengineering, vol. 16, pp. 1875-1883, 2006 (DOI: 10.1088/0960-1317/16/9/017).

[163] S. K. Sia and G. Whitesides, "Microfluidic devices fabricated in poly(dimethylsiloxane) for biological studies," Electrophoresis, vol. 24, pp. 3563-3576, 2003.

[164] T. Sikanen, L. Heikkila, S. Tuornikoski, R. A. Ketola, R. Kostiainen, S. Franssila, and T. Kotiaho, "Performance of SU-8 microchips as separation devices and comparison with glass microchips," Analytical Chemistry, vol. 79, pp. 6255-6263, 2007.

[165] K. Smistrup, B. G. Kjeldsen, J. L. Reimers, M. Dufva, J. Petersen, and M. F. Hansen, "On-chip magnetic bead microarray using hydrodynamic focusing in a passive magnetic separator," Lab on a Chip, vol. 5, pp. 1315-1319, 2005.

[166] K. Smistrup, T. Lund-Olesen, M. F. Hansen, and P. T. Tang, "Microfluidic magnetic separator using an array of soft magnetic elements," Journal of Applied Physics, vol. 99, 2006.

[167] S. Sole, A. Merkoci, and S. Alegret, "New materials for electrochemical sensing III. Beads," trends in analytical chemistry, vol. 20, pp. 102-110, 2001.

[168] T. M. Squires and S. R. Quake, "Microfluidics: Fluid physics at the nanoliter scale," Reviews of Modern Physic, vol. 77, pp. 977-1026, 2005.

[169] V. Srinivasan, V. K. Pamula, and R. B. Fair, "Droplet-based microfluidic lab-on-a-chip for glucose detection," Analytica Chimica Acta, vol. 507, pp. 145-150, 2004.

[170] H. A. Stone and S. Kim, "Microfluidics: Basic Issues, Applications and Challenges," AlChE Journal, vol. 47, pp. 1250-1254, 2001.

[171] H. A. Stone, A. D. Stroock, and A. Ajdari, "Engineering flows in small devices: Microfluidics toward a lab-on-a-chip," Annual Review of Fluid Mechanics, vol. 36, pp. 381-411, 2004.

[172] Y. C. Tan, J. S. Fisher, A. I. Lee, V. Cristini, and A. P. Lee, "Design of microfluidic channel geometries for the control of droplet volume, chemical concentration, and sorting," Lab Chip, vol. 4, pp. 292 - 298, 2004.

[173] T. Taniguchi, T. Torii, and T. Higuchi, "Chemical reactions in microdroplets by electrostatic manipulation of droplets in liquid media," Lab on a Chip, vol. 2, pp. 19-23, 2002.

[174] T. Tartaj and M. del Puerto Morales, "The Preparation of magnetic nanoparticles for applications in biomedicine," Journal of Physics D: Applied Physics, vol. 36, pp. R182-R197, 2003.

[175] H. Tian, A. F. R. Hühmer, and J. P. Landers, "Evaluation of Silica Resins for Direct and Efficient Extraction of DNA from Complex Biological Matrices in a Miniaturized Format," Analytical Biochemistry, vol. 283, pp. 175-191, 2000.

[176] J. D. Tice, H. Song, A. D. Lyon, and R. F. Ismagilov, "Formation of Droplets and Mixing in Multiphase Microfluidics at Low Values of the Reynolds and the Capillary Numbers," Langmuir, vol. 19, pp. 9127-9133, 2003.

[177] R. C. Tolman, "Consideration of the Gibbs Theory of Surface Tension," Journal of Chemical Physics, vol. 16, pp. 758-774, 1948.

[178] R. L. Tornay, T. Braschler, N. Demierre, B. Steitz, A. Finka, H. Hofmann, J. A. Hubbell, and P. Renaud, "Dielectrophoresis-based particle exchanger for the manipulation and surface functionalization of particles," Lab on a Chip, vol. 8, pp. 267-273, 2008.

[179] H. Ueda, K. Tsumoto, K. Kubota, E. Suzuki, T. Nagamune, H. Nishimura, P. A. Schueler, G. Winter, I. Kumagai, and W. C. Mahoney, "Open sandwich ELISA: A novel immunoassay based on the interchain interaction of antibody variable region," Nature Biotechnology, vol. 14, pp. 1714-1718, 1996.

[180] O. D. Velev, B. G. Prevo, and K. H. Bhatt, "On-chip manipulation of free droplets," Nature, vol. 426, pp. 515-516, 2003 (DOI: 10.1038/426515a).

[181] E. Verpoorte, "Beads and chips: new recipes for analysis," Lab on a Chip, vol. 3, pp. 60N-68N, 2003.

[182] J. Vuosku, L. Jaakola, S. Jokipii, K. Karppinen, T. Kamarainen, V. P. Pelkonen, A. Jokela, T. Sarjala, A. Hohtola, and H. Haggman, "Does extraction of DNA and RNA by magnetic fishing work for diverse plant species?," Molecular Biotechnology, vol. 27, pp. 209-215, 2004.

[183] W. Wang, Z. X. Li, R. Luo, S. H. Lu, A. D. Xu, and Y. J. Yang, "Droplet-based micro oscillating-flow PCR chip," Journal of Micromechanics and Microengineering, vol. 15, pp. 1369-1377, 2005.

[184] Y. Wang, Y. Zhao, and S. K. Cho, "Efficient in-droplet separation of magnetic particles for digital microfluidics," Journal of Micromechanics and Microengineering, vol. 17, pp. 2148-2156, 2007.

[185] M. Washizu, "Electrostatic Actuation of Liquid Droplets for Microreactor Applications," IEEE Transactions on Industry Applications, vol. 34, pp. 732-737, 1998.

[186] D. B. Weibel, W. R. DiLuzio, and G. M. Whitesides, "Microfabrication meets microbiology," Nature Reviews Microbiology, vol. 5, pp. 209-218, 2007.

[187] B. H. Weigl, R. L. Bardell, and C. R. Cabrera, “Lab-on-a-chip for drug development,” Advanced Drug Delivery Reviews, vol. 55, pp. 349-377, 2003.

[188] P. Weiss, “The ferromagnetism of crystals,” Physikalische Zeitschrift, vol. 6, pp. 779-781, 1905.

[189] F. M. White, Viscous Fluid Flow: McGraw-Hill, 1974.

[190] G. M. Whitesides, “The origins and the future of microfluidics,” Nature, vol. 442, pp. 368-373, 2006.

[191] S. M. Williams, C. A. Meadows, and E. Lyon, “Automated DNA extraction for real-time PCR,” Clinical Chemistry, vol. 48, pp. 1629-1630, 2002.

[192] D. J. Wilson, A. J. Eccles, T. A. Steele, R. L. Williams, and R. C. Pond, "Surface chemistry and wettability of plasma-treated PTFE," Surface and Interface Analysis, vol. 30, pp. 36-39, 2000.

[193] R. Wirix-Speetjens, “Magnetoresistive Biosensors Based on Manipulation and Detection of Magnetic Particles,” in ESAT Leuven: Katholieke Universiteit Leuven, 2006.

[194] R. Wirix-Speetjens and J. de Boeck, “On-chip magnetic particle transport by alternating magnetic field gradients,” IEEE Transactions on Magnetics, vol. 40, pp. 1944-1946, 2004.

[195] R. Wirix-Speetjens, W. Fyen, K. D. Xu, J. De Boeck, and G. Borghs, “A force study of on-chip magnetic particle transport based on tapered conductors,” IEEE Transactions on Magnetics, vol. 41, pp. 4128-4133, 2005 (DOI: 10.1109/TMAG.2005.855345).

[196] A. Wixforth, C. Strobl, C. Gauer, A. Toegl, J. Scriba, and Z. von Guttenberg, “Acoustic manipulation of small droplets,” Analytical and Bioanalytical Chemistry, vol. 379, pp. 982-991, 2004.

[197] K. A. Wolfe, M. C. Breadmore, J. P. Ferrance, M. E. Power, J. F. Conroy, P. M. Norris, and J. P. Landers, “Toward a microchip-based solid-phase extraction method for isolation of nucleic acids,” Electrophoresis, vol. 23, pp. 727-733, 2002.

[198] H. U. Worm, D. Clark, and M. J. Dekkers, “Magnetic Susceptibility of Pyrrhotite - Grain-Size, Field and Frequency-Dependence,” Geophysical Journal International, vol. 114, pp. 127-137, 1993.

[199] T. T. Wu and I. H. Chang, “Actuating and detecting of microdroplet using slanted finger interdigital transducers,” Journal of Applied Physics, vol. 98, 2005 (DOI: 10.1063/1.1949710).

[200] G. Wyszecki and W. S. Stiles, Color Science: Concepts and Methods, Quantitative Data and Formulae, 2nd ed.: Wiley Interscience, 1982.

[201] Y. N. Xia and G. M. Whitesides, "Soft lithography," Annual Review of Materials Science, vol. 28, pp. 153-184, 1998.

[202] J. Yang, C. X. Bi, Z. G. Su, and G. H. Ma, "A novel process to prepare magnetic polymer microspheres," Chemistry Letters, vol. 36, pp. 1062-1063, 2007.

[203] S. Y. Yang, Y. H. Chao, H. E. Horng, C. Y. Hong, and H. C. Yang, "Tunable one-dimensional ordered structure in a magnetic fluid microstrip under parallel magnetic fields," Journal of Applied Physics, vol. 97, 2005.

[204] B. B. Yellen, R. M. Erb, H. S. Son, R. Hewlin, H. Shang, and G. U. Lee, "Traveling wave magnetophoresis for high resolution chip based separations," Lab on a Chip, vol. 7, pp. 1681-1688, 2007.

[205] S. W. Yeung and I. M. Hsing, "Manipulation and extraction of genomic DNA from cell lysate by functionalized magnetic particles for lab on a chip applications," Biosensors & Bioelectronics, vol. 21, pp. 989-997, 2006.

[206] J. Y. Yoon and R. L. Garrell, "Preventing biomolecular adsorption in electrowetting-based biofluidic chips," Analytical Chemistry, vol. 75, pp. 5097-5102, 2003.

[207] B. Zheng, J. D. Tice, L. S. Roach, and R. F. Ismagilov, "A droplet-based, composite PDMS/glass capillary microfluidic system for evaluating protein crystallization conditions by microbatch and vapor-diffusion methods with on-chip X-ray diffraction," Angewandte Chemie-International Edition, vol. 43, pp. 2508-2511, 2004.

PUBLICATIONS

Journal Articles

U. Lehmann, M. Sergio, S. Pietrocola, E. Dupont, C. Niclass, M.A.M. Gijs and E. Charbon, "Microparticle photometry in a CMOS microsystem combining magnetic actuation and in-situ optical detection". Sensors & Actuators B: Chemical, 2008 (DOI:10.1016/j.snb.2007.10.021).

U. Lehmann, D. de Courten, C. Vandevyver, V.K. Parashar and M.A.M. Gijs, "On-chip antibody handling and colorimetric detection in a magnetic droplet manipulation system". Microelectronic Engineering, vol. 84, pp. 1669-1672, 2007 (DOI: 10.1016/j.mee.2007.01.212).

U. Lehmann, C. Vandevyver, V.K. Parashar and M.A.M. Gijs, "Droplet-Based DNA Purification in a Magnetic Lab-on-a-Chip". Angewandte Chemie International Edition, vol. 45, pp. 3062-3067, 2006 (DOI: 10.1002/ anie.200503624).

U. Lehmann, S. Hadjidj, V.K. Parashar, C. Vandevyver, A. Rida and M.A.M. Gijs, "Two-dimensional magnetic manipulation of microdroplets on a chip as a platform for bioanalytical applications". Sensors and Actuators B:Chemical, vol. 117, pp. 457-463, 2006 (DOI: 10.1016/ j.snb.2005.12.053).

Conference Contributions

U. Lehmann, M. Sergio, S. Pietrocola, C. Niclass, E. Charbon and M.A.M. Gijs, "Particle Shadow Tracking - Combining Magnetic Particle Manipulation with In-Situ Optical Detection in a CMOS Microsystem". MicroTAS 2007, Paris, France, 2007.....*Presentation*

U. Lehmann, M. Sergio, S. Pietrocola, C. Niclass, E. Charbon and M.A.M. Gijs, "CMOS Microsystem Combining Magnetic Acuation and In-Situ Optical Detection of Microparticles". IEEE Transducers 2007, Lyon, France, 2007.....*Presentation*

U. Lehmann, C. Vandevyver, V.K. Parashar, D. DeCourten and M.A.M. Gijs, "Two-Dimensional Magnetic Droplet Manipulation Platform for Miniaturized Bioanalytical Applications". IEEE MEMS 2007, Kobe, Japan, 2007.....*Poster*

U. Lehmann, C. Vandevyver, V.K. Parashar and M.A.M. Gijs, "Droplets and DNA: Extracting and Purifying DNA in a Magnetic Droplet Manipulation System". NanoTech Montreux 2006, Montreux, Switzerland, 2006.....*Poster*

U. Lehmann, C. Vandevyver, V.K. Parashar and M.A.M. Gijs, "Magnetic on-chip DNA Extraction in a Droplet-Based Microsystem". MicroTAS 2006, Tokyo, Japan, 2006.....*Poster + Poster Award*

U. Lehmann, D. DeCourten, C. Vandevyver, V.K. Parashar and M.A.M. Gijs, "On-chip antibody handling and detection in a magnetic droplet manipulation system". MNE 2006, Barcelona, Spain, 2006.....*Presentation*

U. Lehmann, C. Vandevyver, V.K. Parashar and M.A.M. Gijs, "DNA capture and elution in a magnetic droplet manipulation system". 6th International Conference on the Scientific and Clinical Applications of Magnetic Carriers, Krems, Austria, 2006.....*Presentation*

U. Lehmann, V.K. Parashar, C. Vandevyver and M.A.M. Gijs, "On-chip Enzyme-Based Bioanalytical Detection in a Magnetic Droplet Manipulation System". NanoTech Montreux 2005, Montreux, Switzerland, 2005.....*Poster*

U. Lehmann, V. Parashar, S. Hadjidj, A. Rida and M.A.M. Gijs, "Two dimensional magnetic manipulation of microdroplets on a chip". IEEE Transducers 2005, Seoul, Corea, 2005.....*Presentation*

U. Lehmann, S. Hadjidj, A. Rida, V.K. Parashar and M.A.M. Gijs, "Two-dimensional transport of water droplets in oil using magnetic nano-particles". NanoTech Montreux 2004, Montreux, Switzerland, 2004...*Poster*

Conference Abstracts

E. Dupont, U. Lehmann, M. Lombardini, E. Charbon and M.A.M. Gijs, "Detection of fluorescently labelled magnetic particles for lab-on-a-chip applications". NanoTech Montreux 2007, Montreux, Switzerland, 2007.

U. Lehmann, V.K. Parashar, C. Vandevyver and M.A.M. Gijs, "Microfluidic system for analytical applications: a magnetic droplet-based Lab-on-a-Chip". Nanozoom "Applications industrielles des nanotechnologies" , Besançon, France, 2006.

U. Lehmann, V.K. Parashar, C. Vandevyver and M.A.M. Gijs, "A magnetic droplet-based Lab-on-a-Chip". Third Asia Forum on Magnetics, Shimane, Japan, 2006.

U. Lehmann, V.K. Parashar, C. Vandevyver and M.A.M. Gijs, "A Lab-on-a-Chip using magnetic droplets". Nanotech 2006, Boston (MA), USA, 2006.

U. Lehmann, C. Vandevyver, V.K. Parashar and M.A.M. Gijs, "Magnetic particles as mobile substrates on biochips". pHealth2006, International workshop on wearable micro- and nanosystems for personalized Health, Luzern, Switzerland, 2006.

Ulrike Lehmann

Avenue de Morges 26
1004 Lausanne
Switzerland

e-mail: ulrike.lehmann@epfl.ch
tel: +41 21 6259960
mobil: +41 76 3949855

German/ born 18.02.1978

Education

2004-present: **PhD** student at the Institute of Microelectronics and Microsystems at the Ecole Polytechnique Fédérale de Lausanne (EPFL) in Lausanne, Switzerland
PhD Project: "Manipulation of magnetic microparticles in liquid phases for on-chip biomedical analysis methods"

- I developed a new miniaturized bio-analysis system, where small aqueous droplets are actuated magnetically. This multidisciplinary project combined elements of physics, electrical engineering, chemistry, biology and microtechnology.
- During the PhD, I supervised several Master and Bachelor students, as well as students' practical excercises in the clean room.

2001-2002: **Internship** at the University of Delaware in Newark (DE), USA
Project: "Terahertz emitting devices based on SiGe quantum wells"

- I designed a quantum cascade laser based on multiple stacks of SiGe and Si layers, which is able to emit radiation at THz frequencies.

1997-2003: **Dipl.-Ing.** studies in Electrical Engineering at the Chemnitz Technical University in Chemnitz, Germany with a specialization in Microsystems and Device Engineering
Diploma Project: "Resonating scanners with magnetic actuation"

- I studied the feasibility of driving a silicon micromirror via screen-printed permanent micromagnets.

1997: **Abitur** at the Bunsen Gymnasium in Heidelberg, Germany

Languages:

German: mother tongue
English: fluent
French: fluent
Russian: basic knowledge
Latin: school knowledge

IT skills:

AutoCAD, Solid Works
Mathematica, MatLab, COMSOL
LabView
Adobe Photoshop, Illustrator, Corel Draw
C++

Stipends and Awards:

1997-2004: Scholarship of the German National Merit Foundation ("Studienstiftung des deutschen Volkes")

2006: Poster Award at the MicroTAS Conference (Tokyo, November 5-9, 2006)

Interests and extracurricular activities:

2005-2007: President and active member of the EPFL's theatre group "Les Polyssons"

2006-2007: Secretary of the Ultimate Frisbee Club "FlyHigh Lausanne" and member of the organization committee of the "Force Lake" Tournaments 2006 to 2008.